UNIVERSITY OF OKLAHOMA

GRADUATE COLLEGE

ASSIMILATION OF RADAR OBSERVATIONS WITH ENSEMBLE VARIATIONAL HYBRID DATA ASSIMILATION METHOD FOR THE INITIALIZATION AND PREDICTION OF HURRICANES

A DISSERTATION

SUBMITTED TO THE GRADUATE FACULTY

in partial fulfillment of the requirements for the

Degree of

DOCTOR OF PHILOSOPHY

By

YONGZUO LI
Norman, Oklahoma
2015

ASSIMILATION OF RADAR OBSERVATIONS WITH ENSEMBLE

VARIATIONAL HYBRID DATA ASSIMILATION METHOD FOR THE

INITIALIZATION AND PREDICTION OF HURRICANES

A DISSERTATION APPROVED FOR THE
SCHOOL OF METEOROLOGY

BY

_____
Dr. Xuguang Wang, Chair

_____
Dr. Ming Xue, Co-Chair

_____
Dr. Robert Palmer

_____
Dr. Lance Leslie

_____
Dr. Deepak Devegowda

_____
Dr. Yang Hong

Acknowledgements

First and foremost I wish to thank my advisors, Dr. Xuguang Wang and Dr. Ming Xue. I would like to sincerely thank them, for their guidance, teaching, discussion and support during my study and research at the University of Oklahoma (OU). They trained me for many skills at all levels. They gave me many good and important suggestions on my data assimilation research.

I would also like to gratefully acknowledge all the other members of my dissertation committee: Dr. Robert Palmer, Dr. Lance Leslie, Dr. Yang Hong and Dr. Deepak Devegowda, who have spent their time to read my dissertation and offered valuable advices. Without their important comments and suggestions on my research, this dissertation would not be completed.

I am grateful to Dr. Haldun Karan for his help on WRF ARW and WRFDA work. Many thanks go to Dr. Mingjing Tong for her suggestions and discussions on the Gridpoint Statistical Interpolation (GSI) system and to Dr. Henry R. Winterbottom for his suggestions and discussions on the ensemble Kalman filre (EnKF). I thank Dr. Yunheng Wang for helping me on many computer issues patiently. I also acknowledge Dr. Curtis N. James for radar data processing, Shizhang Wang, Alex Schenkman, and Dr. Robin Tanamachi for helpful discussions and assistance.

Thanks also extend to staffs at school of meteorology and CAPS, particularly,Celia Jones, Marcia Pallutto, Eileen Hasselwander and Scott Hill for their kind helps.

Outside the academic community, I shared with my family members. I want to

thank my parents for their endless love, encouragement and support. Many thanks go to my wife, Eva Duo, and my son, Steven Li, for their support and love. They always encourage me on my research and careers with their enthusiasm. Without their constant support and encouragement, the research would not have been possible.

This research was supported by National Ocean and Atmosphere Administration (NOAA) Hurricane Forecast Improvement Project (HFIP) project grant NA12NWS4680012, NA14NWS4830008 and NA14NWS4680021, a subcontract to a grant from the Mississippi State University led by Dr. Haldun Karan. This work was also supported by NSF grant AGS-0802888, DOD-ONR grant N00014-10-1-0775, NOAA THOPREX grant NA08OAR4320904, and NASA NIP grant NNX10AQ78G.

The experiments were performed on the supercomputers of National Ocean and Atmosphere Administration (NOAA), University of Oklahoma, and Mississippi State University..

Table of contents

Acknowledgements iv

Table of contents vi

List of Tables ix

List of Figures x

Abstract xvi

Chapter 1. 1

Introduction and overview 1

1.1 Background and motivation 1

1.2 Overview of the dissertation 8

Chapter 2 9

Assimilation of radar radial velocity data with the WRFEnsemble 3DVAR hybrid system for the prediction of Hurricane Ike (2008) 9

2.1 Introduction 9

2.2 Methodology 12

a. The hybrid ensemble-3DVAR scheme 12

2.3 Experimental design 15

a. The WRF model configuration 15

b. The radar data processing 16

c. The data assimilation setup 18

2.4 Results and discussion 23

a. Single observation test for vertical localization 23

b. Wind increments 24

c. Temperature increments 27
d. Innovation statistics for Vr and minimum sea level pressure in DA cycles ... 29
e. The analyzed hurricane structures 32
f. The track and intensity forecasts 37
g. Verification of forecasts against Vr observations 38
h. Evaluation of rainfall forecasts 40
2.5 Summary and conclusions 42
Chapter 3 46
Assimilation of airborne radar radial velocity data using the unified GSI-based hybrid EnKF-3DVAR system for the prediction of Hurricane Irene (2011) 46
3.1 Introduction 46
3.2 Methodology 49
a. The hybrid ensemble-3DVAR scheme 49
3.3 Experimental design 51
a. The HWRF model configuration 51
b. The airborne radar data processing 52
3.4 Results and discussion 58
a. Wind and temperature analysis increments 59
b. Verification with independent in-flight measurements 61
c. Innovation statistics for Vr and minimum sea level pressure in DA cycles ... 65
d. The analyzed hurricane structures 67
e. The track and intensity forecasts 69
3.5 Summary and conclusions 71

Chapter 4 75

Assimilation of Airborne Radar Data using Dual Resolution, GSI-based Var-EnKF Hybrid System for TC Initialization and Prediction 75

4.1 Introduction 75

4.2 Methodology 80

a. The hybrid ensemble-3DVAR scheme 80

4.3 Experimental design 85

a. The HWRF model configuration 86

b. The airborne radar data processing 87

c. The data assimilation setup 88

4.4 Results and discussion 91

a. Single observation test for equivalence between EnKF and Hybrid 91

b. Wind and temperature analysis increments 93

c. The hurricane structures 96

d. The precipitable water 101

e. The track and intensity forecast RMSEs 104

4.5 Summary and conclusions 106

Chapter 5 110

Summary and Future Plan 110

5.1 General Summary 110

5.2 Future plan 115

References 116

List of Tables

Table 2.1 List of experiments……19

Table 3.1 List of experiments……....56

Table 4.1 List of experiments……....90

List of Figures

Fig. 1.1 The WRF model domain and National Hurricane Center best track positions for Hurricane Ike (2008) from 1800 UTC 12 to 0000 UTC 14 September 2008. Also indicated are the Houston, Texas (KHGX) and Lake Charles, Louisiana (KLCH) WSR-88D radar locations (asterisks) and maximum range (300 km for radial velocity and 460km for the reflectivity) coverage circles. 5

Fig. 1.2 The HWRF model domain and National Hurricane Center best track positions for Hurricane Irene (2011) from 1200 UTC 25 to 0000 UTC 28 August 2011. Also indicated are six flight legs of NOAA P-3 mission in green color. 7

Fig. 2.1 Schematic diagram of the hybrid ensemble-3DVAR forecast-analysis cycle for a hypothetical three-member ensemble. Each member assimilates the observations containing a different set of perturbations. 12

Fig. 2.2 The radial velocity (interval of 20 m s^{-1}) at 0.5^{o} elevation angle from (a) KHGX and (b) KLCH WSR-88D radars at 0000 UTC 13 September 2008. Black dot is for NHC best-track position of Hurricane Ike (2008) at this time. Asterisks are for radar 17

Fig. 2.3 The flow charts for (a) NoDA experiment, (b) 3DVAR experiments (3DVARa and 3DVARb), and (c) hybrid experiments (HybridF and HybridH). 20

Fig. 2.4 The vertical cross section of the wind speed increment (interval of 5 m s^{-1}) using a single KHGX radar radial velocity data located at (28.4^{o}N, 93.7^{o}W, 3176 m) with an innovation of -38.63 m s^{-1} using the configurations of experiment HybridF but (a) without and (b) with vertical localization at 0000 UTC 13 September 2008. 23

Fig. 2.5 The 700 hPa wind analysis increments (m s^{-1}) for (a) 3DVARa, (b) 3DVARb, (c) HybridF, and (d) HybridH at 0000 UTC 13 September 2008. 25

Fig. 2.6 The 850 hPa temperature analysis increments for (a) 3DVARb (at intervals of 0.3 K), (b) HybridF (at intervals of 0.7 K), and (c) HybridH (at intervals of 0.3 K), at 0000 UTC 13 September 2008. 27

Fig. 2.7 The forecast and analysis (sawtooth pattern during DA cycling) of (a) RMSD of radial velocity (m s^{-1}), and (b) the minimum sea level pressures (hPa) together with the NHC best track estimate, for 3DVARb, HybridF, and HybridH from 0000 to 0300 UTC 13 September 2008. 30

Fig. 2.8 The analyzed sea level pressure (interval of 5 hPa, solid contours) and the surface wind vectors (m s^{-1}) for (a) NoDA, (b) 3DVARb, (c) HybridF, and (d) HybridH at 0300 UTC 13 September 2008. The thick solid line indicates the vertical cross section location in Fig. 2.9 and Fig. 2.10. 33

Fig. 2.9 Vertical cross sections of analyzed horizontal wind speed (interval of 10 m s^{-1}, shaded) and potential temperature (interval of 5 K, solid contours) for (a) NoDA, (b) 3DVARb, (c) HybridF, and (d) HybridH, at 0300 UTC 13 September 2008. 34

Fig. 2.10 Vertical cross sections of analyzed temperature anomalies (interval of 2 K) for (a) NoDA, (b) 3DVARb, (c) HybridF, and (d) HybridH, at 0300 UTC 13 September 2008. 35

Fig. 2.11 Deterministic forecast hurricane (a) tracks and (b) minimum sea level pressure (hPa) by NoDA, 3DVARb, HybridF, and HybridH as compared to NHC best track estimates from 0300 UTC 13 through 0000 UTC 14 September 2008. 37

Fig. 2.12 Deterministic forecast RMSEs of Vr (m s^{-1}) by 3DVARb, HybridF, and HybridH from 0300 to 0900 UTC 13 September 2008. 38

Fig. 2.13 The equitable threat scores for 3 h accumulated forecast precipitation by NoDA, 3DVARb, HybridF, and HybridH at thresholds (a) 5 mm, (b) 10 mm, and (c) 25 mm, verified against NCEP Stage-IV precipitation analyses valid at 0600, 0900, 1200, and 1500 UTC 13 September 2008. 40

Fig. 2.14 Three-hour accumulated precipitation (mm) by (1^{st} column) NCEP Stage-IV precipitation analyses, (2^{nd} column) NoDA, (3^{rd} column) 3DVARb, and (4^{th} column) HybridF valid at (top) 0600 and (bottom) 0900 UTC 13 September 2008. 41

Fig. 3.1 Schematic diagram of the GSI-based EnKF-variational one way coupled hybrid data assimilation system. 49

Fig. 3.2 Horizontal distribution of the airborne Doppler radar radial velocity observations. 54

Fig. 3.3 Vertical distribution of the airborne Doppler radar radial velocity observations. 55

Fig. 3.4 The flow charts for (a) NoDA experiment, (b) GSI3DVar experiments, (c) 3DEnsVar experiments, and (d) EnKF experiments. 57

Fig. 3.5 The 700 hPa wind analysis increments (m s^{-1}) for (a) GSI3DVar, (b) EnKF, and (c) 3DEnsVar at 2130 UTC 25 August 2011. 59

Fig. 3.6 The 700 hPa temperature analysis increments (at intervals of 0.5 K) for (a) GSI3DVar, (b) EnKF, and (c) 3DEnsVar at 2130 UTC 25 August 2011. 60

Fig. 3.7 Flight level wind speed (m s^{-1}) observed by in-flight instrument (black line) and interpolated from model prior (green line), and post (red line). First flight leg at

2048 – 2157 UTC: (a) GSI3DVar, (b) EnKF, (c) 3DEnsVar. Last flight leg at 2531 – 2627 UTC: (d) GSI3DVar, (e) EnKF, (f) 3DEnsVar 62

Fig. 3.8 Surface wind speed (m s^{-1}) retrieved by SFMR (black line) and interpolated from model lowest level for prior (green line), and post (red line). First flight leg at 2048 – 2157 UTC: (a) GSI3DVar, (b) EnKF, (c) 3DEnsVar. Last flight leg at 2531 – 2627 UTC: (d) GSI3DVar, (e) EnKF, (f) 3DEnsVar. 64

Fig. 3.9 The forecast and analysis (sawtooth pattern during DA cycling) of (a) RMSD of TDR radial velocity (m s^{-1}), and (b) the minimum sea level pressures (hPa) verified against the NHC best track estimate, for GSI3DVar, EnKF, and 3DEnsVar from 2130 UTC 25 to 0200 UTC 26 August 2011. 66

Fig. 3.10 Wind vector and speed (shaded) at 1-km height. (a) HRD TDR Vr analysis. The HWRF model simulation of wind, together with sea level pressure (interval of 5 hPa, solid contours) for (b) GSI3DVar, (c) 3DEnsVar at 0200 UTC 26 September 2011. 67

Fig. 3.11 Vertical cross section of wind speed (interval of 10 m s^{-1}, shaded). (a) HRD TDR Vr analysis. The HWRF model simulated wind, together with potential temperature (interval of 5 K, solid contours) for (b) GSI3DVar, (c) 3DEnsVar at 0200 UTC 26 September 2011. 68

Fig. 3.12 Deterministic forecast hurricane (a) tracks and (b) minimum sea level pressure (hPa) by NoDA, GSI3DVar, EnKF, 3DEnsVar, EMC as compared to NHC best track estimates from 0200 UTC 26 through 0000 UTC 28 August 2011. 69

Fig. 4.1 Hurricane Irene (2011) tracks based on National hurricane Center best-track locations. Also indicated are flight tracks of NOAA aircraft missions in red, green, blue, and orange color. 79

Fig. 4.2 Schematic diagram of the GSI-based EnKF-variational one/two-way coupled hybrid data assimilation system..... 80

Fig. 4.3 An example of the HWRF model domain. D01 and D02 denote 9 and 3 km grids respectively. 87

Fig. 4.4 Vertical cross sections of the wind speed increment (interval of 1 m s^{-1}) using a single radial velocity with an innovation of 8 m s^{-1} located at (34.78^{o}N, 76.78^{o}W; 535 hPa) for 2130 UTC 25 August 2011. Axis are marked by vertical levels and horizontal grid points. 92

Fig. 4.5 The 700 hPa wind analysis increments (interval of 5 m s^{-1}) with background from nested grids at (a) 9 km, (b) 3 km at 0930 UTC 26 August 2011. 94

Fig. 4.6 The 700 hPa temperature analysis increments (at intervals of 0.5 K) for (a) dualHYBe2w93, (b) sinHYBe1w9 at 0930 UTC 25 August 2011. 95

Fig. 4.7 Wind vector and speed (shaded, interval of 10 m s^{-1}) at 1-km height. (a) HRD TDR Vr analysis. The final analyzed wind for (b) dualHYBe2w93, and (c) sinHYBe1w93 at 1300 UTC 26 September 2011. 96

Fig. 4.8 Vertical cross section of wind speed (interval of 10 m s^{-1}, shaded). (a) HRD TDR Vr analysis. The final analysis wind for (b) dualHYBe2w93, and (c) sinHYBe1w93 at 1300 UTC 26 September 2011. Error! Reference source not found. 97

Fig. 4.9 Wind vector and speed (interval of 10 m s^{-1}, shaded) at 1-km height. (a) HRD TDR Vr analysis. The HWRF forecast wind for (b) dualHYBe2w93, (c) sinHYBe1w93, and (d) sinHYBe1w9 at 0000 UTC 27 September 2011. 99

Fig. 4.10 Vertical cross section of wind speed (interval of 10 m s-1, shaded). (a) HRD TDR Vr analysis. The HWRF forecast wind for (b) dualHYBe2w93, (c) sinHYBe1w93, and (d) sinHYBe1w9 at 0000 UTC 27 September 2011. 100

Fig. 4.11 Precipitable water (interval of 5 mm) for final analysis by (a) dualHYBe2w93, (b) sinHYBe1w93, and (c) sinHYBe1w9 at 1300 UTC 26 September 2011 and forecast by (a) dualHYBe2w93, (b) sinHYBe1w93, and (c) sinHYBe1w9 at 0000 UTC 27 September 2011. 103

Fig. 4.12 Deterministic forecast RMSEs for (a) tracks and (b) central sea level pressure (hPa), (c) maximum wind by dualHYBe2w93, dualHYBe1w93, sinHYBe1w93, and sinHYBe1w9 as compared to NHC best track estimates from 1300 UTC 26 through 1200 UTC 28 August 2011..... 105

Abstract

Data assimilation is a critical component for accurate model forecast. This dissertation investigated the ensemble-variational hybrid data assimilation methods using land based radar and airborne radar data for the prediction of Hurricanes.

In the first part of this dissertation, an enhanced version of the hybrid ensemble-3DVAR data assimilation system for the WRF model is applied to the assimilation of radial velocity (Vr) data from two coastal WSR-88D radars for the prediction of Hurricane Ike (2008) before and during landfall. In this hybrid system, flow-dependent ensemble covariance is incorporated into the varitional cost function using the extended control variable method. The analysis ensemble is generated by updating each forecast ensemble member with perturbed radar observations using the hybrid scheme itself. The Vr data are assimilated every 30 minutes for 3 hours immediately after Ike entered the coverage of the two coastal radars. The hybrid system is compared with the WRF 3DVAR results after tuning to its background error covariance correlation scale.

The hybrid method produces temperature increments showing rainband structures and positive increments in the vortex core region, and a warm core throughout the hurricane depth in the final analysis. In contract, the 3DVAR produces much weaker and smoother increments with negative values at the vortex center at lower levels. The unturned WRF 3DVAR produces wind increments that are inconsistent with the hurricane vortex circulations. Forecasts from the hybrid analyses fit the observed radial velocity better than that from 3DVAR, and the 3-h accumulated precipitation forecasts are also more skillful. The track forecast is slightly improved by

the hybrid method and slightly degraded by the 3DVAR compared to the forecast from GFS analysis. All experiments assimilating the radar data show much improved intensity analyses and forecasts compared to the experiment without assimilating radar data. The forecast results indicate that the hybrid method produces dynamically more consistent state estimations that lead to lower error growth in the forecast than the 3DVAR method does, and there is little benefit of including the static component of background error covariance for hurricane and radar data assimilation.

In the second part of this dissertation, the unified Gridpoint Statistical Interpolation (GSI) based hybrid ensemble Kalman filter (EnKF)-three dimensional variational data assimilation (3DVAR, DA) system interfaced with the Hurricane Weather Research and Forecasting (HWRF) model, is used to assimilate the airborne tail Doppler radar (TDR) radial velocity data for tropical cyclone (TC) prediction. In this hybrid system, flow-dependent covariance estimated from an ensemble forecast updated by the ensemble square root filter (EnSRF) is incorporated into the 3DVAR cost function via extended control variables. The thinning algorithm for TDR data was also enhanced.

The system was first explored using a single resolution configuration where both analysis and forecast ensemble perturbations are defined at 9 km grid . We compared with the flight level wind and temperature, SFMR remote sensed wind, and air borne Doppler radar wind composite produced by HRD, we see that the hybrid analyses successfully capture the inner-core structure of the hurricane vortex in terms for both wind and temperature fields during the analysis time. The subsequent deterministic

forecasts initialized by assimilating airborne radar observations using the hybrid method improved the hurricane track and intensity forecasts, compared with EMC operational forecast, the forecast initialized by GSI 3DVar with static background covariance, and forecast without assimilating TDR data.

One advantage of the hybrid method is its easiness to implement the dual resolution configuration. In the third part of the study, dual resolution hybrid DA method, where the ensemble forecast perturbation and extended control variable are configured at 9-km grid while the analysis is performed at 3-km grid, was investigated,. The one-way and two-way coupling hybrid DA systems are inter-compared. For dual resolution study, a case study and statistics of multiple missions are conducted. Given a weaker TC in background fields, the dual resolution method enhanced it by producing more detailed cyclonic wind increment and inner core positive temperature increment than single low resolution. Verification against radar observed wind analysis and National Hurricane Center (NHC) best track shows that the dual resolution applied for both analysis and forecast produces more accurate forecast winds than single low resolution. On average of 4 missionscases, the experiment with a combination of dual resolution hybrid DA method and two-way coupling produces the smallest track and intensity forecast errors among various configurations.

Chapter 1.

Introduction and overview

1.1 Background and motivation

Numerical Weather Prediction (NWP) requires accurate initial conditions to produce subsequent weather forecast by complex numerical models. Due to the chaotic nature of the atmosphere, small errors initial conditions can be amplified during model integration and result in big differences between the forecast and true atmosphere state. Thus various data assimilation methods that combine observations and model forecast state have been developed and applied for model initialization.

Firstly three dimensional variational (3DVAR) data assimilation method has been used by many research and operational centers. Traditionally 3DVAR uses static covariance that is a statistics of the atmosphere for a period (e.g., 15 days or 30 days). Such a static covariance does not reflect current atmosphere flow and the analysis by 3DVAR could be wrong, especially for some strong weather system such as hurricane, where covariance may change dramatically with time and space. The four dimensional variational (4DVAR) data assimilation method was developed by assimilating observation during a time period, which uses a tangent-linear version of an often simplified forecast model implicitly evolves the background error covariance over the assimilation period, starting from a typically static estimate of the covariance at the beginning of the time window (Courtier et al. 1994). The computational cost for 4DVAR increased tremendously in comparison with 3DVAR. In addition, great effort is

needed to developing and maintaining the complex adjoint model. Nevertheless, the 4DVAR has been implemented at several operational centers, including European Centre for Medium-Range Weather Forecasts (ECMWF), MeteoFrance, and Japan Meteorological Agency (JMA). Recently Ensemble Kalman filter (EnKF) proposed by Evensen (1994), has been widely used for model initialization. The background error covariance of EnKF is estimated from an ensemble forecast perturbations and evolves with data assimilation cycling. Such a covariance can be consistent with current flow pattern. The ensemble analyses provided by EnKF are the natural choice for initializing ensemble forecasts. Without the need for developing and maintaining the adjoint code for variational data assimilation algorithm, the implementation of an EnKF is relatively straightforward and simple. Given a proper interface, a general EnKF system can be interfaced with multiple numerical models. For example, the EnKF in Data Assimilation Research Testbed (DART) developed at the National Center for Atmospheric Research (NCAR) is applied to various numerical models. Among other limitations, one disadvantage of EnKF is that it not easy to incorporate physical constraints (e.g., continuity constraint). On the contrary, physical constraints can be easily added to variational algorithm.

One better choice is to incorporate flow dependent covariance estimated from ensemble forecast into variational algorithm (e.g., Hamill and Snyder 2000; Lorenc 2003; Etherton and Bishop 2004; Zupanski 2005; Wang et al. 2007ab, 2008ab, 2009; Wan 2010, 2011; Wang et. al 2013; Wang and Lei 2014). Hamill and Snyder (2000) proposed that the background error statistics for the data assimilation are estimated from a linear combination of static 3DVAR covariances and flow-dependent covariances

estimated from the ensemble of short-range forecasts. Such a hybrid scheme allows the user to weight the relative contributions of the 3DVAR and ensemble-based background covariances. They found that, for large ensemble size, the hybrid analysis performs best when background error covariances are estimated almost fully from the ensemble. For small ensemble size, some lessened weighting of ensemble-based covariances is desirable. Meanwhile hybrid scheme improves analysis in sparse data area more than in data-rich area. Lorenc (2003) proposed the hybrid method where forecast ensemble perturbations used to estimate background covariance are directly incorporated into variational cost function through extended control variables. This hybrid method is relatively straight-forward when it is coded into existing variational assimilation (3DVAR or 4DVAR) system. Wang et al. (2007a) proved the theoretical equivalence of these two hybrid methods. The potential advantages of a hybrid method compared to a standalone Var and EnKF are summarized in Wang 2010.

Based on existing WRF 3DVAR system, the hybrid system was first developed for WRF ARW model by combining ensemble covariances with the static covariances to estimate the complex, flow-dependent forecast-error statistics, using the extended control variable method during the variational minimization (Wang et al. 2008a). This system laid the foundation for the study documented in chapter 2 of this dissertation. Wang (2010) derives the mathematical framework to incorporate ensemble covariance in variational minimization for the US NWS's operational data assimilation system Gridpoint statistical interpolation (GSI), Both the 3D and 4D hybrid method have been implemented in US NWS's operational Global Forecast System (Wang et al. 2013; Wang and Lei 2014) . Such hybrid system interfaced with HWRF

model laid foundation for the study in chapter 3 and 4 of this dissertation. Buehner et al. (2010) implemented the hybrid method at the Canadian Meteorological Centre for their operational global data assimilation system.

Radar data is one of the most important observations. It has high temporal and spatial resolution. Proper use of radar data could obtain both thermodynamic and dynamic information. The coastal ground based radar could cover as far as about 200 km offshore, where there is little three dimensional meteorological data. This area is a key for hurricane landfall forecast. Airborne Doppler radar data is another important observation oversea for hurricane analysis and forecast, especially for hurricane inner core structure. Compared with conventional data such as sounding, radar data need additional effort for data quality control process and dealiasing. As the radar data is not model quantity additional steps are needed during data assimilation.

In this research we assimilate land based radar to the hybrid ensemble-3DVAR system developed for the WRF model (Wang et al. 2008a) and assimilate airborne radar radial velocity data into the Grid Statistics Interpolation (GSI)-based EnKF-Var system extended for Hurricane Weather Research and Forecast (HWRF) model.

Initial condition is one of the important aspects for a numerical model to forecast hurricane accurately. Many previous studies adopted the vortex relocation and/or bogussing (e.g., Liu et al. 2000; Kurihara et al. 1995; Zou and Xiao 2000) techniques. While such techniques are non-trivial and have been shown to improve the hurricane forecast, how to maintain the dynamical and thermo-dynamical coherency of the hurricane and its environment is probably the biggest challenge with such methods. Thus advanced data assimilation is needed to initialize the model forecast. Such data

assimilation (DA) system can effectively use the observations to accurately estimate the initial TC vortex and the environment where the TC is embedded in.

In Chapter 2 of this study, we assimilate land-base radar radial velocity with hybrid ensemble-3DVAR system for WRF model. As a first step of such research, we focus on assimilating radar radial velocity data. Meanwhile, this research also performs detailed diagnostics to understand the fundamental differences between the roles and effects of flow-dependent and static covariances in the TC analysis and forecast.

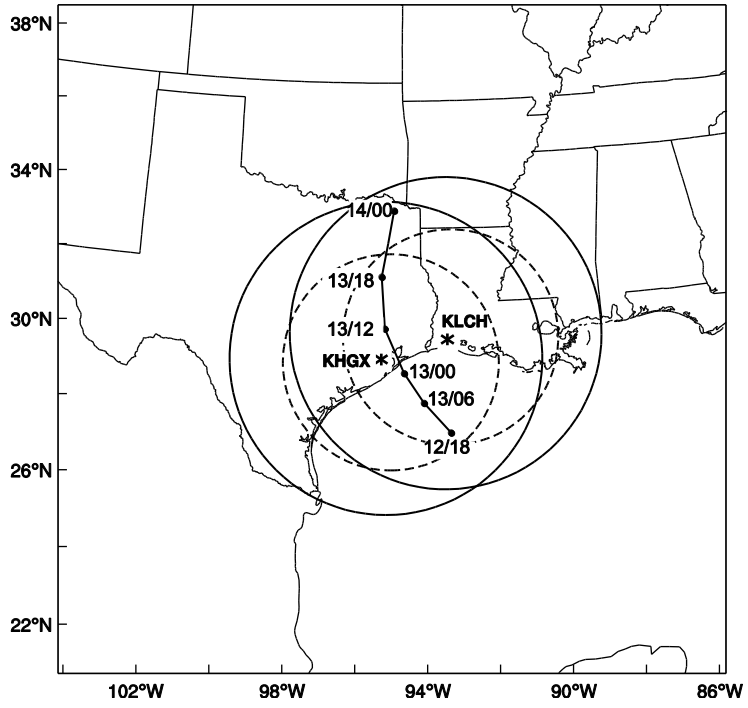

Fig. 1.1 The WRF model domain and National Hurricane Center best track positions for Hurricane Ike (2008) from 1800 UTC 12 to 0000 UTC 14 September 2008. Also indicated are the Houston, Texas (KHGX) and Lake Charles, Louisiana (KLCH) WSR-88D radar locations (asterisks) and maximum range (300 km for radial velocity and 460km for the reflectivity) coverage circles.

More specifically, this research applies and explores the WRF ensemble-3DVAR hybrid system (Wang et al. 2008ab) to the assimilation of coastal WSR-88D radar radial velocity data for the prediction of Hurricane Ike (2008) (Fig. 1.1). Ike is the second costliest tropical cyclones in the recorded history (1900-2010) over the mainland United States (http://www.nhc.noaa.gov/pdf/nws-nhc-6.pdf).

In Chapter 3 of this study, assimilation of airborne radar radial velocity with GSI based EnKF-Var system for HWRF model is performed. Traditionally, GSI system, operationally adopted by NCEP, uses a static background error covariance matrix. In this study, the flow-dependent ensemble covariance estimated from the ensemble Kalman filter (EnKF) is incorporated into GSI cost function using the extended control variable method. Here the EnKF is a serial implementation of the square root ensemble Kalman filter (EnSRF) system, by which the analysis ensemble is generated by updating each forecast ensemble member. Both EnKF and GSI are interfaced with each other (i.e., the EnKF is using the same observation operator from GSI), and interfaced with HWRF model.

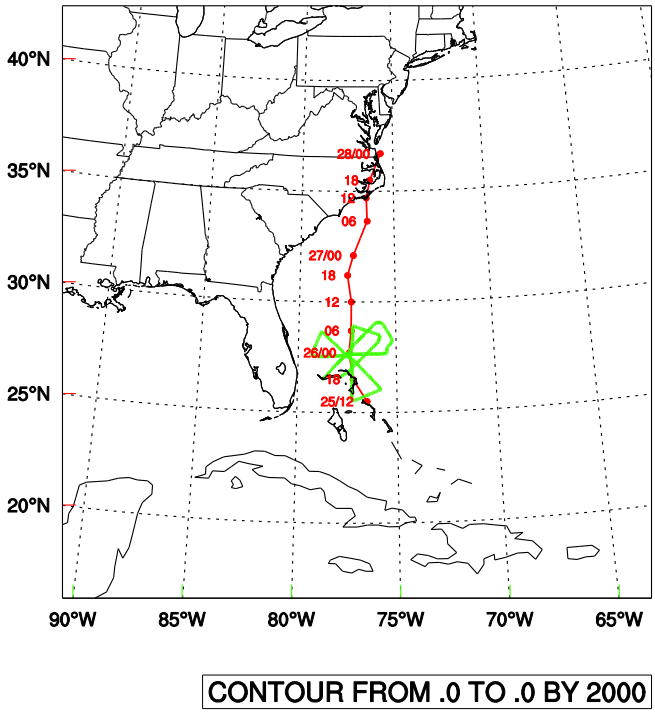

Fig. 1.2 The HWRF model domain and National Hurricane Center best track positions for Hurricane Irene (2011) from 1200 UTC 25 to 0000 UTC 28 August 2011. Also indicated are six flight legs of NOAA P-3 mission in green color.

In this research, we assimilate airborne radar radial velocity data. Meanwhile, this study also performs detailed diagnostics to understand the fundamental differences between the roles and effects of flow-dependent and static covariances in the TC analysis and forecast. More specifically, this study applies the GSI 3DVar-based ensemble–3DVAR hybrid system to explore the assimilation of NOAA P-3 airborne Doppler radar radial velocity data for the prediction of Hurricane Irene (2011) (Fig. 1.2). Irene (2011) is currently ranked as the seventh costliest hurricane in the United States history (interested readers are referred to en.wikipedia.org/wiki/Hurricane_Irene).

1.2 Overview of the dissertation

This dissertation is organized as follows. Chapter 2 presents the application of hybrid ensemble-3DVAR system for WRF model for assimilation of coastal land-base radar radial velocity. Chapter 3 presents the research on assimilating airborne radar radial velocity using GSI based 3DEns-Var system for HWRF model using a single resolution configuration. Chapter 4 presents the research on assimilating airborne radar radial velocity using GSI based 3DEns-Var system for HWRF model using a dual resolution configuration. A general summary and future plan is given in Chapter 5.

Chapter 2

Assimilation of radar radial velocity data with the WRFEnsemble 3DVAR hybrid system for the prediction of Hurricane Ike (2008)

2.1 Introduction

Tropical cyclones (TCs) are among the most costly forms of natural disaster (Pielke et al. 2008). An accurate TC forecast will require not only a numerical model to realistically simulate both the TC itself and its environment, but also a data assimilation (DA) system that can effectively use the observations to accurately estimate the initial Hurricane structure and its environment.

To address the TC initialization issue, many previous studies adopted the vortex relocation and/or bogussing (e.g., Liu et al. 2000; Kurihara et al. 1995; Zou and Xiao 2000) techniques. While such techniques are non-trivial and have been shown to improve the hurricane forecast, how to maintain the dynamical and thermo-dynamical coherency of the hurricane and its environment is probably the biggest challenge with such methods.

Recently, several studies have explored the use of ensemble-based DA methods to initialize hurricane forecasts and have shown great promise (e.g., Torn and Hakim 2009; Zhang et al. 2009a; Li and Liu 2009; Hamill et al. 2011; Wang 2011; Weng et al. 2011; Zhang et al. 2011; Aksoy et al. 2012; Weng and Zhang 2012; Dong and Xue 2012). The key with ensemble-based DA is the use of an ensemble to estimate the forecast error statistics in a flow-dependent manner. Therefore, the observation

information will be properly weighted and spread consistent with the background hurricane forecasts; and perhaps more importantly, the ensemble covariance can realistically infer the flow-dependent cross-variable error statistics and therefore update state variables not directly observed in a dynamically and thermodynamically consistent manner.

One candidate in ensemble-based DA is the hybrid ensemble-variational DA method. It has been proposed (e.g., Hamill and Snyder 2000; Lorenc 2003; Etherton and Bishop 2004; Zupanski 2005; Wang et al. 2007b, 2008a; Wang 2010), implemented and tested with numerical weather prediction (NWP) models recently (e.g., Buehner 2005; Wang et al. 2008b; Liu et al. 2008, 2009; Buehner et al. 2010a,b; Wang 2011; Wang et al. 2011; Whitaker et al. 2011; Kleist et al. 2011). A standard variational method (VAR) typically uses static background error covariance, but a hybrid ensemble-variational DA system incorporates ensemble-dervied flow-dependent covariance into the VAR framework. The ensemble can be generated by an ensemble Kalman filter (EnKF). Recent studies have suggested that hybrid DA systems may represent the "best of both worlds" by combining the best aspects of the variational and EnKF systems (e.g., Buehner 2005; Wang et al. 2007a, 2008a,b, 2009; Zhang et al. 2009b; Buehner et al. 2010ab; Wang 2010). While preliminary tests of the hybrid DA system with real NWP models and data have shown great potential of the method for non-TC forecasts (e.g., Wang et al. 2008b; Buehner et al. 2010ab) and for forecasts of TC tracks (e.g., Wang 2011; Whitaker et al. 2011), and there has been a growing body of literature documenting the success of using the EnKF to assimilate inner core data for TC

initialization at convection-allowing resolutions (e.g., Zhang et al. 2009a, Weng et al. 2011; Zhang et al. 2011; Aksoy et al. 2012; Weng and Zhang 2012; Dong and Xue 2012), to the author's best knowledge, to date there is no published research applying a hybrid DA method to the assimilation of radar data at a convection-allowing resolution for TC predictions. This study serves as a pilot study applying the hybrid ensemble-3DVAR system developed for the WRF model (Wang et al. 2008a) to explore its potential for assimilating radar observations for hurricane forecasts. As a first step of such study, we focus on assimilating radar radial velocity data. Meanwhile, this study also performs detailed diagnostics to understand the fundamental differences between the roles and effects of flow-dependent and static covariances in the TC analysis and forecast.

More specifically, this study applies and explores the WRF ensemble-3DVAR hybrid system to the assimilation of coastal WSR-88D radar radial velocity data for the prediction of Hurricane Ike (2008) (Fig. 1.1). Ike is the second costliest tropical cyclones in the recorded history (1900-2010) over the mainland United States (http://www.nhc.noaa.gov/pdf/nws-nhc-6.pdf). Previous studies (e.g., Zhao and Xue 2009) have shown significant impact of the radar data for this case using ARPS 3DVAR/cloud analysis package.

The remainder of this section is organized as follows: Section 2.2 presents the methodology and section 2.3 discusses the experiment design. The experiment results are discussed in Section 2.4 while the final section summarizes the main conclusions of this study.

2.2 Methodology

a. The hybrid ensemble-3DVAR scheme

A diagram of the hybrid DA system is shown in Fig. 2.1 Similar to Hamill and Snyder

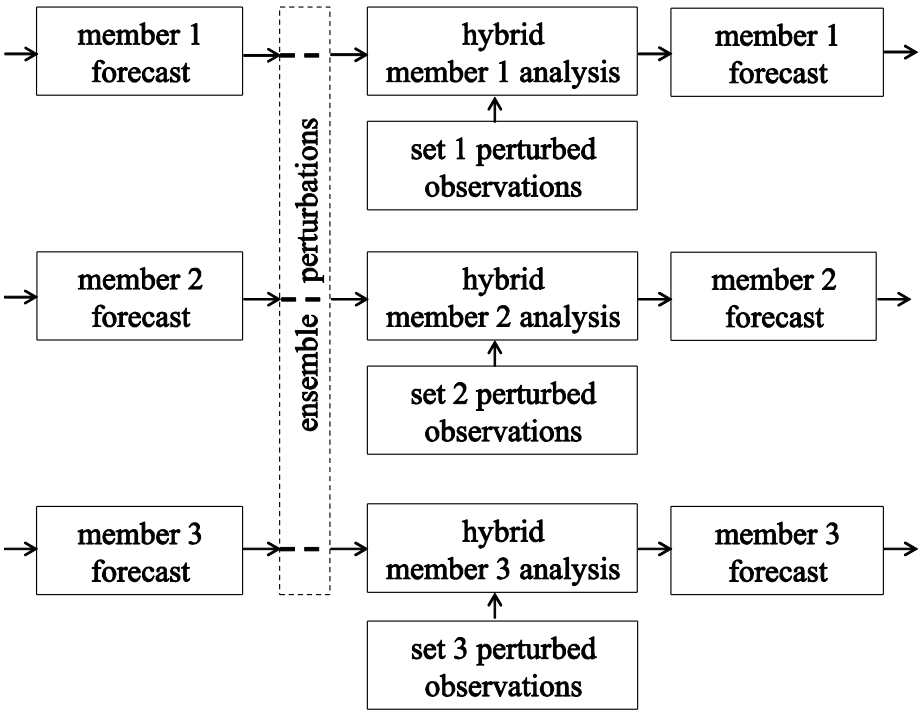

Fig. 2.1 Schematic diagram of the hybrid ensemble-3DVAR forecast-analysis cycle for a hypothetical three-member ensemble. Each member assimilates the observations containing a different set of perturbations.

(2000), the following four steps are repeated for each DA cycle: 1. Perform K (K is the ensemble size) number of ensemble forecasts to generate background forecast fields at the time of analysis; 2. Calculate ensemble forecast perturbations to be used by the hybrid cost function for flow-dependent covariance by subtracting ensemble mean from

each member; 3. Generate K independent sets of perturbed observations by adding random perturbations to the observations; 4. Obtain the analysis increment for each ensemble member through minimization of the hybrid cost function using one set of perturbed observations. Steps 1 through 4 are repeated for each of the follow-on cycles, with the ensemble analyses providing initial conditions for step 1. In step 3, the random perturbations added to the observations are drawn from a Gaussian distribution with a mean of zero and a standard deviation of the observation error. This 'perturbed observation method' was used in Hamill and Snyder (2000), which corresponds to the classic stochastic ensemble Kalman filters (Burgers et al. 1998; Houtekamer and Mitchell 1998; Evensen, 2003). In the original work of Wang et al. (2008a), the ensemble transform Kalman filter (ETKF) was used to update forecast perturbations.

A brief review on the extended control variable method for incorporating ensemble covariance into a WRF 3DVAR framework is given here. For detailed discussions, readers are referred to Wang et al. (2007b, 2008a).

For state vector **x,** the analysis increment of the hybrid scheme, **x'**, is the sum of two terms,

$$\mathbf{x}^{'} = \mathbf{x}_1^{'} + \sum_{k=1}^{K} \left(\mathbf{a}_k \circ \mathbf{x}_k^e \right). \tag{1}$$

The first term $\mathbf{x}_1$**'** in Eq. (1) is the increment associated with WRF 3DVAR static background covariance and the second term is the increment associated with flow-dependent covariance. Here, the vectors $\mathbf{a}_k$, $k = 1, \ldots, K,$ denote extended control

variable (Lorenc 2003) for each ensemble member; and the second term of Eq. (1) represents a local linear combination of ensemble perturbations. The coefficient $\mathbf{a}_k$ for each member varies in space as discussed later, which determines the ensemble covariance localization scale. Specifically, each element of $\mathbf{a}_{k,}$ is a sum of the products of the ensemble perturbations of state variables multiplied by the corresponding traditional control variables, respectively, at the same grid point. $\mathbf{x}_k^e$ is the k^{th} ensemble perturbation state vector. The symbol 'o' denotes the Schur product (element by element product) of the vectors $\mathbf{a}_k$ and $\mathbf{x}_k^e$.

The cost function for WRF hybrid ensemble-3DVAR is

$$J(\mathbf{x}_1^{'}, \mathbf{a}) = \beta_1 J_b + \beta_2 J_e + J_o,$$

$$= \beta_1 \frac{1}{2}(\mathbf{x}_1^{'})^T \mathbf{B}^{-1}(\mathbf{x}_1^{'}) + \beta_2 \frac{1}{2}(\mathbf{a})^T \mathbf{A}^{-1}(\mathbf{a}) + \frac{1}{2}(\mathbf{y}^{o'} - \mathbf{H}\mathbf{x}^{'})^T \mathbf{R}^{-1}(\mathbf{y}^{o'} - \mathbf{H}\mathbf{x}^{'}). \qquad (2)$$

J_b is the traditional WRF 3DVAR background term associated with the static covariance **B** and J_e is the hybrid term associated with flow-dependent covariance. **a** is defined as $\mathbf{a}^{\mathrm{T}} = (\mathbf{a}_1^{\mathrm{T}}, \mathbf{a}_2^{\mathrm{T}}, \cdots, \mathbf{a}_{\mathrm{K}}^{\mathrm{T}})$. J_o is the observation term associated with observation error covariance **R**. The innovation vector $\mathbf{y}^{\mathrm{o}\prime}$ is defined as, $\mathbf{y}^{\mathrm{o}\prime} = \mathbf{y}^{\mathrm{o}} - \mathbf{H}(\mathbf{x}^{\mathrm{b}})$, where $\mathbf{y}^{\mathrm{o}}$ is the observation vector, $\mathbf{x}^{\mathrm{b}}$ is the background forecast state vector, and **H** is the linearized observation operator.

The weights of the static covariance and flow-dependent covariance are determined by factors β_1 and β_2 according to relationship

$$\frac{1}{\beta_1} + \frac{1}{\beta_2} = 1, \qquad (3)$$

which conserves the total variance.

As described in Wang et al. (2008a), the ensemble covariance localization, denoted as **A**, has horizontal and vertical components. In this study, both the horizontal and vertical localization are applied. Specifically, the horizontal localization is modeled by a recursive filter transform as in Wang et al. (2008a). The vertical localization is implemented by transforming the extended control variable **a** in Eq. (2) with empirical orthogonal functions (EOFs). The correlation matrix, denoted as Cov, from which the EOFs is derived, follows

$$\mathrm{Cov}(k_1, k_2) = \exp\left(-\frac{d^2}{L^2}\right), \qquad (4)$$

where d is the distance between model levels k_1 and k_2 and L is the vertical localization radius. Existing EOF codes in the WRF 3DVAR for modeling the vertical static error covariance is used for the vertical ensemble covariance localization purpose.

2.3 Experimental design

a. The WRF model configuration

The Advanced Research WRF (ARW) model version 3 (Skamarock et al. 2008) is used in this study. The model is compressible, three-dimensional, non-hydrostatic, discretized on an Arakawa C grid with terrain-following mass-based sigma coordinate levels. In this study, the WRF model is configured with 401x401 horizontal grid points at 5-km grid spacing (Fig. 1.1), and 41 vertical levels with the model top at 100 hPa.

The WRF single-moment six-class scheme (Hong et al. 2004) is chosen for the explicit microphysics processes. Since the grid resolution may not fully resolve the hurricane convective features, the Grell-Devenyi cumulus parameterization scheme (Grell; Devenyi 2002) is included. Other physics parameterizations schemes used include the Yonsei University (YSU) (Noh et al. 2003) scheme for planetary boundary layer parameterization, the 5-layer thermal diffusion model for land surface processes (Skamarock et al. 2008), the Rapid Radiative Transfer Model (RRTM) longwave (Mlawer et al. 1997), and the MM5 shortwave (Dudhia 1989) radiation parameterization.

b. The radar data processing

The radial velocity data from coastal WSR-88D radars at Houston, Texas (KHGX) and Lake Charles, Louisianan (KLCH) are processed using a modified version of the Four Dimensional Dealiasing Algorithm (James and Houze 2001). The algorithm was originally designed for Doppler radars in European Alps. The modified algorithm by this study is capable of reading level-II WSR-88D data and dealiasing the radial velocities.

To dealias radial velocity data, the following steps are performed: First, a wind profile is created based on model background, rawindsonde, or wind profiler data. The background radial velocity in radar observation space is calculated from the wind profile, assuming the wind is horizontally homogeneous. Second, the WSR-88D radial velocity is compared with the background radial velocity for a gross check. In this step,

aliased radial velocity that needs to be corrected is identified. Third, at each elevation angle, spatial dealiasing is performed. The aliased velocity V_a will be recovered by factored Nyquist velocity V_n,

$$V_d = V_a + 2NV_n \ , \qquad (5)$$

where N is a positive or negative integer whose sign and value are determined by a gate-to-gate shear threshold of $0.4V_n$ (James and Houze 2001). After dealiasing is finished, the radial velocity interpolated to the Cartesian coordinates is thinned to 10 km spacing horizontally and 500 meter vertically.

Figure 2.2 shows the processed radial velocity at 0.5° elevation angle for KHGX (Fig. 2.2a) and KLCH (Fig. 2.2b) at 0000 UTC 13 September 2008. These two radars

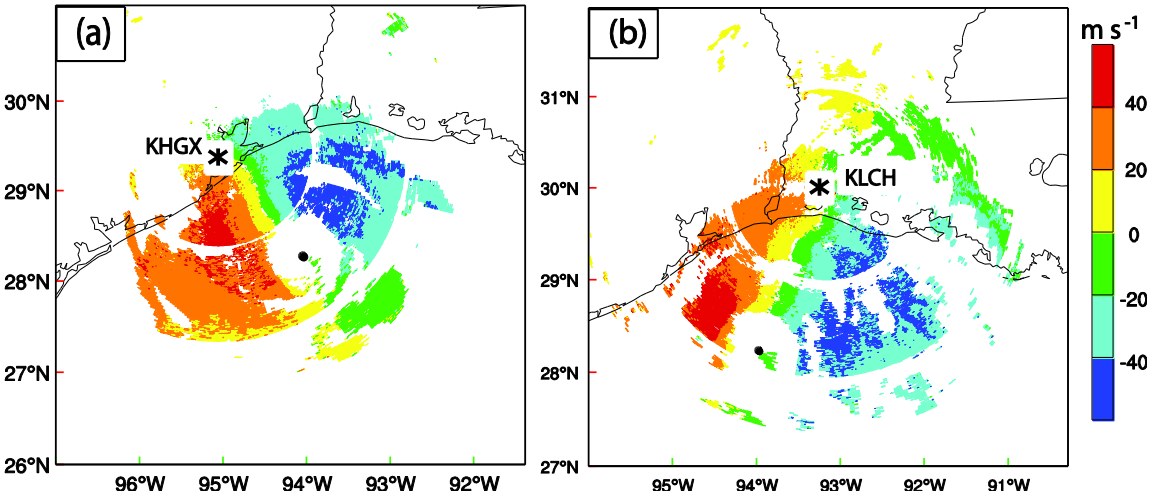

Fig. 2.2 The radial velocity (interval of 20 m s^{-1}) at 0.5° elevation angle from (a) KHGX and (b) KLCH WSR-88D radars at 0000 UTC 13 September 2008. Black dot is for NHC best-track position of Hurricane Ike (2008) at this time. Asterisks are for radar locations.

complement each other by providing scans that are approximately the right angle at the

location of Ike's eye. KHGX covers almost all of Ike's eye and eye wall. The outbound radial velocity on the left side of the eye and inbound radial velocity on the right side of the eye reflect the circulation of the hurricane. KLCH covers only about half of eye and eye wall. The outbound radial velocity on the front side of the eye and inbound radial velocity on the back side of the eye also reflect the circulation of the hurricane.

The observation error standard deviation for the radial velocity is set to 2 m s^{-1} during the DA. This error value is similar to the values used in (Dowell; Wicker 2009), (Xu; Gong 2003), and (Xiao et al. 2009).

c. The data assimilation setup

This paper presents five experiments denoted as NoDA, 3DVARa, 3DVARb, HybridF, and HybridH (Table 2.1). Experiments differ based on what, if any, assimilation system is used for radar data. The experiments are designed to examine the difference of using flow-dependent versus static background covariance when assimilating the radar data and the impact of DA on the subsequent forecast.

The NoDA experiment did not assimilate any radar data, instead the WRF model initial condition at 0300 UTC 13 September 2008 simply comes from the 1ºx1º degree

Table 2.1 List of experiments

Experiment	Description
NoDA	No radar data assimilation. WRF model initial condition interpolated from NCEP 1^{o}x1^{o} analysis
3DVARa	Radar DA using WRF 3DVAR with static covariance from NMC method
3DVARb	Same as 3DVARa, except the horizontal spatial correlation in the static covariance is multiplied by 0.3.
HybridF	Radar DA using hybrid method with full weight given to flow dependent covariance, with $1/\beta_1 = 1/1001$ and $1/\beta_2 = 1/1.001$ in Eq. (1)
HybridH	Hybrid method with equal weight given to static covariance (which is the same as 3DVARb) and flow-dependent covariance, with $1/\beta_1 = 1/2$ and $1/\beta_2 = 1/2$ in Eq. (1)

NCEP (National Centers for Environmental Prediction) operational GFS (Global Forecast System) analysis. The 6-hourly GFS analyses also provide the lateral boundary conditions (LBCs).

The "3DVARb" experiment assimilated the radar data using the traditional 3DVAR

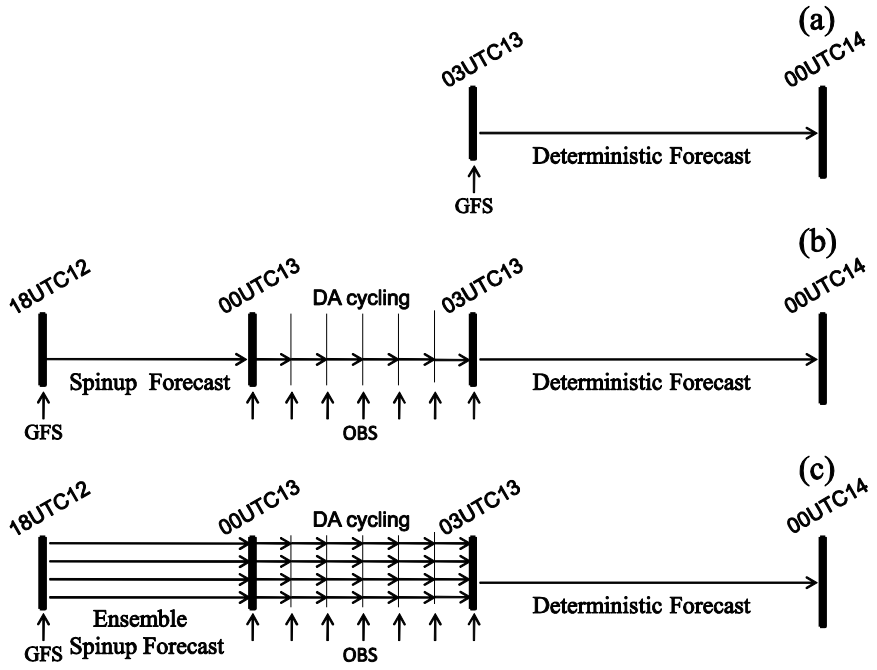

Fig. 2.3 The flow charts for (a) NoDA experiment, (b) 3DVAR experiments (3DVARa and 3DVARb), and (c) hybrid experiments (HybridF and HybridH).

method where the static background covariance is adopted. The static covariance is generated and further tuned as followed. The NMC method (Parrish and Derber 1992) was first employed to generate the static background covariance statistics based on 12-h and 24-h WRF model forecasts, starting at 00 UTC and 12 UTC every day, during the period from 01 to 15 September 2008. The experiment using the static covariance generated by the above procedure without further tuning is denoted as 3DVARa. Because the default correlation length scales derived from the NMC method reflects mostly large-scale error structures, their direct use may not be appropriate for storm-scale radar DA (Liu et al. 2005). The horizontal correlation length scale of the static covariance is reduced by a factor of 0.3 in experiment 3DVARb and this factor is found

to be optimal through experimentations. The 3DVAR experiments contains three stages (Fig. 2.3b): (1) a single 6-h spinup forecast initialized from the GFS analysis at 1800 UTC, September 12, to produce an initial first guess at 0000 UTC, September 13 for radar DA cycles. The spin-up time of 6 hours is based on past experiences and other published studies (e.g., Zhang et al. 2009, spin-up time of 9 hours; Aksoy et al. 2012, spin-up time of 6 hours); (2) assimilation of radial velocity data from KHGX and KLCH radars every 30 minutes for 3 hours; (3) a 21-h deterministic forecast initialized by the analysis at the end of the assimilation cycles in (2). The WRF model boundary conditions for all three stages are also provided by the operational GFS analyses at 6 hourly intervals. Experiment 3DVARb serves as a base line for evaluating the performance of the hybrid method.

Experiments HybridF and HybridH are identical except that the different weighting factors β_1 and β_2 are used in Eq. (2). For HybridF, the full weight is assigned on the flow-dependent ensemble covariance (using $1/\beta_1 = 1/1001$ and $1/\beta_2 = 1/1.001$). For HybridH, the static covariance and the flow-dependent ensemble covariance are equally weighted ($1/\beta_1 = 1/2$ and $1/\beta_2 = 1/2$), i.e., only half of the flow-dependent covariance is used, hence the 'H' in the name. The horizontal correlation scale of static covariance in HybridH is also reduced by a factor of 0.3 as in 3DVARb. Meanwhile, HybridH uses the same flow dependent covariance localization as HybridF, which will be discussed in detail in section 2.4.a.

Each of the hybrid experiments, HybridF and HybridH, has 40 ensemble members. Similar to the 3DVAR experiments, the hybrid experiments have three stages (Fig.

2.3c): (1) 6-h ensemble forecasts to spin up a first guess ensemble and provide flow-dependent covariance at the beginning of the radar DA cycles. The initial and boundary conditions for each member are the GFS analysis plus correlated random perturbations following Torn et al. (2006) and Wang et al. (2008a,b); (2) assimilation of perturbed radial velocity data from KHGX and KLCH radars every 30 minutes for 3 hours by variationally minimizing the hybrid cost function, according to the description given in the previous section (see also Fig. 2.3); (3) a 21-h deterministic forecast initialized from the ensemble mean analysis at the end of the DA cycles in (2). To generate the random perturbations in (1), the random-cv facility in the WRF 3DVAR system is employed (Barker et al. 2004). First, a random control variable vector is created with a normal distribution having a zero mean and unit standard deviation. Then the perturbation control variable vector is transformed to the model space to obtain perturbations to the model state variables including the horizontal wind components, pressure, potential temperature, and mixing ratio of water vapor. The perturbation standard deviations are roughly 1.9 m s^{-1} for the horizontal wind components, 0.6 K for temperature, 0.3 hPa for model pressure perturbation, and 0.9 g kg^{-1} for water vapor mixing ratio and these values are based on the NMC-method-derived background error statistics.

Like other ensemble based data assimilation algorithm, the hybrid ensemble-3DVAR quickly reduces ensemble spread after assimilating observations. To mitigate quick reduction of the spread, the relaxation method of Zhang et al. (2004) for ensemble covariance inflation was adopted. Specifically, the inflated ensemble posterior perturbation $\mathbf{x}'_{new}$ is a weighted average of prior perturbation $\mathbf{x}'_{f}$ and posterior

perturbation $\mathbf{x'}_a$, $\mathbf{x'}_{new} = (1 - b)\,\mathbf{x'}_f + b\,\mathbf{x'}_a$, the relaxation coefficient, denoted as b, is set to 0.5 in this study. This formulation retains part of prior perturbation to mitigate quick spread reduction.

2.4 Results and discussion

The analysis increment of the first DA cycle, the cycling process, the final analysis fields, and the deterministic forecasting results will be presented and discussed in this section. The subsection organization roughly follows the experiment flow charts in Fig. 2.3.

a. Single observation test for vertical localization

Before complete DA experiments are performed, the vertical covariance localization in the hybrid scheme is tested by assimilating a single radial velocity observation.

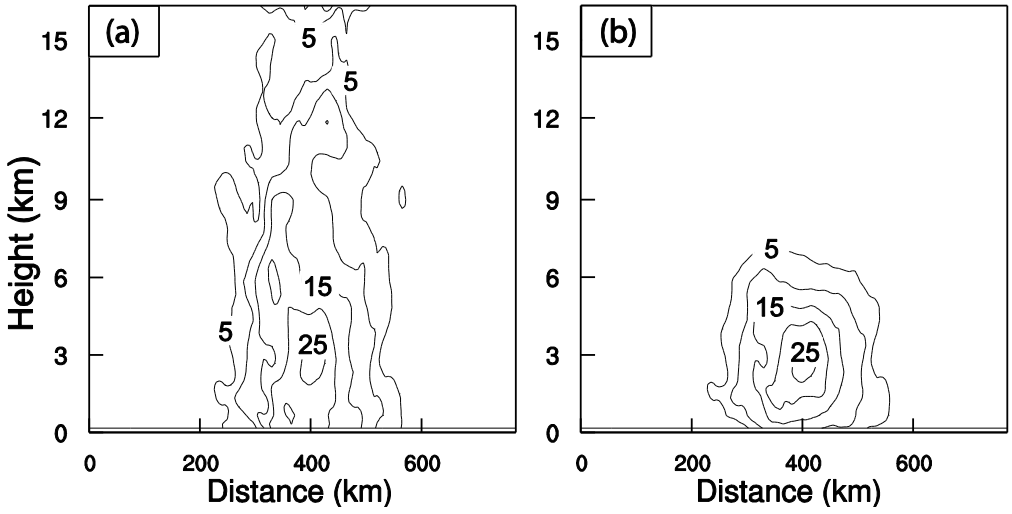

Fig. 2.4 The vertical cross section of the wind speed increment (interval of 5 m s^{-1}) using a single KHGX radar radial velocity data located at (28.4°N, 93.7°W, 3176 m) with an innovation of -38.63 m s^{-1} using the configurations of experiment HybridF but (a) without and (b) with vertical localization at 0000 UTC 13 September 2008.

Figure 2.4 shows the wind speed increment produced by HybridF analyzing a single radial velocity observation located 3176 m above sea level at 0000 UTC 13 September 2008. The innovation (i.e., the observed radial velocity minus forecast ensemble mean valid at 0000 UTC 13 September) for this observation is -38.63 m s^{-1}. Without the vertical localization, nonzero increment reaches the top of the model with relatively noisy increments at the upper levels (Fig. 2.4a). The horizontal and vertical localization radii of 60 and 3 km, respectively, are used in hybrid experiment HybridF (and in HybridH). The localization radii were empirically determined. For example, we tested 20 km, 60km, 200 km, 600 km for horizontal localization and found the 60km showed the most reasonable increment. The vertical localization was also tested. The radar observation over Ike inner core area is about 3 km above the surface. With 3 km vertical localization scale, the influence of radar data could reach the surface. Figure 2.4b shows that with such localizations, the analysis increment is more confined around the observation location. This single observation test shows that our implementation of the vertical localization is taking effect.

b. Wind increments

To see the differences in analyzing the radar data using flow-dependent and static covariances, the analysis increments from the 3DVAR and hybrid experiments after the first analysis time are compared. We first look at the wind increments and will look at indirectly related cross-variable increments in the next subsection.

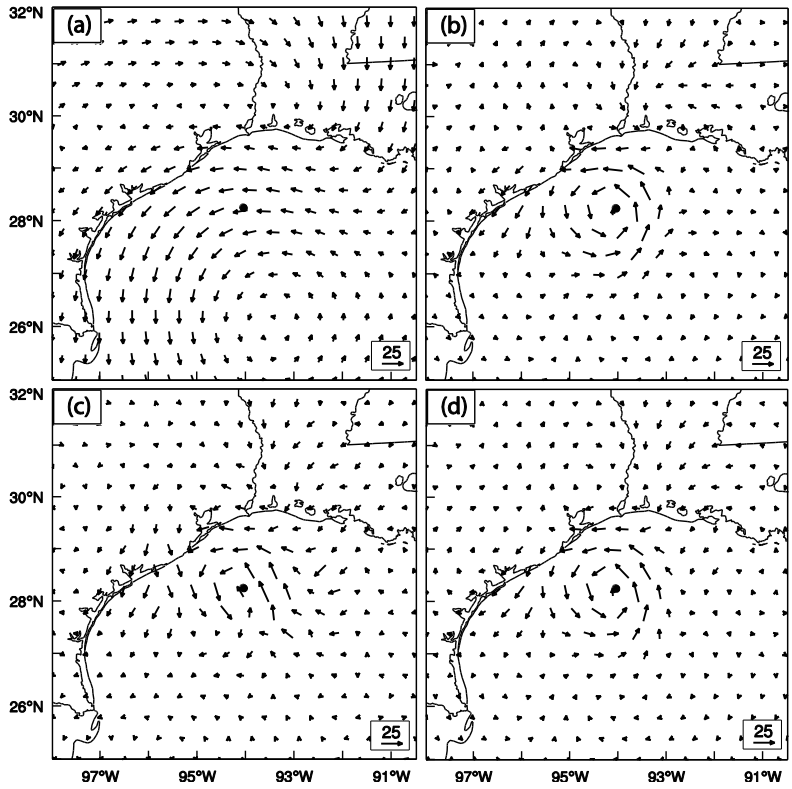

Fig. 2.5 The 700 hPa wind analysis increments (m s^{-1}) for (a) 3DVARa, (b) 3DVARb, (c) HybridF, and (d) HybridH at 0000 UTC 13 September 2008.

Figure 2.5 shows the wind analysis increments at 850 hPa, at 0000 UTC 13 September 2008, the time of first analysis for 3DVARa, 3DVARb, HybridF, and HybridH. The increment in 3DVARa using the default NMC-method-derived static covariance shows cyclonic and anti-cyclonic increment patterns of rather large scales (Fig. 2.5a); the cyclonic increment circulation is centered almost 2 degrees off the observation hurricane center to the southsoutheast, while at the hurricane center location the wind increment is mostly easterly. To the north the increment circulation shows an anti-cyclonic pattern. Such cyclonic and anti-cyclonic increments are also found in a previous studies assimilating radar radial velocity data using WRF 3DVAR (e.g., Xiao

et al. 2007), but are clearly unrealistic, and do not reflect the fact that a strong vortex exists where the background strongly underestimate the strength of the vortex. The default background error covariance derived from the NMC method is unaware of the hurricane vortex and its spatial correlation scales mostly reflect synoptic scale error structures. The net result is the inappropriately large amount of smoothing of the radar data in the data dense region and inappropriately large spreading of the information outside the data coverage region. The radar data, being collected at high spatial resolution, should be analyzed using much smaller spatial correlation scales. This had been pointed out in Liu et al. (2005). The use of smaller correlation scales for radar data is a common practice in the ARPS 3DVAR system (e.g., Hu et al. 2006; Schenkman et al. 2011). Sugimoto et al (2009) also tested the sensitivity of WRF 3DVAR to the correlation length scale and the variance of the background covariance for radar data assimilation.

In 3DVARb, the default horizontal spatial correlation scale is reduced by a factor of 0.3. The resulting wind increment now shows a more or less symmetric cyclonic pattern around the observed center of Ike (Fig. 2.5b). Compared with 3DVARa, the large increments are more limited to the region of vortex in 3DVARb, and the increment is consistent with the inbound and outbound radial velocity couplets associated with the hurricane vortex as observed by KHGX and KLCH radars (Fig. 3). Such results are more realistic.

In HybridF with full weight given to the flow-dependent covariance, the wind increment also shows a cyclonic pattern centered around the eye of Ike (Fig. 2.5c), but

the increment circulation is less axisymmetric, reflecting the contribution of spatially inhomogeneous flow-dependent covariance. When equal weights are placed on the ensemble covariance and static covariance in HybridH, the wind increments show a pattern that is close to that of 3DVARb, but the increment magnitude is between those of the HybridF and 3DVARb (Fig. 2.5d).

c. Temperature increments

Because radar radial velocity is the only data type assimilated in this study, any increment in temperature is the result of balance relationship applied (if any) and/or due to cross-covariance in the background error. Figure 2.6 shows the 850 hPa temperature increments for 3DVARb, HybridF, and HybridH after assimilating radial velocity data for the first cycle. For 3DVARb, negative temperature increments are found in the

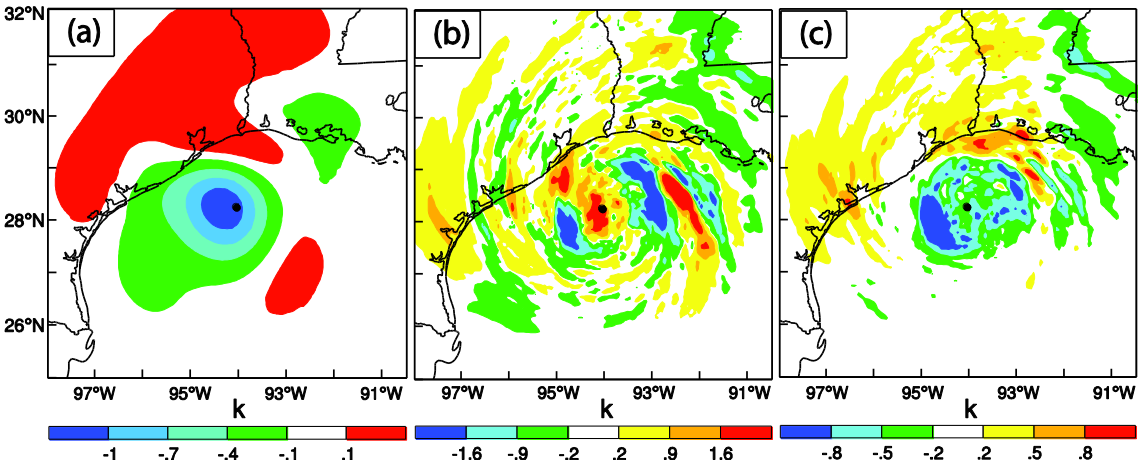

Fig. 2.6 The 850 hPa temperature analysis increments for (a) 3DVARb (at intervals of 0.3 K), (b) HybridF (at intervals of 0.7 K), and (c) HybridH (at intervals of 0.3 K), at 0000 UTC 13 September 2008.

vortex region, and the magnitude is largest near the hurricane enter (Fig. 2.6a). Physically, enhanced hurricane vortex circulation should be accompanied by warming of the vortex core region, to give a warmer core vortex; hence the 3DVAR temperature increment is inconsistent with expected hurricane structures. The negative increment is expected of the 3DVAR, because the increment is obtained through a balance relationship between temperature and wind and this relationship reflects the thermal wind relation. More specifically, the 'balanced temperature' increment T_b at a vertical level k, in WRF 3DVAR is related to the stream function ψ by a regression relation, $T_b(k) = \Sigma_1 G(l,k) \psi(l)$, where G is the regression coefficient and the summation is over the vertical index l. Such a regression relation derived using the NMC-method generally reflects hydrostatic, geostrophic, and thermal wind relations (Barker et al. 2004). A colder core at 850 hPa is consistent with an enhanced cyclonic circulation at the 700 hPa seen in Fig. 2.5. Note that at this distance, the lowest radar beams do not reach below 850 hPa, hence the enhancement of wind is larger above 850 hPa. Therefore the cyclonic wind increment increases with height in the lower atmosphere. We note that negative temperature increment is also seen in the low-level eye region of analyzed hurricanes in previous studies using Airborne Doppler radar data and WRF 3DVAR (e.g., Xiao et al. 2009)

Different from 3DVAR, the temperature increment obtained in HybridF shows positive increments in the eye region (Fig. 2.6b) and spiral patterns in the eye wall and outer rainband regions. In this case, the hurricane in the background forecast at 0000 UTC 13 September 2008 is much weaker than the observation (Fig. 2.7b), which is

accompanied by lower temperatures at the core of the vortex than observed. When radar observations are assimilated, the background TC vortex is strengthened and therefore the core temperature is expected to be increased to be consistent with the warm core structure of TCs. The more realistic increment structures in HybridF are the result of temperature-wind cross covariances derived from the ensemble, which have knowledge of the vortex as a tropical cyclone. In addition, the magnitude of the temperature increments in HybridF is an order of magnitude larger than that of 3DVARb; the temperature increment in the 3DVAR analysis of Xiao et al. (2009) for Hurricane Jeanne (2004) was also weak, reflecting the relative weak thermal wind relationship in 3DVAR.

Same as the wind increment, the temperature increment from HybridH is in-between those of HybridF and 3DVARb (Fig. 2.6c). The magnitude is about half that of HybridF. The structure of the increment resembles that of HybridF more but the eye region has negative instead of positive increments. From this aspect, HybridH is poorer than HybridF.

d. Innovation statistics for Vr and minimum sea level pressure in DA cycles

The behaviors of 3DVARb, HybridH, and HybridF are further compared by examining

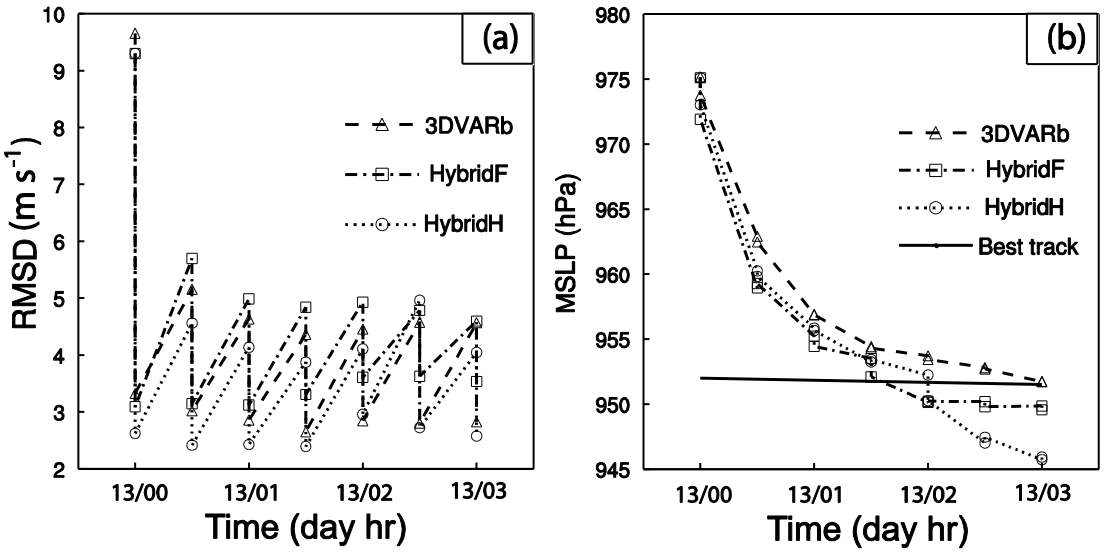

Fig. 2.7 The forecast and analysis (sawtooth pattern during DA cycling) of (a) RMSD of radial velocity (m s^{-1}), and (b) the minimum sea level pressures (hPa) together with the NHC best track estimate, for 3DVARb, HybridF, and HybridH from 0000 to 0300 UTC 13 September 2008.

the fit of their analyses and forecasts to Vr observations during the DA cycles. The fit is defined as the root mean square difference (RMSD) between the model state and observations, after the model state is converted to the observed quantities; and such difference is also called observation innovation. Figure 2.7 shows the RMSDs for Vr and minimum sea level pressure (MSLP) from HybridH, HybridF and 3DVARb. Vr data of both KHGX and KLCH are used in the innovation calculation and for the hybrid, the ensemble mean is used. In all three experiments, the RMSD for Vr is reduced significantly by the analysis within each cycle and the largest reduction occurs in the first analysis cycle at 0000 UTC when the observation innovations are the greatest. In later cycles, the innovations for the analyses remain roughly between 2.5 and 3.5 m s^{-1}, which is reasonable given the 2 m s^{-1} expected observation error. The 30-

minute forecasts following each analysis generally increase the Vr innovation by about 2 m s^{-1}, reaching 4-5 m s^{-1} levels. In general, HybridH produces analyses that fit Vr observations tightest while HybridF the least and 3DVARb is in-between. Similar is true of the 30-minute forecasts. Note that although the analysis increment of HybridH is in general (Fig. 2.5 and Fig. 2.6) in-between HybridF and 3DVARb, the root-mean-square Vr fit to observations in HybridH is not necessarily between HybridF and 3DVARb. The observation innovation statistics can help us to see if the DA system is doing about the right things, but being 'verification' against the same set of observations that is also used in the DA, it cannot really tell us the true quality of the analyses. True measures of the analysis quality require verifications against independent observations or verification of subsequent forecasts, which will be presented later.

Figure 2.7b shows the fit of the analysis and forecast MSLPs to the best track data from the National Hurricane Center. The best track MSLP is more or less constant during this 3 hour period, being at about 952 hPa. At the beginning of DA cycling (0000 UTC 13 September), the MSLP is about 23 hPa higher than the best track estimate. Most of the reductions in MSLP in all cases are actually achieved through adjustment during the forecasting process, with more than 15 hPa reduction achieved during the first analysis cycle between 0000 and 0030 UTC. This is not surprising because wind is the only parameter directly measured, and pressure analysis increments are only achieved through balance relationships and/or cross covariance, which are apparently weak.

We note in general, the MSLP decreases faster in the short forecasts between the

analyses in the hybrid experiments than in 3DVARb. This is consistent with the fact that the hybrid method tends to build a warmer vortex core, and warmer temperature tends to induce a lower surface pressure due to hydrostatic balance. A stronger vortex circulation will also induce lower central pressure due to cyclostrophic balance. During the final 3 cycles, there is clearly over-deepening of the central pressure in HybridH in the short forecasts, resulting in a fall of MSLP that is about 5.5 hPa too low compared to best track. The final analyzed MSLP in HybridF is about 2.0 hPa too low, which should be within the uncertainty range of MSLP best track data. We also note that in this study, since the dense radar data define the TC center location rather well (Fig. 2.2) and are assimilated every 30 minutes, the TC locations in the first guess ensembles do not diverge too much in the 30-minute forecasts throughout the assimilation cycles.

Overall, errors in the maximum surface wind (MSW) and MSLP are greatly reduced after assimilating radar data in all DA experiments. At 0300 UTC 13 September, the end of the DA cycles, the best track MSW and MSLP are 47.5 m s^{-1} and 951 hPa respectively. For 3DVARb, HybridF, and HybridH, after assimilating radar radial wind, the MSW errors are 1, 0.8, and 2.7 m s^{-1} and the MSLP errors are 0.2, 1.9, and 5.6 hPa, respectively. The larger MSW (which is not directly observed) error in HybridH suggests that there is over-fitting of the analyzed wind to Vr observations (Fig. 2.7a). For NoDA experiment without assimilating radar data, the MSW error is 9 m s^{-1} and MSLP error is 29 hPa.

e. The analyzed hurricane structures

We examine next the structure of the hurricane at the end of the DA cycles by

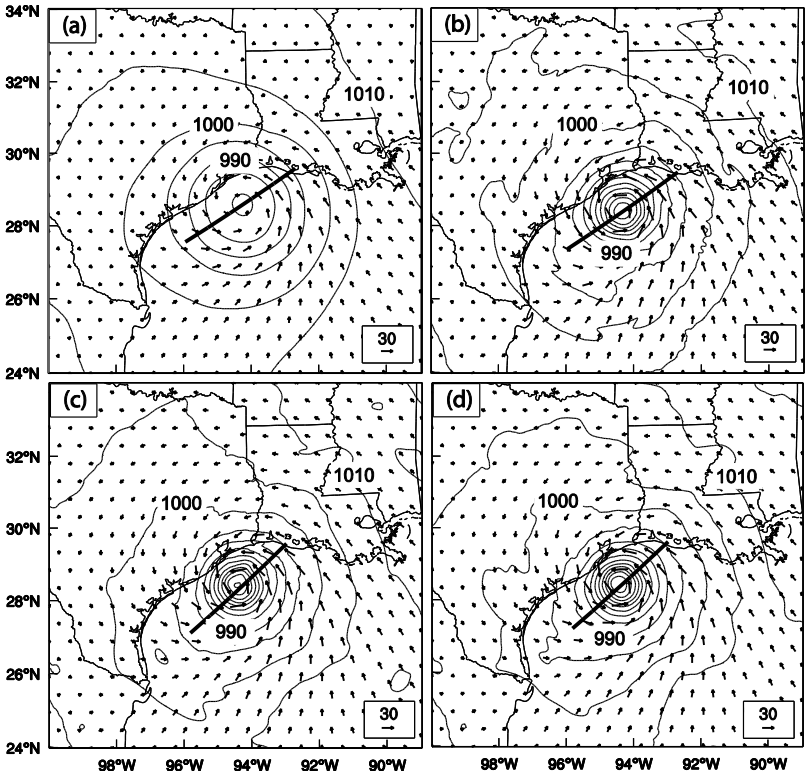

Fig. 2.8 The analyzed sea level pressure (interval of 5 hPa, solid contours) and the surface wind vectors (m s^{-1}) for (a) NoDA, (b) 3DVARb, (c) HybridF, and (d) HybridH at 0300 UTC 13 September 2008. The thick solid line indicates the vertical cross section location in Fig. 2.9 and Fig. 2.10.

plotting fields at the surface and in vertical cross sections through the analyzed hurricane center. Figure 2.8 shows the analyzed mean sea level pressure and surface wind vectors for NoDA, 3DVARb, HybridF and HybridH. Compared with NoDA (Fig. 2.8a), the analyzed vortex circulations are stronger and the minimum sea level pressure is much lower in 3DVARb, HybridF, and HybridH (Fig. 2.8b-d). Such primary

hurricane circulations (Willoughby 1990) are captured well by the assimilation of radar radial velocity data.

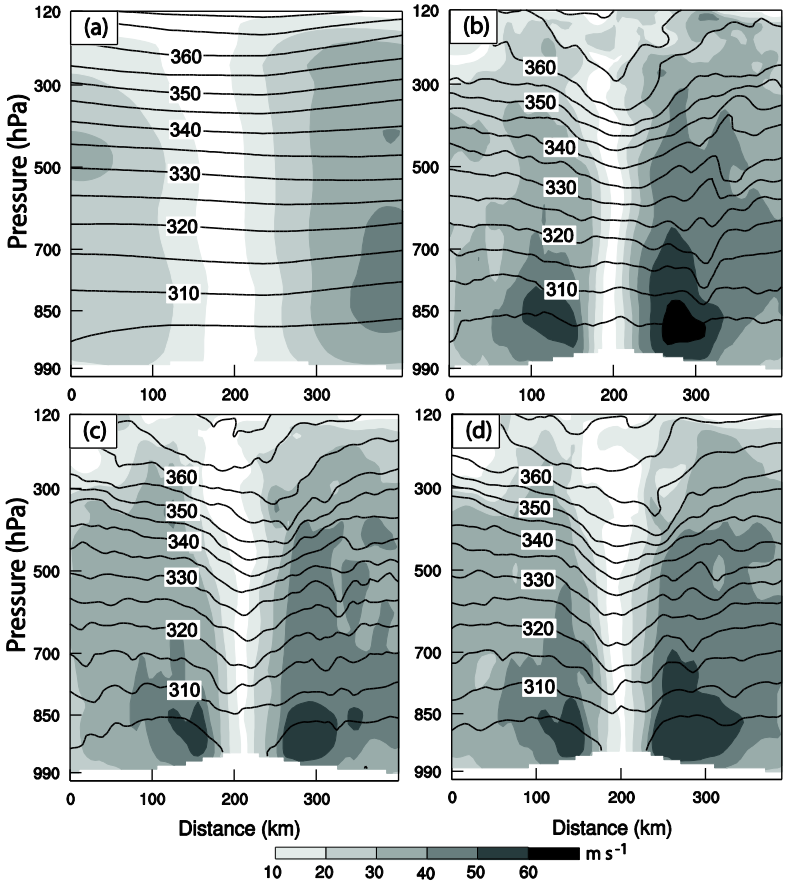

Fig. 2.9 Vertical cross sections of analyzed horizontal wind speed (interval of 10 m s^{-1}, shaded) and potential temperature (interval of 5 K, solid contours) for (a) NoDA, (b) 3DVARb, (c) HybridF, and (d) HybridH, at 0300 UTC 13 September 2008.

Figure 2.9 shows the vertical cross sections of horizontal wind speed and potential temperature for all four experiments. The locations of cross sections are through the analyzed hurricane center and the location of maximum wind speed of each experiment as indicated by the thick lines in Fig. 2.8; the locations of MSLP and maximum wind

for the four experiments are slightly different. In NoDA, the hurricane eye is much wider and the intensity is much weaker than in the three radar DA experiments. Unlike the hybrid experiments, the potential temperature contours of 3DVARb (Fig. 2.9b) do not bend downward below ~600 hPa. The downward extruion of potential temperature contours in

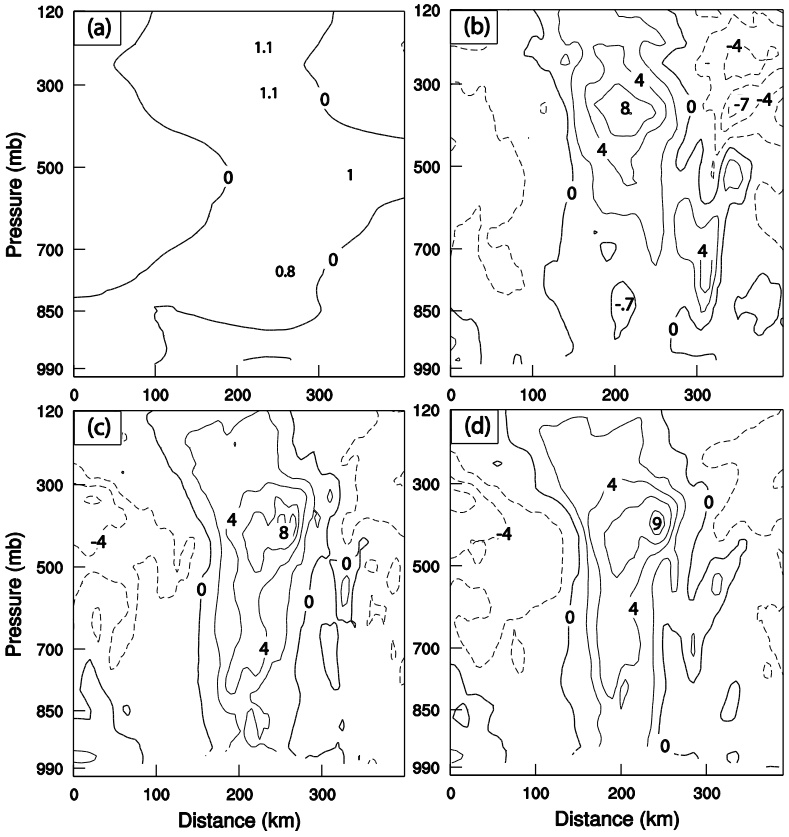

Fig. 2.10 Vertical cross sections of analyzed temperature anomalies (interval of 2 K) for (a) NoDA, (b) 3DVARb, (c) HybridF, and (d) HybridH, at 0300 UTC 13 September 2008.

HybridF and HybridH indicates a warm core structure (Fig. 2.9c, d). In experiment 3DVARb (Fig. 2.9b), the maximum wind speed at ~850 hPa on the right side of eye

wall is about 10 m s^{-1} larger than those in HybridF and HybridH (Fig. 2.9c, d), but this larger wind speed is not accompanied by a warmer core expected of a stronger TC; this is an indication that the 3DVAR analysis is not dynamically and thermodynamically balanced.

Given the inner eye pressure deficit, the warm core should extend through the depth of the troposphere based on the hydrostatic approximation (Haurwitz 1935). The warm core structure is seen clearly in the vertical cross sections of horizontal temperature anomaly, which is the deviation from the mean at the pressure levels (Fig. 2.10). The temperature anomaly in NoDA is very small (less than 2 K, Fig. 2.10a) while that in 3DVARb, HybridF and HybridH exceeds 8 K, with the maximum anomaly found between 300 and 500 hPa levels (Fig. 2.10b-d). This result is consistent with observational studies; the strength of hurricane warm core has been shown to negatively correlate with MSLP (Halverson et al. 2006; Hawkins and Imbembo 1976).

The near-zero or negative temperature anomaly below 700 hPa is clear in Fig. 2.10b for 3DVARb. This is related to the negative 3DVARb temperature increment discussed earlier. It is worth noting that the 3DVARb analysis does produce a reasonable warm core aloft. In HybridF and HybridH, the positive anomaly extends to the surface (Fig. 2.10c and 2.10d). In the latter two, the maximum anomaly is found to be at the inner edge of hurricane eye wall at about 400 hPa, which should be associated with the eye wall warming (LaSeur and Hawkins 1963; Holland 1997).

f. The track and intensity forecasts

To further evaluate the quality of analyses produced by different DA methods, deterministic forecasts initialized from the (ensemble mean in the hybrid cases) analyses at 0300 UTC 13 September, the end of the DA cycles, are launched. The track

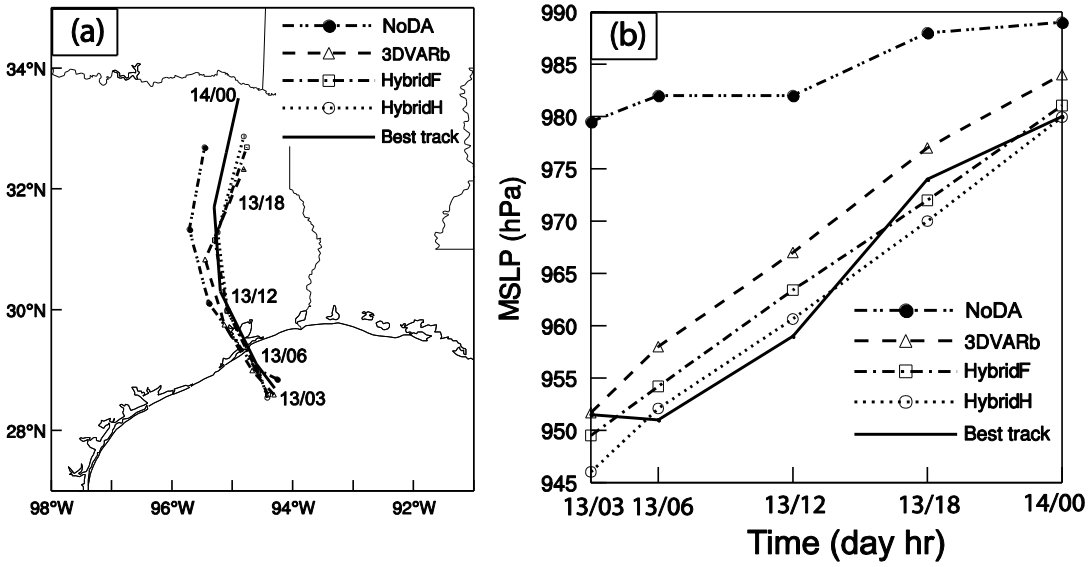

Fig. 2.11 Deterministic forecast hurricane (a) tracks and (b) minimum sea level pressure (hPa) by NoDA, 3DVARb, HybridF, and HybridH as compared to NHC best track estimates from 0300 UTC 13 through 0000 UTC 14 September 2008.

forecasts are compared in Figure 2.11a. The center of hurricane is defined as the location of MSLP. The initial track errors at 0300 UTC are less than 20 km for all four experiments. By 0000 UTC 14 September, the track errors are 98, 117, 84, 64 km for NoDA, 3DVARb, HybridF and HybridH respectively. The mean track errors based on the hurricane positions at 6-h interval during the period from 0300 UTC 13 to 0000 UTC 14 September are 41, 57, 41, and 34 km for NoDA, 3DVARb, HybridF, and HybridH respectively. Given that our DA experiments do not include environmental

observations, the main effect on the track should come from the changes to the structure and intensity of the analyzed hurricane.

Figure 2.11b shows the intensity forecasts in terms of MSLP, together with the best track MSLP. At 0300 UTC 13 September, the MSLP errors are 28, 0.2, 2.0, and 5.5 hPa for NoDA, 3DVARb, HybridF and HybridH respectively. NoDA has the largest MSLP error throughout the forecast. The MSLP error in 3DVARb is smaller at the initial time, but becomes larger than those of HybridF and HybridH at the later forecast times. Overall, the forecast MSLP in the two hybrid experiments is closer to the best track MSLP than that of 3DVARb. None of the forecasts capture the slight deepening during the first 3 hours of forecast.

g. Verification of forecasts against Vr observations

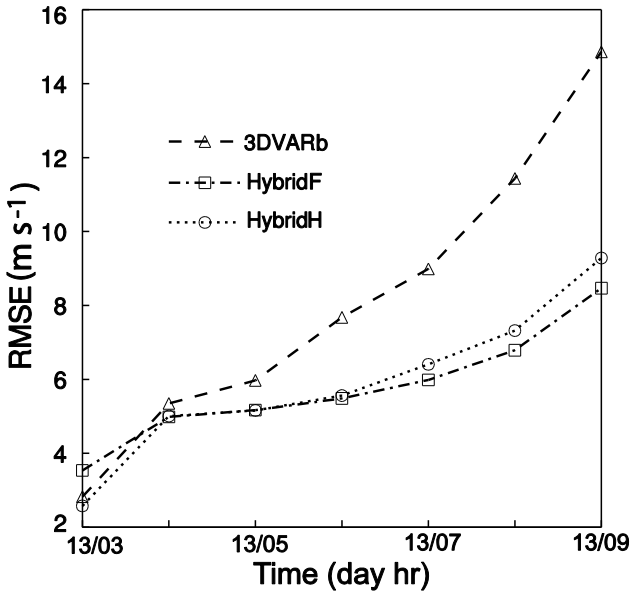

Fig. 2.12 Deterministic forecast RMSEs of Vr (m s^{-1}) by 3DVARb, HybridF, and HybridH from 0300 to 0900 UTC 13 September 2008.

The wind forecasts are further verified against observed radar radial velocity data. Figure 2.12 shows the root mean squared errors (RMSEs, strictly it is RMSD because observations also contain error) of forecast against observed Vr for 3DVARb, HybridF and HybridH. Compared to the best track estimation of wind speed, the radar Vr observations are more reliable. At the initial time of 0300 UTC, the RMSE of 3.5 m s^{-1} from HybridF is slightly larger than those from HybridH (2.6 m s^{-1}) and 3DVARb (2.8 m s^{-1}). After the first hour, the HybridF wind forecast fits the observed radial wind best, especially after 6 hours of forecast where the error in 3DVARb grows much faster and reaching 14.8 m s^{-1} compared to the 8-9 m s^{-1} in the hybrid cases. The much faster error growth in 3DVARb, even though its fit to Vr observations at the start of free forecast is comparable to that of HybridH and better than HybridF, again suggests that other model fields in the 3DVARb analysis are dynamically less consistent with the wind field than in the hybrid cases. As shown in Fig. 2.6, major differences exist between the 3DVAR and hybrid methods with the cross variable updating. This is further confirmed with the performance of HybridH in Fig. 2.12. Even though the HybridH analysis is even more over-fitting to observations than the 3DVAR (Fig. 2.7a), the forecast of HybridH was better than the 3DVAR due to the use of ensemble covariance. Interestingly, this over-fitting to conventional temperature and wind observations in 3DVAR analysis and worse fitting to observations in the forecast, compared with Hybrid where the forecast ensemble perturbations were used to estimate background error covariance, is also seen in other studies with quite different application (Fig. 2 of Wang et al. 2008b). The slight better forecast in HybridF than in HybridH at 6 hours suggests the fully flow-dependent

covariance during the assimilation cycles is beneficial.

h. Evaluation of rainfall forecasts

Rainfall forecasts are evaluated by calculating equitable threat scores (ETSs) of 3-h

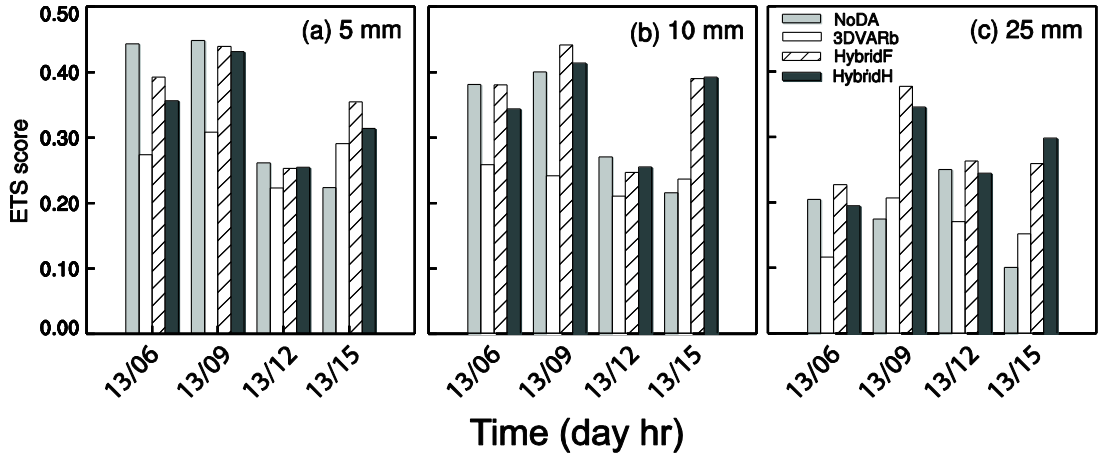

Fig. 2.13 The equitable threat scores for 3 h accumulated forecast precipitation by NoDA, 3DVARb, HybridF, and HybridH at thresholds (a) 5 mm, (b) 10 mm, and (c) 25 mm, verified against NCEP Stage-IV precipitation analyses valid at 0600, 0900, 1200, and 1500 UTC 13 September 2008.

accumulated precipitation against NCEP Stage IV precipitation analyses (Fig. 2.13). For the thresholds of 5, 10, and 25 mm/3 hr and all forecast lead times, the hybrid experiments have higher ETSs than 3DVARb. Furthermore, the improvement of the hybrid over 3DVARb increases with precipitation threshold, indicating again the superior quality of the hybrid DA method. In addition, HybridF has slightly higher ETS scores than HybridH for most times and thresholds. The ETS of the hybrid experiments is higher than the NoDA for larger threshold and longer forecast lead times. By further

looking at the precipitation patterns, it is found that the precipitation forecasts of HybridF more closely match the observed convective spiral band patterns in the inner core region while 3DVARb produces too much precipitation in the southeast quadrant in the outer band region (the region is within the reflectivity coverage of coastal radars, from which the Stage IV precipitation is estimated, c.f. Fig. 1.1) and the radius of the

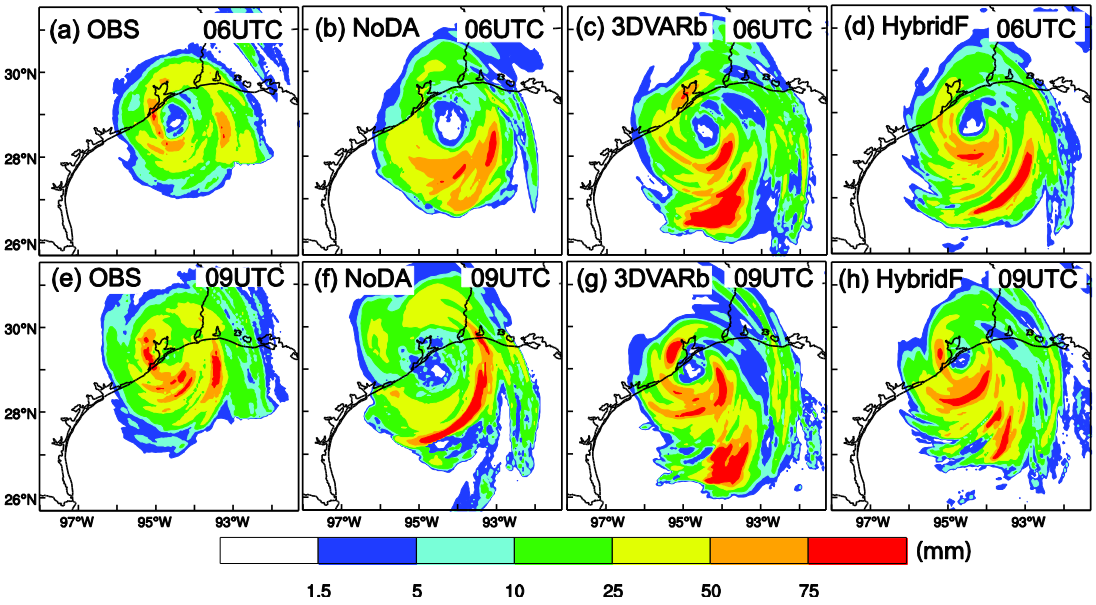

Fig. 2.14 Three-hour accumulated precipitation (mm) by (1st column) NCEP Stage-IV precipitation analyses, (2nd column) NoDA, (3rd column) 3DVARb, and (4th column) HybridF valid at (top) 0600 and (bottom) 0900 UTC 13 September 2008.

inner core eye wall appears larger than observed (Fig. 2.14). In comparison, the precipitation pattern from NoDA case is poorer than the DA experiments especially for inner rain bands. We do note that during the earlier hours and for lower threholds, the ETSs of NoDA are compariable to those of hybrid schemes and higher than those of 3DVARb. The exact cause is difficult to acertain. Imblances and adjustments in the

3DVAR analyses with short analysis-forecast cycles might have been a cause for the poorer performance but this is only a hypothesis.

2.5 Summary and conclusions

In this study, the WRF hybrid ensemble-3DVAR data assimilation (DA) system is applied for the first time to the assimilation of radial velocity data for a landfalling hurricane. More specifically, radial velocity data from two operational WSR-88D radars along the Gulf of Mexico coast are assimilated over a three-hour period after Hurricane Ike (2008) moved into the coverage of the two radars, using an enhanced version of the WRF hybrid DA system. Instead of using an ensemble transformation Kalman filter as in an earlier study to generate the analysis ensemble, we employ in this study the 'perturbed observation' method. Further, we applied vertical localization based on empirical orthogonal functions while continuing to use recursive filters for horizontal localization for the flow-dependent ensemble-estimated background error covariance. The flow-dependent ensemble covariance is incorporated into the 3D variational framework by using the extended control variable method.

The radial velocity data are assimilated every 30 minutes over a 3 hour period. Results mainly from five experiments are presented. A forecast experiment without assimilating any radar data is first carried out to serve as a baseline against which the radar-assimilating experiments are compared; this forecast experiment (NoDA) started directly from the operational GFS analysis, which contained too weak a hurricane vortex. The four radar DA experiments used the WRF 3DVAR using the static

covariance derived from the NMC method (3DVARa), the WRF 3DVAR using further tuned static covariance (3DVARb), the hybrid DA system with purely flow-dependent background covariance (HybridF), as well as half static and half flow-dependent covariance (HybridH), respectively. In the tuned 3DVAR experiment (3DVARb) as well as HybridH, the horizontal spatial correlation scale in the static covariance derived from the NMC-method is reduced by a factor of 0.3 to produce much more realistic wind increments than the default scale (in 3DVARa). The results of analyses and forecasts from the five experiments are inter-compared and verified against best track data, radar wind measurements, and precipitation data. The main conclusions are summarized in the following.

(1) HybridF produces the most realistic temperature increments with positive values at the hurricane center, corresponding to the warm core structure, while 3DVARb produces much weaker and smoother temperature increments that are negative at the center of hurricane. At the end of assimilation cycles, negative temperature anomalies are found at lower levels in the eye region of 3DVARb analysis while the hybrid analyses show deep warm core structures.

(2) All three DA experiments are able to create analyses that fit the Vr data well, and the error reduction by analysis is the largest in the first analysis cycle. Most of the minimum sea level pressure (MSLP) reduction is achieved through model adjustment during the forecast step of the assimilation cycles.

(3) The hybrid experiments improve the Ike track forecast slightly, over the track forecast by NoDA starting from the GFS analysis. 3DVARb slightly degrades the track

forecast. All radar DA experiments produce MSLP forecasts closer to the best track observation than NoDA does.

(4) The fit of forecast radial velocity to radar observations of 3DVARb is much worse than those of HybridF and HybridH. The forecast results indicate that the overall quality of hybrid analyses is better than that of 3DVARb, producing more dynamically consistent state estimations that lead to later slower error growth during forecast. The forecast error of HybridF is slightly lower than that of HybridH starting from hour three.

(5) The equitable threat scores (ETSs) for 3-hour accumulated precipitation forecasts in the hybrid experiments are higher than those of 3DVARb for the thresholds and lead times considered, and the improvement increases with precipitation threshold, indicating again the superior quality of the hybrid DA method. Among the hybrid experiments, HybridF produced slightly better ETSs than HybridH at most verification times.

(6) The results of this study also show positive impacts of assimilating radar data for hurricane initialization, and the hybrid-method-analyzed hurricane has kinematic and thermodynamic structures that are consistent with tropical cyclone conceptual models.

Finally a point worth noting: the inclusion of static background covariance in HybridH in general did not improve the results over HybridF in this case study; i.e., the use of flow-dependent covariance in full in general gives better results. Earlier studies (Hamill and Snyder 2000; Wang et al. 2007a) suggested that the optimal combination of the static and flow-dependent covariance depends on their relative quality. The results

in this case study suggest that for hurricanes and radar data, there is likely little benefit of including static covariance because if the static covariance is not capable of appropriately reflecting the mesoscale and convective-scale nature of hurricanes.

We also note that this study represents the first attempt of applying a variational-ensemble hybrid data assimilation method to hurricane and radar data assimilation. While the results are positive and encouraging, more robust conclusions will need to be drawn by testing the method on many more cases.

Chapter 3

Assimilation of airborne radar radial velocity data using the unified GSI-based hybrid EnKF-3DVAR system for the prediction of Hurricane Irene (2011)

3.1 Introduction

In the previous studies, the vortex bogussing techniques have been used to improve the TC initialization (Kurihara et al. 1995; Liu et al. 2000; Zou and Xiao 2000). Such techniques usually create a bogus TC vortex that is inserted in the model initial conditions. The bogus vortex may be generated from analytical equation with input of observed TC intensity and size or extracted from model forecast TC structure that has the similar intensity to the observed one. Although bogussing techniques have been shown to improve the hurricane forecast, how to maintain the dynamical and thermodynamical balances among state variables representing the hurricane remains probably the biggest challenge with these algorithms.

A series of studies has explored the use of ensemble-based DA methods to initialize hurricane forecasts and made great progress (Li and Liu 2009; Torn and Hakim 2009; Zhang et al. 2009; Hamill et al. 2011; Li et al. 2011; Wang et al. 2011; Weng et al. 2011; Zhang et al. 2011; Aksoy et al. 2012; Li et al. 2012; Weng and Zhang 2012; Dong and Xue 2013; Wang and Lei 2014). The important aspect with ensemble-based DA is the use of an ensemble to estimate the forecast error statistics using flow-dependent error. With flow dependent covariance, the observation will be properly spread over surrounding area. Meanwhile, the state variable that is not observed can be

updated through the flow-dependent cross-variable error statistics in dynamically and thermodynamically consistence.

A currently advanced ensemble-based DA method is the hybrid ensemble-variational DA method. It has been widely investigated during last decade (Hamill and Snyder 2000; Lorenc 2003; Etherton and Bishop 2004; Buehner 2005; Zupanski 2005; Wang et al. 2007ab, 2008ab, 2009; Wang 2010, 2011; Buehner et al. 2010ab, Wang et al. 2013; Wang and Lei 2014;). While a standard variational method (VAR) typically uses static background error covariance, a hybrid ensemble variational DA system incorporates ensemble-derived flow-dependent covariance into the VAR framework. The ensemble can be generated by an ensemble Kalman filter (EnKF). Recent studies have suggested that hybrid DA systems may combine the best aspects of the variational and EnKF systems (Wang et al. 2007b; 2008ab; 2009; Wang 2010; Buehner et al. 2010b, a; Wang et. al 2013). While preliminary tests of the hybrid DA system with NWP models and real time data have shown great potential for TC forecasts, further studies on operational hybrid DA system applying to TC forecast are practically urgent.

Traditionally, global statistical interpolation (GSI) system, operationally adopted by NCEP, uses a static background error covariance matrix. In this study, the flow-dependent ensemble covariance estimated from the ensemble Kalman filter (EnKF) is incorporated into GSI cost function using the extended control variable method (Wang 2010; Wang et. al 2013). Here the EnKF is a serial implementation of the square root ensemble Kalman filter (EnSRF) system, by which the analysis ensemble is generated by updating each forecast ensemble member. Both EnKF and GSI are interfaced with

each other (i.e., the EnKF is using the same observation operator from GSI), and interfaced with HWRF model.

A previous study using a hybrid ensemble-variational data assimilation system for assimilating coastal ground-based radar has shown promising results (Li et al. 2012). The ground-based radars cover the hurricanes only when they are near coast. Usually hurricanes spend most of life time over sea where observations are rare or not available at all. Therefore, National Oceanic and Atmospheric Administration (NOAA) Hurricane Research Division (HRD) sent out aircraft equipped with airborne radar, Stepped Frequency Microwave Radiometer (SFMR), and other in-flight instruments to obtain hurricane inner core observations. Although assimilation of these observations has been carried out (Aksoy et al. 2012; Du et al. 2012; Weng and Zhang 2012), further research to use more advanced DA system is still necessary. In this study, we focus on assimilating airborne radar radial velocity data. Meanwhile, this study also performs detailed diagnostics to understand the fundamental differences between the roles and effects of flow-dependent and static covariances in the TC analysis and forecast. More specifically, this study applies and explores the GSI based ensemble–3DVAR hybrid system to the assimilation of NOAA P-3 airborne Doppler radar radial velocity data for the prediction of Hurricane Irene (2011) (Fig. 1). Irene (2011) is currently ranked as the seventh costliest hurricane in the United States history (en.wikipedia.org/wiki/Hurricane_Irene).

The remainder of this section is organized as follows: section 3.2 presents the methodology and section 3.3 discusses the experiment design. The experiment results

are discussed in section 3.4, while the final section summarizes the main conclusions of this study.

3.2 Methodology

a. The hybrid ensemble-3DVAR scheme

A diagram of the hybrid DA system is shown in Fig. 3.1 The following four steps

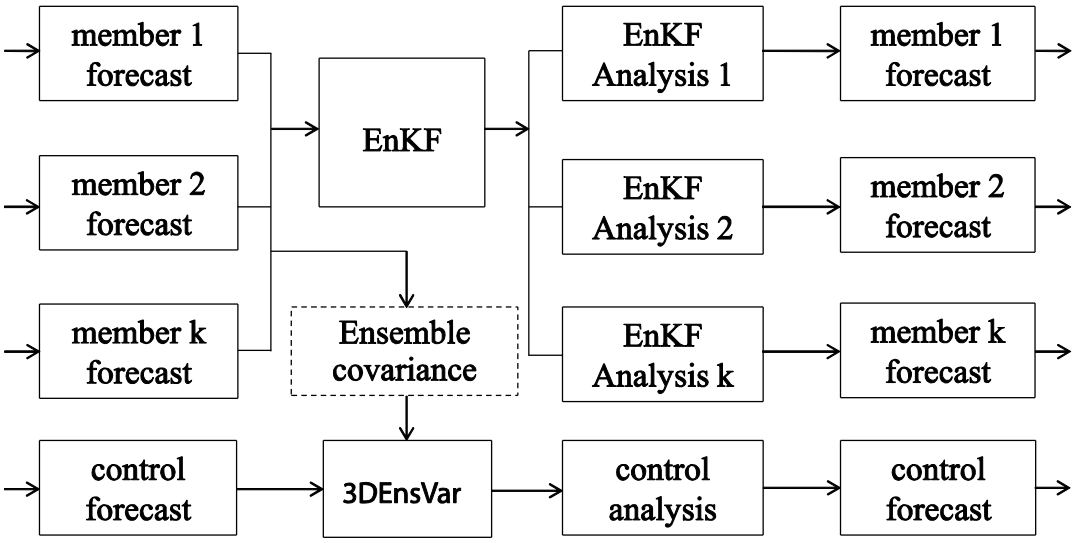

Fig. 3.1 Schematic diagram of the GSI-based EnKF-variational one way coupled hybrid data assimilation system.

Are repeated during each DA cycle: 1) Perform K (K is the ensemble size) number of ensemble forecasts to generate background forecast fields at the time of analysis. 2) Meanwhile, perform a control forecast for hybrid 3DVAR analysis background. 3) The

hybrid 3DVAR system reads ensemble forecast fields and calculates ensemble perturbations to be used by the hybrid cost function for flow-dependent covariance. Perform hybrid 3DVAR analysis with the observations. 4) The ensemble members are updated by EnKF with the same observations in step 3. Step 1 through step 4 are repeated for each of the follow-on cycles, with the hybrid 3DVAR analysis in step 3 and EnKF analysis in step 4 providing initial conditions for step 2 and step 1 respectively.

Similar to WRFDA hybrid, extended control variable method is also used for incorporating ensemble covariance into GSI system. Yet, recursive filter is used for both vertical and horizontal localization. For detailed discussions, readers are referred to Wang (2010).

The ensemble for the hybrid ensemble-3DVAR system is updated by using an EnKF. The square root filter algorithm (Whitaker and Hamill 2002) was adopted in this study. This EnKF code has been efficiently parallelized following Anderson and Collins (2007). In this algorithm, both the model state variables and the observation priors (the predicted observation variable ensemble members) are updated so as to avoid re-computing the forward operator after each observation is assimilated. The EnKF is interfaced with HWRF model by inputting HWRF forecast data and outputting HWRF initial condition data. Meanwhile, the EnKF is interfaced with GSI 3DVAR system by using GSI's observation operators, pre-processing and quality control of assimilated data. Covariance localization is used to limit the impact of the observation being assimilated. Cut-off distances of 450 km in the horizontal direction and 1.0 scale height in the vertical direction are used for the localization. Temporal localization using a 10^3-hour cut-off distance is also implemented. Usually, the ensemble based data

assimilation algorithm will quickly reduce ensemble spread after assimilating observations. To mitigate quick reduction of the spread, the multiplicative inflation method is applied. The posterior ensemble perturbations are inflated by a factor proportional to the amount of the reduction of the ensemble covariance due to the assimilation of observations. .

3.3 Experimental design

a. The HWRF model configuration

The Hurricane Weather Research and Forecasting system (HWRF) model is used in this study. (Documentation about this model is available online:

http://www.dtcenter.org/HurrWRF/users/docs/users_guide/HWRF_v3.5a_Users_Guide.pdf

http://www.dtcenter.org/HurrWRF/users/docs/scientific_documents/HWRFv3.5a_ScientificDoc.pdf)

The model is a nonhydrostatic primitive equation model using rotated-E grid dynamic core. In this study the HWRF is configured with 224X448 horizontal grid points at 9-km grid spacing with time step of 20 minutes, and 61 vertical levels with the model top at 2 hPa. This configuration except grid points is also used by EMC so that EMC and our forecasts can be compared straightforwardly. The microphysics scheme is based on the Eta Grid-scale Cloud and Precipitation scheme (Ferrier 2005). Since the grid resolution may not fully resolve the hurricane convective features, the Simplified Arakawa-Schubert scheme (SASS) cumulus parameterization (Han and Pan 2011) is included. Other physics parameterizations schemes include non-local planetary boundary layer parameterization (Troen and Mahrt 1986), surface layer

parameterization (Sirutis and Miyakoda 1990) and Land/water surface parameterization scheme (Tuleya 1994), HWRF short wave (Lacis and Hanson 1974) and long wave (Fels and Schwarzkopf 1975; Schwartzkopf and Fels 1991) radiation parameterization schemes.

b. The airborne radar data processing

The radial velocity data retrieved from the tail Doppler radar aboard NOAA P-3 aircraft are assimilated in this study. The airborne radar observations are collected and processed for data quality control during flight missions. The data quality control includes several passes such as removing the observations that represent a reflection off sea surface, subtracting the projection of aircraft motion on the radials, and radar Nyquist velocity de-aliasing (HRD; Gamache 2005). Then the data, encoded in Binary Universal Form for the Representation (BUFR) format, are sent off the aircraft to Environmental Modeling Center (EMC) operational use, shared by this study. The flight mission for this study was performed by NOAA N42RF aircraft on 25 August 2011. The aircraft took off at 1949 UTC from MacDill Air Force Base and made five legs of the observations (2048-2157, 2157-2308, 2308-2416, 2416-2531, 2531-2627 UTC). Fig. 3.2 shows the five legs and Hurricane Irene (2011) track.

The NOAA P-3 tail Doppler radar is a vertical scanning. The scanning procedure of each cycle consists of two sweeps for collecting data: one pointing about ~25^{o} forward from a plane normal to the flight track and the other pointing about ~25^{o} afterward. The antennas switch forward and afterward alternatively when the radial beam reaches the highest elevation angle. The radial beams of each sweep form a cone surface. Such a

technique is called as fore/aft scanning technique (FAST). As the aircraft moves on roughly straight track, FAST scans sweep out a three dimensional region of space surrounding the aircraft's track. The space between two adjacent forward or afterward sweeps along the flight track is about 1.4 km.

The spacing of radial velocity encoded in BUFR is about 1.2 km along a radial beam. Such a radar data spatial resolution is much higher than model resolution, which causes that the model resolution is not able to fully resolve the data. Meanwhile, a large amount of original data may be potentially correlated. Therefore thinning is conducted to reduce the high density of radial velocity observations. The data are organized as one sweep scan followed by another. Thinning is performed by three steps: 1) We separate forward and afterward scans at a radial with highest earth-relative elevation angle (e.g., a radial with elevation angle 88^o that is greater than those of two radials immediately before and after this radial). 2) Then the three dimensional model space is divided into many adjacent cubic boxes. 3) For one cubic box, we keep two radial velocities from forward and afterward scans respectively that represent wind components from different directions (i.e., about 50^o apart from each other). These two radial velocities are chosen as close as possible to the center of the cubic box.

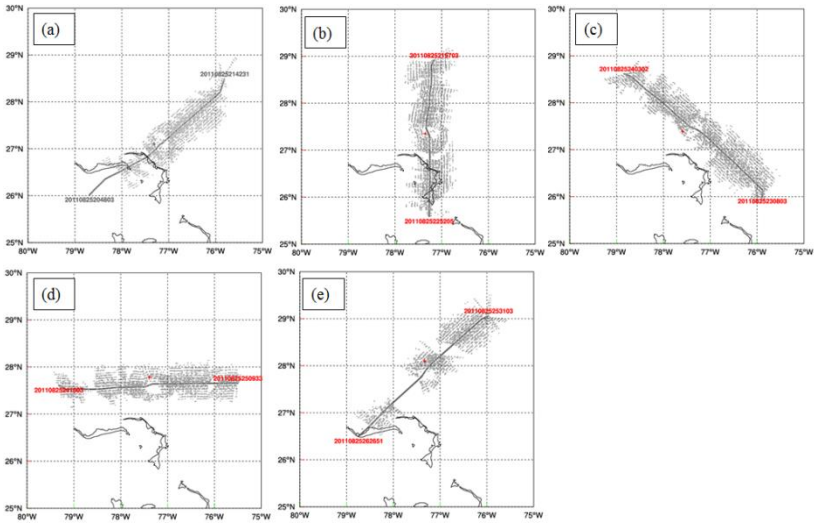

Fig. 3.2 Horizontal distribution of the airborne Doppler radar radial velocity observations.

Fig. 3.2 shows TDR data horizontal distributions of the airborne Doppler radar radial velocity observations aggregated from all levels for the five legs. We can see the width of the swath of TDR data is up to 1 latitude/longitude degree. The hurricane eye whose center is indicated by red dot has sparse or void data. Nevertheless we may expect TDR data assimilation mainly improve the hurricane inner core fields.

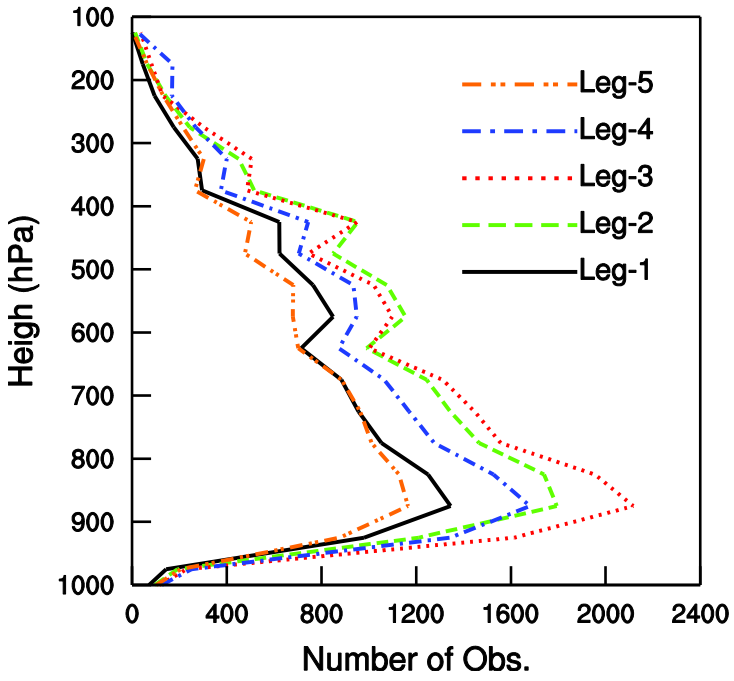

Fig. 3.3 Vertical distribution of the airborne Doppler radar radial velocity observations.

Fig. 3.3 shows vertical distributions of TDR radial velocity data at five legs used by data assimilation. The greatest observation density is generally around 880 hPa for all five legs where there is plenty of raindrops.

The radial velocity observation error is assumed to be 3 m s^{-1}. This error value is close to the values used in Dowell and Wicker (2009), Xu and Gong (2003), and Xiao et al. (2009). The threshold of a radial velocity innovation is set to 15 m s^{-1}. The observation is discarded if the difference between this observation and background is larger than this threshold.

c. The data assimilation setup

This paper presents five experiments denoted as NoDA, GSI3DVar, 3DEnsVar,

and EnKF (Table 1). Experiments differ based on what, if any, assimilation system is used for airborne radar data. The experiments are designed to examine the difference of using flow-dependent versus static background covariance when assimilating the airborne

Table 3.1 List of experiments

Experiment	Description
NoDA	No radar data assimilation. WRF model initial condition is average of 40 members of GFS/EnKF ensemble analysis
GSI3DVar	Radar DA using GSI 3DVar with static covariance
3DEnsVar	Same as GSI3DVar, except using flow dependent covariance for EnKF
EnKF	Ensemble Kalman filter with 40 members

radar data and the impact of DA on the subsequent forecast. We assimilate only airborne TDR radial velocity data. Other available observations are used for verification. We define “prior (background)” and “post (analysis)” for the model fields before and after data assimilation respectively.

Fig. 3.4 shows flow chart of experiments carried out in this study. The NoDA experiment did not assimilate any observation data, instead the HWRF model initial condition at 1200 UTC on 25 August 2011 simply comes from the average of the 40

ensemble members from the GFS/EnKF ensemble system at the same time (Fig. 3.4a). The forecast of a control run from the GFS/EnKF ensemble system provides the lateral boundary conditions (LBCs).

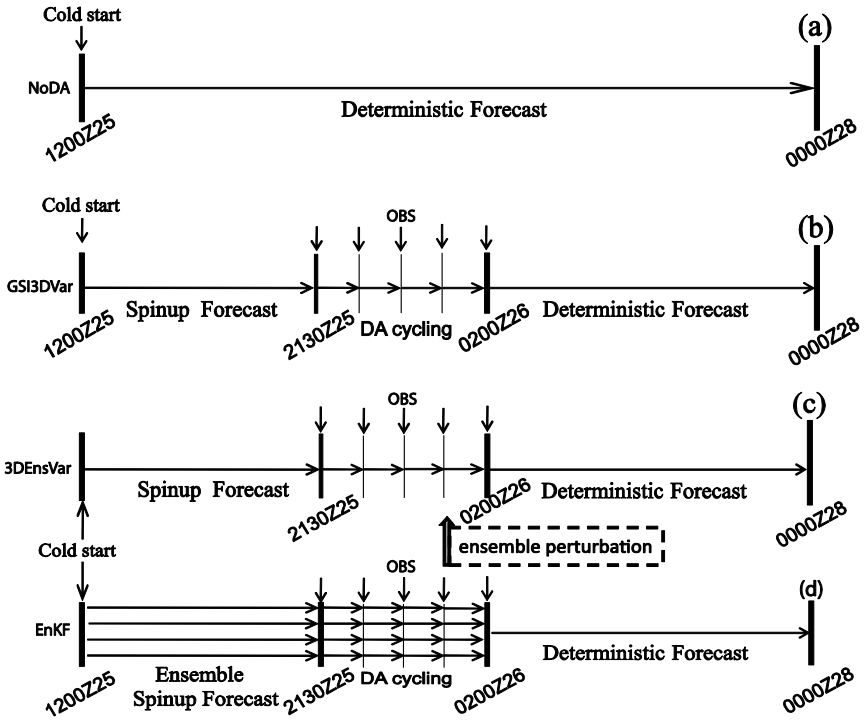

Fig. 3.4 The flow charts for (a) NoDA experiment, (b) GSI3DVar experiments, (c) 3DEnsVar experiments, and (d) EnKF experiments.

The GSI3DVar experiment assimilated the radar data using the traditional GSI 3DVAR method where the static background covariance is adopted. The horizontal and vertical correlation length scales of original static covariance are reduced by factors of 0.4 and 0.6 respectively in experiment GSI3DVar. The GSI 3DVAR experiment contains three stages (Fig. 3.4b). 1) A single 9.5-h spinup forecast initialized from the average of the 40 ensemble members from the GFS/EnKF ensemble system at 1200

UTC 25 August 2011 to produce an initial first guess at 2130 UTC, August 25 for radar DA cycles. The spin-up time of 9.5 hours is based on past experiences and other published studies (e.g., Zhang et al. 2009, spin-up time of 9 hours; Aksoy et al. 2012, spin-up time of 6 hours. 2) Assimilation of tail Doppler radial velocity data one flight leg by the other. We choose times of the assimilation as close to the center of each leg as possible, which are 2130, 2230, 2330 UTC August 25, 0030, 0200 UTC August 26. 3) A 46-h deterministic forecast initialized by the analysis at the end of the assimilation cycles in step 2. The WRF model boundary conditions for all three stages are the same as in NoDA.

The 3DEnsVar has the same three stages as GSI3DVar except that the background covariance is estimated from EnKF ensemble perturbations (Fig. 3.4c).

EnKF experiment has 40 ensemble members. Similar to the GSI3DVar/3DEnsVar experiments, the EnKF experiment has three stages (Fig. 3.4d). 1) 9.5-h ensemble forecasts to spin up a first guess ensemble and provide flow-dependent covariance at the beginning of the radar DA cycles. The initial and boundary conditions for each member are the GFS/EnKF ensemble member forecast. 2) Assimilation of tail Doppler radial velocity data. 3) A 46-h deterministic forecast initialized from the ensemble analysis mean at the end of the DA cycles in step 2.

3.4 Results and discussion

a. Wind and temperature analysis increments

To evaluate the impact of assimilated radial velocity data and the differences of assimilation methods using flow-dependent and static covariances, we first look at the structure and magnitude of analysis increments for wind and then look at that for temperature

Fig. 3.5 shows the wind increment for experiment GSI3DVar, EnKF, and 3DEnsVar at 700 hPa for first DA cycle that assimilates radial velocity from first flight

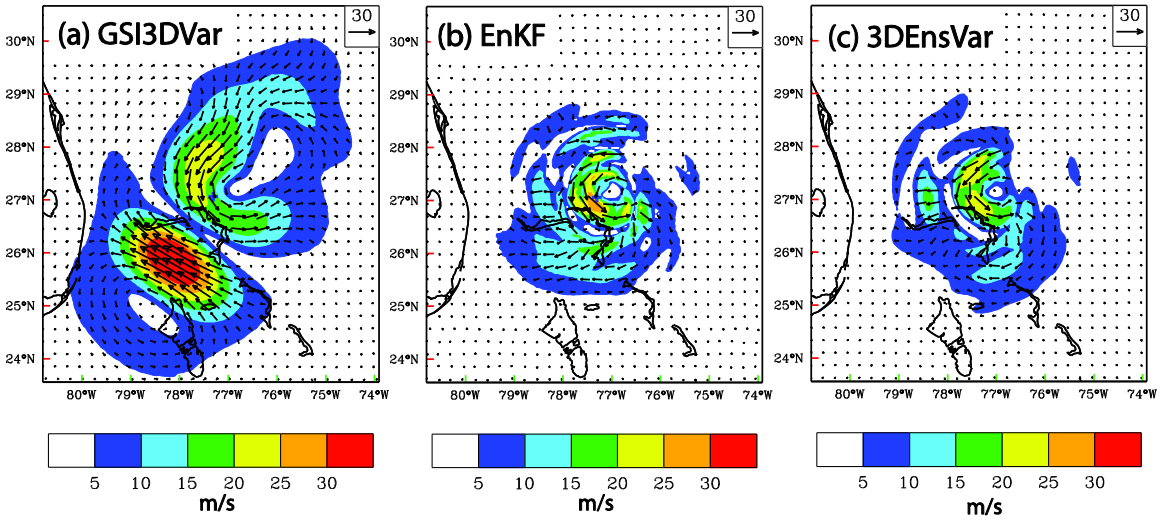

Fig. 3.5 The 700 hPa wind analysis increments (m s^{-1}) for (a) GSI3DVar, (b) EnKF, and (c) 3DEnsVar at 2130 UTC 25 August 2011.

leg. For GSI3DVar, there is cyclonic increment around observed hurricane center indicated by a cross sign. However, an anti-cyclonic increment centered at 26° N, 78°W, with the maximum wind speed increment larger than 30 m s^{-1}, is found. We will see that increment is not consistent with observed flight level wind. In a previous study (Li et al. 2012) such a dual pole pattern of cyclonic and anti-cyclonic wind increment is also

produced by static covariance 3DVAR method. For 3DEnsVar and EnKF, we can see cyclonic wind increment is found around the hurricane center, with larger wind increment at the left of the center, which can be explained well later by comparing with flight level wind observation.

Because only radial velocity data is assimilated in this study, any increment in temperature is a result of balance relationship applied (if any) and/or due to cross covariance in the background error. Fig. 3.6 shows the 700-hPa temperature increments

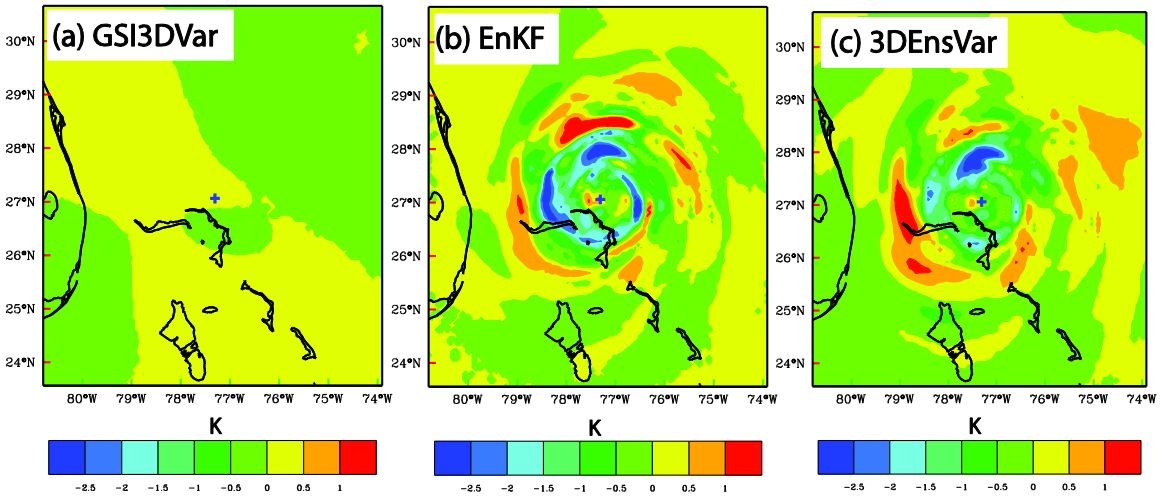

Fig. 3.6 The 700 hPa temperature analysis increments (at intervals of 0.5 K) for (a) GSI3DVar, (b) EnKF, and (c) 3DEnsVar at 2130 UTC 25 August 2011.

for GSI3DVar, 3DEnsVar, and EnKF after assimilating radial velocity data for the first cycle/leg. For GSI3DVar, the temperature increment is relatively smooth and small (-0.25^{o} – 0.5^{o}). No hurricane circulation pattern is found due to the use of static covariance which is homogeneous. There is even negative increment near hurricane center. Physically, the warmer core results in lower central pressure and stronger

hurricane. As the hurricane in background field is weaker than observation, the analysis increment of temperature near hurricane center should be positive in order to raise the strength. In other words, we expect a warmer hurricane core after analysis. The inconsistence is caused by use of static covariance. More detailed explanation is given in Chapter 2. For 3DEnsVar and EnKF, the temperature increments show hurricane-like spiral bands with warmer increment near hurricane center. Both the increment pattern and enhanced warmer core are a benefit of the use of flow-dependent covariance between wind and temperature. Such a result is also shown in the previous study (Li et al. 2012).

b. Verification with independent in-flight measurements

While TDR radial velocity data is assimilated, the aircraft in-flight measurements and the Stepped Frequency Microwave Radiometer (SFMR) retrieved surface winds are used as independent observations for verification. In this section, we will inter-compare the model simulated hurricane inner-core structures, before DA analysis (named as "prior") and after DA analysis (named as "post"), among NoDA, GSI3DVar, EnKF (ensemble mean), and 3DEnsVar, and then verify each experiment result against the observations from the NOAA P-3 aircraft in-flight measurements and the SFMR-retrieved surface winds based on that observed wind speeds, hurricane center, and other parameters are obtained. For the purpose of conciseness, we look at the results for first and last data assimilation cycle out of total five cycles.

Fig. 3.7 shows the comparison between the wind speeds, derived from numerical model of GSI3DVar, EnKF, and 3DEnsVar, and that observed by in-flight instruments

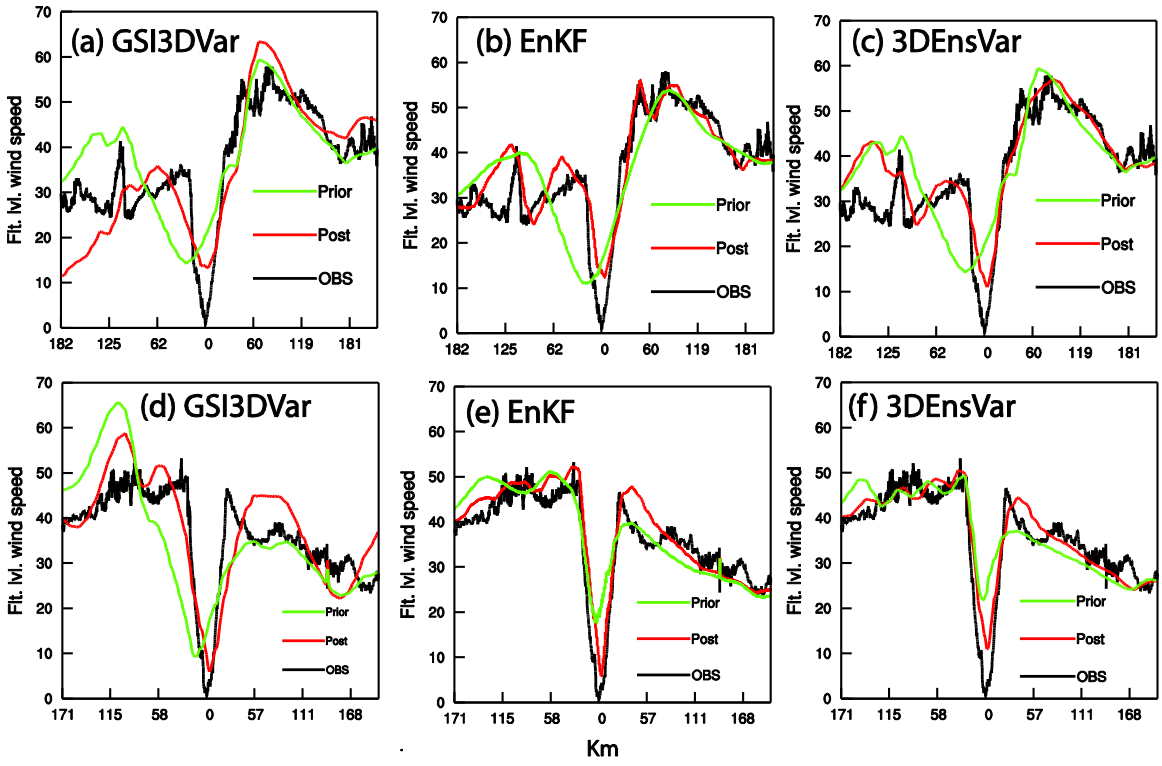

Fig. 3.7 Flight level wind speed (m s^{-1}) observed by in-flight instrument (black line) and interpolated from model prior (green line), and post (red line). First flight leg at 2048 – 2157 UTC: (a) GSI3DVar, (b) EnKF, (c) 3DEnsVar. Last flight leg at 2531 – 2627 UTC: (d) GSI3DVar, (e) EnKF, (f) 3DEnsVar

At flight level. Here the model-derived wind speeds are interpolated along aircraft flight track at 2130 UTC 25 August for first leg (Figs. 3.7a,b,c) and 0200 UTC 26 August 2011 for 5th leg (Figs. 3.7d,e,f). We notice that model-derived wind speeds, according to time and location of observed wind speeds, can be interpolated from time-dependent model states during model integration (Du et al. 2012). In Fig. 3.7 the hurricane center can be identified by the lowest wind speed at the middle of the curves. We first look at wind speeds for first data assimilation cycle at first leg (Figs. 3.7a,b,c). For all experiments of GSI3DVar (Fig. 7a), EnKF (Fig. 3.7b), and 3DEnsVar (Fig. 3.7c), it is

obvious that the model-defined hurricane center was shifted to the left of observed hurricane center before data assimilation and corrected to the observed hurricane center after data assimilation. It means that assimilation of TDR Vr improves model simulated hurricane position. The observed hurricane central wind speed (black line) is almost zero while that interpolated from models of GSI3DVar, EnKF, and 3DEnsVar is about 10 m s^{-1}. We expect such a difference of 10 m s^{-1} will be reduced in later on data assimilation cycles. We look at the wind speeds on the left part of the curves. For all of GSI3DVar, EnKF, and 3DEnsVar, there is large difference of wind speeds between prior (green line) and post (red line), which is consistent with the largest wind analysis increment on the left side of hurricane center in Fig. 3.5. For EnKF (Fig. 3.7b), and 3DEnsVar (Fig. 3.7c), model-derived wind speeds of post are much closer to observed wind speed than that of prior. On the contrary, for GSI3DVar (Fig. 3.7a), compared with observed wind speed on the most left (182-125 km), the wind speeds of post (red line) is about 5 - 20 m s^{-1} below it and that of prior (green line) is about 5 - 10 m s^{-1} above it. Here the large difference (10 -30 m s^{-1}) of model-derived wind speeds between prior and post is also consistent with the large wind analysis increment on the very left part in Fig. 3.5a. Now Figs. 3.7d, e, f show the results for last data assimilation cycle for 5th leg. Verification of model-derived wind speeds against observed one at flight level also shows superiority of EnKF (Fig. 3.7e) and 3DEnsVar (Fig. 3.7f) over GSI3DVar (Fig. 3.7d). For EnKF and 3DEnsVar, model-defined hurricane center of both prior and post is very near observed hurricane center. On

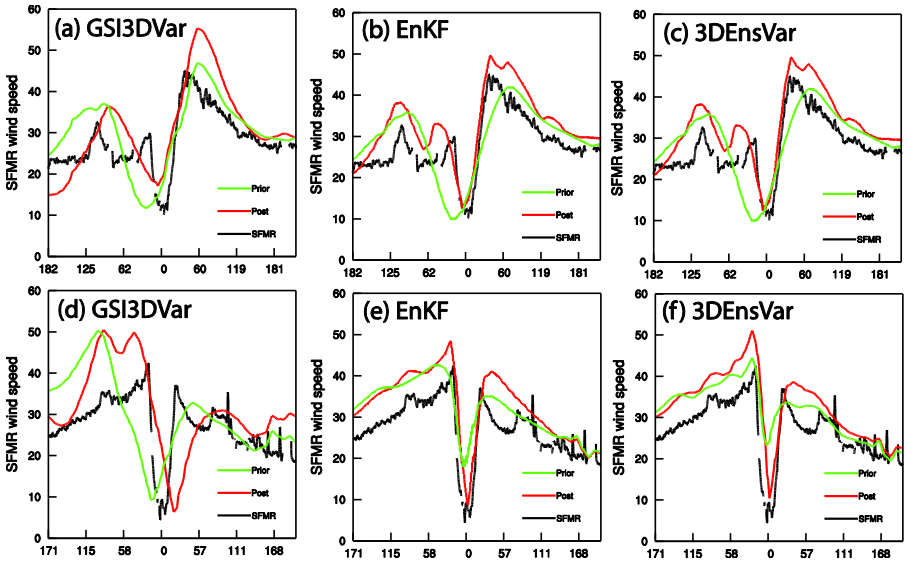

Fig. 3.8 Surface wind speed (m s^{-1}) retrieved by SFMR (black line) and interpolated from model lowest level for prior (green line), and post (red line). First flight leg at 2048 – 2157 UTC: (a) GSI3DVar, (b) EnKF, (c) 3DEnsVar. Last flight leg at 2531 – 2627 UTC: (d) GSI3DVar, (e) EnKF, (f) 3DEnsVar.

the contrary, for GSI3DVar, model-defined hurricane center is deviated to the left of observed hurricane center in prior and corrected to be near observed hurricane center in post. For wind speed on the eye wall, especially on the left side, EnKF and 3DEnsVar also show smaller errors than GSI3DVar for both prior and post. We may deduce that the prior of EnKF and 3DEnsVar receive better benefit than GSI3DVar from previous data assimilation cycles.

The verification of model surface wind speeds against SFMR-retrieved surface wind speeds is shown in Fig. 3.8. The data from all of experiments are interpolated from the model lowest level along aircraft flight track at 2130 UTC 25 August 2011 for first leg (Figs. 3.8a,b,c) and at 0200 UTC 26 August 2011 for 5th leg (Figs. 3.8d,e,f). Generally speaking, verification of model surface wind speed against SMFR-retrieved

measurements show similar results to that of the flight level wind speed (Fig. 3.7). Moreover, in last data assimilation cycle, for EnKF (Fig. 3.8e) and 3DEnsVar (Fig. 3.8f), model hurricane centers of both prior and post are very near observed hurricane center. On contrary, for GSI3DVar (Fig. 3.8d), model hurricane centers are deviated from observed hurricane center, shifting to the left side in prior and right side in post. Meanwhile, EnKF and 3DEnsVar show smaller errors of wind speeds on eye walls than GSI3DVar for both prior and post. Again, EnKF and 3DEnsVar using flow-dependent covariance show superiority over GSI3DVar using static covariance.

c. Innovation statistics for Vr and minimum sea level pressure in DA cycles

The behaviors of GSI3DVar, EnKF, and 3DEnsVar are further compared by examining the fit of their analyses and forecasts to TDR Vr observations during the DA cycles. The fit is defined as the root-mean-square difference (RMSD) between the observation and model state that is converted to the observed quantities; and such difference is also called as observation innovation. Figure 3.9a shows the RMSDs for TDR Vr and minimum sea level pressure (MSLP) from GSI3DVar, EnKF, and 3DEnsVar. The TDR Vr data are used as observation in the innovation calculation. For the EnKF, the ensemble mean is used as model state. In all three experiments, the RMSD for Vr is reduced significantly by the analysis within each cycle. However, the

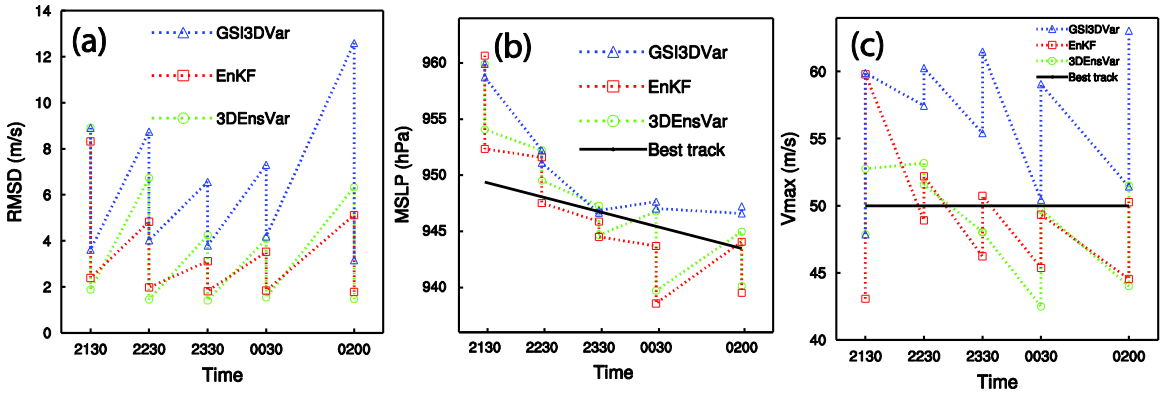

Fig. 3.9 The forecast and analysis (sawtooth pattern during DA cycling) of (a) RMSD of TDR radial velocity (m s^{-1}), and (b) the minimum sea level pressures (hPa) verified against the NHC best track estimate, for GSI3DVar, EnKF, and 3DEnsVar from 2130 UTC 25 to 0200 UTC 26 August 2011.

RMSD of Vr for GSI3DVar is larger than that from EnKF, and 3DEnsVar at both forecast and analysis. Another phenomenon is that the forecast RMSD of TDR Vr for 3DEnsVar is a little larger than that from EnKF.

Figure 3.9b shows the fit of the analysis and short forecast MSLPs to the best-track data from the National Hurricane Center. The best-track MSLP decreased from about 950 hPa at 2130 UTC 25 to 945 hPa at 0200 UTC 26 August 2011. At the beginning of DA cycling (2130 UTC August), the MSLP for GSI3DVar and EnKF is about 11 hPa higher than the best-track estimate. Generally speaking, MSLPs for all three experiments tend to be close to the best-track. Both forecast and analysis MSLPs for GSI3DVar are above best-track while, for EnKF and 3DEnsVar, short forecast MSLPs are above best track and analysis MSLPs are below best-track. From MSLP evolution we are not able to say which experiment is superior over others. But it is obvious that a weaker hurricane in background fields is strengthened towards observation by assimilation of TDR Vr.

d. The analyzed hurricane structures

We now examine the structure of the hurricane at the end of the DA cycles at 1 km height and at vertical cross section through the analyzed hurricane center. The model winds from GSI3DVar and 3DEnsVar (EnKF wind field, not shown, is similar to that of 3DEnsVar) are compared with the three dimensional hurricane-relative wind

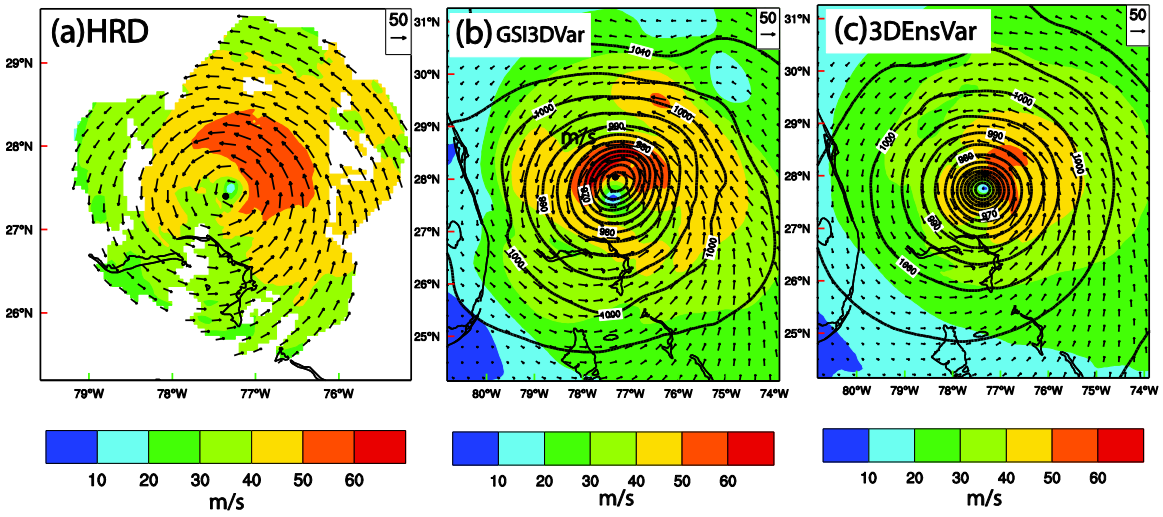

Fig. 3.10 Wind vector and speed (shaded) at 1-km height. (a) HRD TDR Vr analysis. The HWRF model simulation of wind, together with sea level pressure (interval of 5 hPa, solid contours) for (b) GSI3DVar, (c) 3DEnsVar at 0200 UTC 26 September 2011.

analysis derived by HRD based on the quality-controlled TDR radial velocity from all five legs. Fig. 3.10 shows the model wind and TDR Vr wind analysis at 1 km height. The Vr wind analysis covers most area of the hurricane inner core with maximum wind speed at northeast quadrant to the hurricane center. Similar to Vr wind analysis, maximum wind speed in 3DEnsVar was also located northeast quadrant to the hurricane center. The maximum wind speed (>60 m s^{-1}) in GSI3DVar is stronger than that in Vr wind analysis (50 – 60 m s^{-1}) located at northwest to the hurricane center, which is

inconsistent with Vr wind analysis. We can see in 3DEnsVar hurricane centers defined by wind and sea level pressure are co-located. On contrary, the hurricane center defined by sea level pressure is at north of that defined by wind speed in GSI3DVar (Fig. 3.10b), which is dynamically inconsistent.

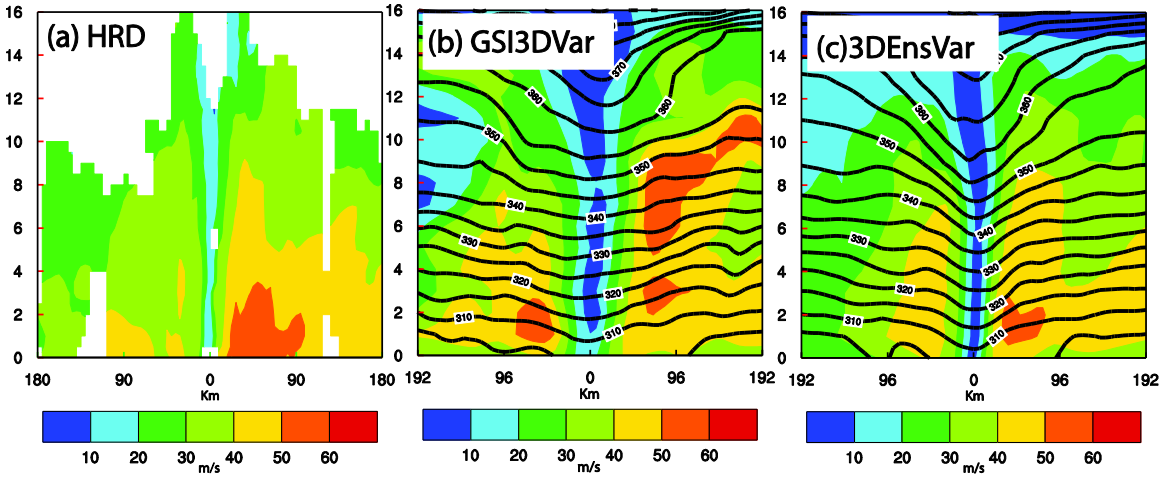

Fig. 3.11 Vertical cross section of wind speed (interval of 10 m s^{-1}, shaded). (a) HRD TDR Vr analysis. The HWRF model simulated wind, together with potential temperature (interval of 5 K, solid contours) for (b) GSI3DVar, (c) 3DEnsVar at 0200 UTC 26 September 2011.

Figure 3.11 shows the vertical cross sections of horizontal wind speed and potential temperature for all four experiments. The locations of cross sections are west-east through the analyzed hurricane center. In HRD Vr wind analysis (Fig. 3.11a), the hurricane eye is clearly shown with maximum wind speed on east eye wall where the large wind for 50 – 60 m s^{-1} is below 3 km height. Similar to Vr wind analysis, in 3DEnsVar (EnKF wind field, not shown, is similar to that of 3DEnsVar), there is also large wind for 50 – 60 m s^{-1} on east eye wall below 3 km height. On the contrary, in GSI3DVar, the large wind for 50 – 60 m s^{-1} on east eye wall extends to about 11 km

height and an extra large wind for 50 – 60 m s^{-1} appears on west eye wall, which is considered as noises. Unlike the 3DEnsVar experiments, the potential temperature contours of GSI3DVar (Fig. 3.11b) do not bend downward for 2 – 10 km. The downward extrusion of potential temperature contours in 3DEnsVar indicates a warm core structure (Figs. 3.11c).

e. The track and intensity forecasts

To further evaluate the quality of analyses produced by different DA methods, deterministic forecasts initialized from the (ensemble mean in the EnKF cases) analyses at 0200 UTC 26 August, the end of the DA cycles, are launched. The track forecasts of EMC official, NoDA, GSI3DVar, EnKF, and 3DEnsVar are verified against NHC best

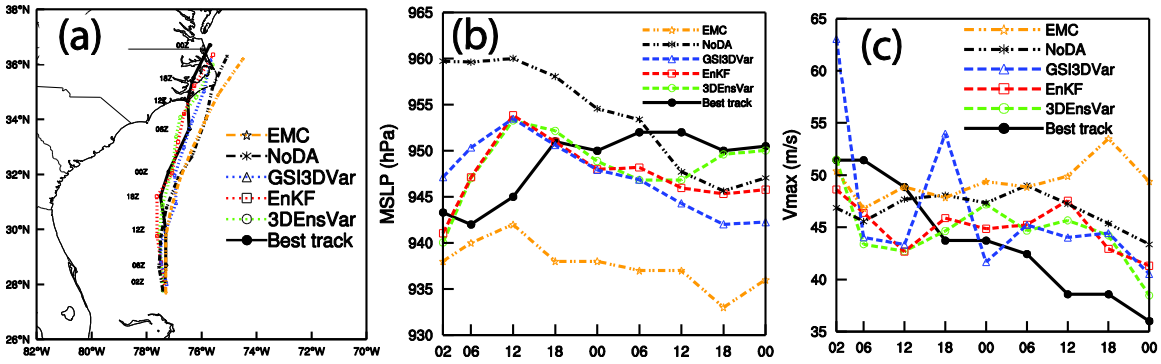

Fig. 3.12 Deterministic forecast hurricane (a) tracks and (b) minimum sea level pressure (hPa) by NoDA, GSI3DVar, EnKF, 3DEnsVar, EMC as compared to NHC best track estimates from 0200 UTC 26 through 0000 UTC 28 August 2011.

track (Fig. 3.12a). The central position of the forecast hurricane is defined as the location of MSLP. The initial track errors at 0200 UTC 26 are less than 20 km for all

experiments. By 0000 UTC 28 August, the mean track errors are 67, 58, 47, 32, and 44 km for EMC official, NoDA, GSI3DVar, EnKF, and 3DEnsVar, respectively. We can see the forecast tracks of NoDA and EMC deviate, towards the right (over sea), from best track while that of 3DEnsVar and EnKF oscillate along the best track. When Irene made landfall at 1200 UTC 27 the sequence (from large to small) of forecast track errors are for EMC official, NoDA, GSI3DVar, EnKF, and 3DEnsVar, respectively. The mean track errors based on the hurricane positions at 6-h interval during the period from 0200 UTC 26 to 0000 UTC 28 August are 58, 47, 32, and 44 km for NoDA, GSI3DVar, EnKF, and 3DEnsVar respectively. Given that our DA experiments do not include environmental observations, the main effect on the track should come from the changes to the inner core structure and intensity of the analyzed hurricane.

Figure 3.12b shows the intensity forecasts in terms of MSLP verified against the best-track MSLP. According to best track, the Irene strengthened during first 4 hours, and then weakened until 1800 UTC 28, maintain almost the same intensity until 0000 UTC 28 August. At 0200UTC 26 August, the MSLP errors are 5, 17, 4, 2.0, and 3.0 hPa for EMC official forecast, NoDA, GSI3DVar, EnKF, and 3DEnsVar, respectively. NoDA has the largest MSLP error throughout the forecast due to its too weak at initial time. EMC over deepens too much during the whole forecast. The mean MSLP errors are 3.3, 4.2, 5.8, 8.2, 10.8 hPa for 3DEnsVar, EnKF, GSI3DVar, NoDA and EMC official forecast, respectively. Overall, the forecast MSLP in the two flow dependent covariance experiments is closer to the best-track MSLP than that of GSI3DVar. None of the forecasts capture the slight deepening during the first 3 h of forecast. Figure 12c

shows the intensity forecasts in terms of Vmax at model lowest levels verified against the NHC best-track Vmax. Unlike MSLP that generally strengthens first and then maintains the same strength level, the best track Vmax generally weakens, from 53 m s^{-1} to 37 m s^{-1}, during the whole forecast time. The Vmax of NoDA and GSI3DVar do not depart from Vamx of EnKF and 3DEnsVar very much except that GSI3DVar has too strong wind speed at beginning and a spike at 18 UTC 26 August. EMC Vmax has too strong wind speed after 18 UTC 26 which is consistent with its MSLP for the same time. EMC Vmax shows weaker wind speed than best track for first 12 hours which is consistent with its MSLP. NoDA Vmax shows a transition time at 12 UTC 26 where NoDA Vmax is lower than best track before it and stronger than best track after it. Differently, NoDA MSLP transition time is at about 6 UTC 27. In other words, model Vmax values are not subject to model MSLP values exactly.

3.5 Summary and conclusions

In this study, the GSI 3DVar-based hybrid EnKF-Var data assimilation system including both the Var and EnKF components were expanded to HWRF for the prediction of hurricane Irene (2011). In the hybrid DA system, the flow-dependent ensemble covariances were estimated from an EnKF-generated ensemble and incorporated into the variational minimization by using the extended control variable method. A 40 member ensemble and single control forecasts are performed. The analysis ensemble is generated by updating each forecast ensemble member with a serial implementation of the square root ensemble Kalman filter (EnSRKF) system. The

air borne Doppler radar radial velocity is for first time assimilated by this EnKF system, which is interfaced with GSI by using the same data quality control and observation operator. In GSI system, the radar data thinning method is further enhanced (e.g., fore and aft sweeps are separated when thinning). Thus in a three dimensional box two radial velocities are selected from two different directions (e.g., 50^o from each other). Such an enhanced part of the thinning method is implemented into EMC operational data assimilation system.

The tail Doppler radar radial velocity is assimilated leg by leg of an NOAA P-3 flight mission on 25 – 26 August 2011. We examine the difference of using flow-dependent and static background covariance when, and the impact of, assimilating airborne radar observations by comparing both analysis and forecast with various kinds of observations. The examinations are based on four experiments in this study. A forecast experiment without assimilating any radar data is first carried out to serve as a baseline against which the radar-assimilating experiments are compared; this forecast experiment (NoDA) started directly from the average of global GFS/EnKF 40 member analysis, which contained too weak a hurricane vortex. The three radar DA experiment employed the WRF 3DVAR using the static covariance (GSI 3DVar), the hybrid DA system with purely flow-dependent background covariance (3DEnsVar), and EnKF. The results of analyses and forecasts from the four experiments are intercompared and verified against EMC operational forecast, best-track data, radar wind measurements, in situ data, and remote sensed observations. The main conclusions are summarized in the following.

Compared with the flight level wind, remote sensed wind, and air borne Doppler radar wind synthetic fields, we see that the hybrid analyses (3DEnsVar and EnKF components) successfully capture the inner-core structure of the hurricane vortex in terms for both wind and temperature fields during the analysis time. The subsequent deterministic forecasts of 3DEnsVar and EnKF initialized by assimilating airborne radar observations improved the hurricane track and intensity forecasts, compared with EMC operational forecast, the forecast initialized by GSI 3DVar with static background covariance, and NoDA.

Through one Vr observation test, we see that the analysis increment 3DEnsVar and EnKF are very similar to each other. There are a little more difference between 3DEnsVar and EnKF when many observations are used. This may be caused by the complex interactions among data and DA methods. We need to do further investigation on the difference and similarity between 3DEnsVar and EnKF.

The 3DEnsVar has no large superiority over EnKF. However, 3DEnsVar has a potential function to include some constraint or extent. 3DEnsVar is also straightforward to implement dual resolution capability, which will be a focus of Chapter 4 of this dissertation. In Chapter 4, we will test dual resolutions of 3km grid nested in 9 km grid for 3DEnsVar and EnKF. We will investigate and expect that the dual resolution of 9 km and 3 km grids produces better hurricane track and intensity forecast than single 9 km grid.

We note that this study represents the first attempt of applying the GSI 3DVar-based hybrid EnKF-Var data assimilation method interfaced with HWRF model to

hurricane and radar data assimilation. We also note that the above conclusions and findings are based on only one flight mission of a hurricane reconnaissance. This study may be considered as a pioneer of future research for many hurricane cases (missions) and operational runs with the same procedures presented in this study.

Chapter 4

Assimilation of Airborne Radar Data using Dual Resolution, GSI-based Var-EnKF Hybrid System for TC Initialization and Prediction

4.1 Introduction

Variational data assimilation methods have been implemented in many operational and research centers. In National Center for Environmental Prediction (NCEP), the community Gridpoint Statistical Interpolation (GSI), a three-dimensional variational data assimilation (3DVAR) system is used to initialize global and regional model (Wu et al. 2002; Kleist et al. 2009; Tallapragada et al. 2014). Traditionally, the background error covariance for GSI is derived with assumptions of spatial and temporal homogeneity and isotropy (Usually using NMC method (Parrish and Derber 1992)). For the analysis of strong nonlinear and discontinuous features such as TC inner core circulation, the use of static background error covariance may be problematic. Some GSI 3DVAR experiments show that inner core observations cannot be used due to the potential negative impacts caused by static covariance on vortex structure (Tallapragada et al. 2014). More advanced ensemble based variational hybrid data assimilation methods could address this problem.

Ensemble-based DA methods, most of which are in various forms of EnKF (Evensen 1994), have been explored to initialize hurricane forecasts and have shown great promise (Li and Liu 2009; Torn and Hakim 2009; Zhang et al. 2009; Hamill et al. 2011; Wang et al. 2011; Weng et al. 2011; Zhang et al. 2011; Aksoy et al. 2012; Li et al. 2012; Weng and Zhang 2012; Cavallo et al. 2013; Dong and Xue 2013; Wang and

Lei 2014). In ensemble-based DA, background error covariance is estimated for the ensemble forecasts that reflect current flow characteristics. Therefore, the observation information will be properly spread consistent with current hurricane flow. Meanwhile state variable that are not observed could be realistically updated through cross variable covariance.

A hybrid data assimilation method that combine ensemble-based and variational DA systems has become an alternative approach (Hamill and Snyder 2000; Lorenc 2003; Etherton and Bishop 2004; Buehner 2005; Zupanski 2005; Wang et al. 2007ab, 2008ab, 2009; Liu et al. 2008, 2009; Buehner et al. 2010a, b; Wang 2010, 2011; Zhang and Zhang 2012; Schwartz et al. 2013; Wang et al. 2013; Zhang et al. 2013a; Zhang et al. 2013b; Gao and Stensrud 2014; Schwartz and Liu 2014; Wang and Lei 2014). While a standard three- or four-dimensional variational method (3D/4DVAR) typically uses static background error covariance, a hybrid ensemble variational DA system incorporates ensemble-derived flow-dependent covariance into the VAR framework. The ensemble can be generated by an EnKF. Furthermore, how to efficiently couple EnKF and hybrid DA systems is investigated. In addition to one-way coupling where EnKF is not affected by VAR system, two-way coupling where ensemble mean is replaced by VAR analysis is also examined (Zhang and Zhang 2012; Wang et al. 2013; Zhang et al. 2013a; Gao and Stensrud 2014). Compared with one-way coupling, two-way coupling allows EnKF perturbations to evolve around the trajectory of the control forecast whose error statistics may be better represented.

Due to limitation of computer resource, it is not practical to put all ensemble members at high resolution grids that are needed to simulate convective circulations.

Several studies tried to incorporate ensemble at multiple resolution in data assimilation, mimicking a typical 4DVar system where the tangnent linear adjoint model is typically run at reduced resolution. Du (2004) proposed a hybrid ensemble prediction system introducing low-resolution ensemble perturbations into a high-resolution forecast that produced new high quality ensemble. Gao and Xue (2008a) tested a dual-resolution EnKF DA system with a single high-resolution forecast and a low-resolution ensemble. The low-resolution ensemble and the high-resolution control forecast run in parallel. The background error covariance estimated from the low-resolution ensemble is used to update a single high-resolution forecast in producing quality analysis on high resolution grid. Rainwater and Hunt (2013) proposed a mixed-resolution ensemble DA system (local ensemble transform Kalman filter (LETKF)) obtaining background covariance from a combination of a high-resolution ensemble and a low-resolution ensemble that produce more accurate analysis than single resolution analysis. In these studies, it is noticed that high resolution grid is defined at the same domain as low resolution grid which is still very costly (Gao and Xue 2008a).

In this chapter, we propose to implement the dual resolution in hybrid ensemble-variational framework using the nested grids, which further reduce the computational cost.

A previous study using a hybrid ensemble-variational data assimilation system for assimilating coastal ground-based radar has shown promising results (Li et al. 2012). The ground-based radars cover the hurricanes only when they are near coast. Usually hurricanes spend most of life time over sea where observations are rare or not available at all. Therefore, National Oceanic and Atmospheric Administration (NOAA) Hurricane

Research Division (HRD) sent out aircraft equipped with tail Doppler radar (TDR), Stepped Frequency Microwave Radiometer (SFMR), and other in-flight instruments to obtain hurricane inner core observations. Assimilation of TDR data has been carried out using 3DVAR (Du et al. 2012), EnKF (Zhang et al. 2011; Weng and Zhang 2012; chapter 3 of this dissertation). In this study, hybrid DA method with dual resolution technique for assimilating TDR data is explored first time. More specifically, unified GSI based EnKF-3DVAR hybrid DA system is employed to the assimilation of TDR data for the hurricane prediction with Hurricane Weather and Research Forecast model (HWRF). The EnKF configured at 9-km grid adopts the square root ensemble Kalman filter (EnSRF) system (Whitaker et. al. 2002). In addition to 9-km single resolution hybrid DA, 9/3 km dual resolution hybrid DA is a focus of this study.

In addition to detailed case study for one P-3 mission that shows how dual and single resolution hybrid system works step by step, statistics based on multiple missions of the same case is also collected. For case study, we apply hybrid system to the assimilation of NOAA P-3 airborne Doppler radar radial velocity data for the prediction of Hurricane Irene (2011) initialized at 12 UTC 26 Aug. 2011. Irene (2011) is currently ranked as the seventhcostliest hurricane in the United States history (en.wikipedia.org/wiki/Hurricane_Irene). Data assimilation and forecast experiments are then carried out for all 4 flight missions around 12 UTC 24, 12 UTC 25, 00 UTC 26, 12 UTC 26 Aug. 2011 for IRENE. (Fig. 4.1)

The remainder of this chapter is organized as follows: section 2 presents the methodology and section 3 discusses the experiment design. The experiment results are

discussed in section 4, while the final section summarizes the main conclusions of this study.

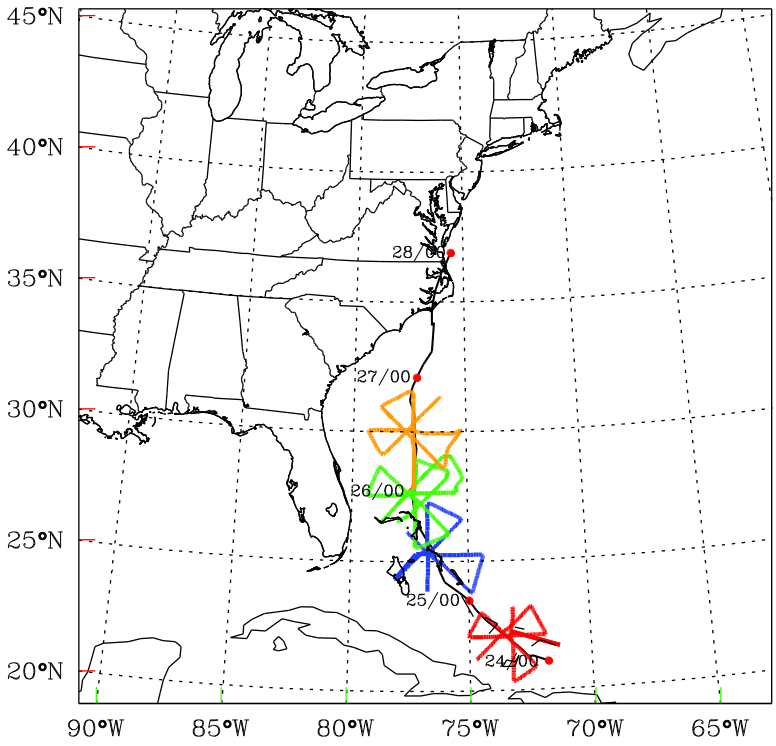

Fig. 4.1 Hurricane Irene (2011) tracks based on National hurricane Center best-track locations. Also indicated are flight tracks of NOAA aircraft missions in red, green, blue, and orange color.

4.2 Methodology

a. The hybrid ensemble-3DVAR scheme

Following Wang et al. 2013, a diagram of the one-way coupled hybrid DA system is shown in Fig. 4.2a. The following four steps are repeated during each DA cycle: 1) Perform K (K is the

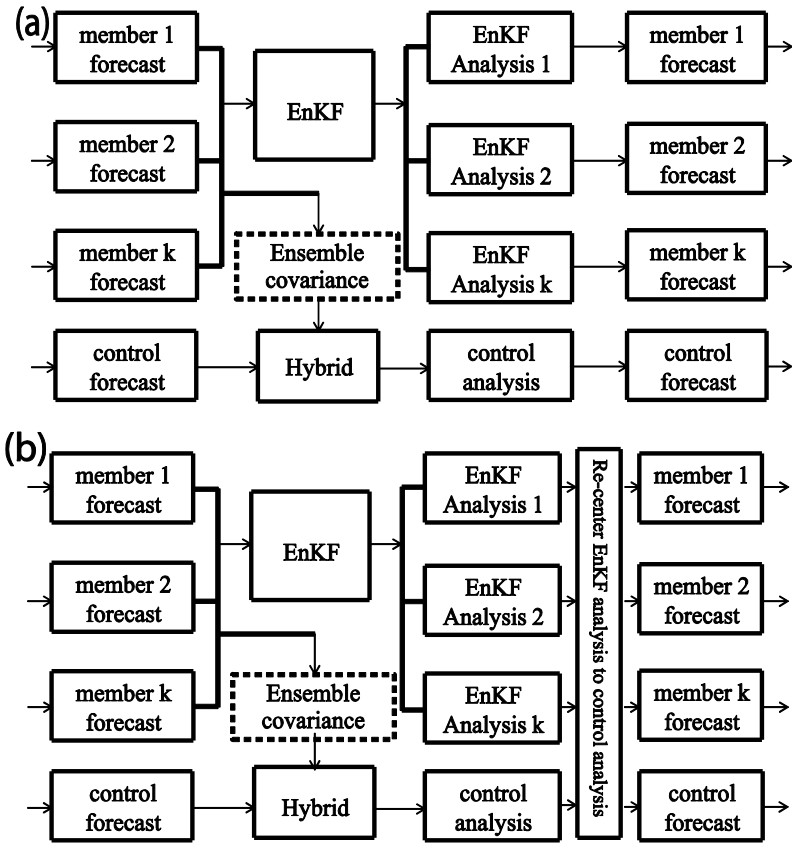

Fig. 4.2 Schematic diagram of the GSI-based EnKF-variational one/two-way coupled hybrid data assimilation system**.**

ensemble size) number of ensemble forecasts to generate background forecast fields at the time of analysis. 2) Meanwhile, perform control run forecast for hybrid 3DVAR analysis background which are configured at single grid and nested grids. 3) The hybrid 3DVAR system reads ensemble forecast fields and calculates ensemble perturbations for flow-dependent covariance used by the hybrid cost function. Perform hybrid 3DVAR analysis at each grid with the observations. 4) The ensemble members are updated by EnKF with the same observations in step 3. Step 1 through step 4 are repeated for each of the follow-on cycles, with the hybrid 3DVAR analysis in step 3 and EnKF analysis in step 4 providing initial conditions (IC) for step 2 and step 1 respectively. For two-way coupled hybrid DA system, step 4 is modified by re-centering the analysis ensemble around the hybrid analysis that replaces ensemble mean to produce final analysis ensemble (Fig. 4.2b). It is expected that with such a modification EnKF perturbations may evolve with the trajectory of the control forecast so that the ensemble covariance may potentially better represent the error statistics of the control forecast.

In addition to single resolution application, the extended control variable method used for GSI hybrid described in Chapter 3 is further modified here into dual resolution manner. For state vector **x,** the analysis increment of the hybrid scheme, **x'**, is the sum of two terms,

$$\mathbf{x}^{'} = \mathbf{x}_1^{'} + \mathbf{L}\sum_{k=1}^{K}\left(\mathbf{a}_k \circ \mathbf{x}_k^e\right). \qquad (1)$$

Most of the explanation of equation (1) is provided in chapter 2 except that **L** represents linear interpolation from ensemble grid at low resolution to analysis grid at high

resolution. Specificcally, $\mathbf{x}$' and $\mathbf{x}_1^{'}$ are defined at high resolution while $\mathbf{a}_k$ and $\mathbf{x}_k^{e}$ are at low resolution.

The dual cost function for hybrid ensemble-3DVAR is

$$J(\mathbf{x}_1^{'},\mathbf{a}) = \beta_1 J_b + \beta_2 J_e + J_o,$$

$$= \beta_1 \frac{1}{2}(\mathbf{x}_1^{'})^T \mathbf{B}^{-1}(\mathbf{x}_1^{'}) + \beta_2 \frac{1}{2}(\mathbf{a})^T \mathbf{A}^{-1}(\mathbf{a}) + \frac{1}{2}(\mathbf{y}^{o'} - \mathbf{H}\mathbf{x}^{'})^T \mathbf{R}^{-1}(\mathbf{y}^{o'} - \mathbf{H}\mathbf{x}^{'}). \quad (2)$$

Note that J_b and J_o are at high resolution while J_e is at low resolution. The other description of equation (2) is provided in chapter 2 and will not be repeated here. We further define a new control variable as

$$\mathbf{x} = \begin{pmatrix} \mathbf{x}_1^{'} \\ \mathbf{a} \end{pmatrix} \quad (3)$$

Equation (1) for hybrid increment can be rewritten as

$$\mathbf{x}^{'} = \mathbf{x}_1^{'} + \mathbf{LDa} = \mathbf{Cx}$$

Where $\mathbf{D}$ = [diag($\mathbf{x_1}^{e}$) … diag($\mathbf{x_k}^{e}$)]. $\mathbf{a}$ is a vector with elements ($\mathbf{a_1}^T$,$\mathbf{a_2}^T$,…$\mathbf{a_k}^T$). **C=(I, LD)**

We define hybrid background covariance

$$\mathbf{B} = \begin{pmatrix} \frac{1}{\beta_1}\mathbf{B}_1 & \cdots & 0 \\ \vdots & \ddots & \vdots \\ 0 & \cdots & \frac{1}{\beta_2}\mathbf{A} \end{pmatrix}$$

The hybrid is preconditioned by a new variable

$$\mathbf{z} = \mathbf{B}^{-1}\mathbf{x} = \begin{pmatrix} \beta_1\mathbf{B}_1^{-1} & \cdots & 0 \\ \vdots & \ddots & \vdots \\ 0 & \cdots & \beta_2\mathbf{A}^{-1} \end{pmatrix} \begin{pmatrix} \mathbf{x}_1^{'} \\ \mathbf{a} \end{pmatrix} = \begin{pmatrix} \beta_1\mathbf{B}_1^{-1}\mathbf{x}_1^{-1} \\ \beta_2\mathbf{A}^{-1}\mathbf{a} \end{pmatrix} \quad (4)$$

According to Wang (2010), the gradients of the cost function (2) with respect to the original control variables $\nabla_{\mathbf{x}_1'} J$ and the extended control variables $\nabla_{\mathbf{a}} J$ are given as

$$\nabla_{\mathbf{x}_1'} J = \beta_1 \mathbf{B}_1^{-1} \mathbf{x}_1' + \mathbf{H}^T \mathbf{R}^{-1} (\mathbf{H}\mathbf{x}' - \mathbf{y}^{0'}) \tag{5}$$

$$\nabla_{\mathbf{a}} J = \beta_2 \mathbf{A}^{-1} \mathbf{a} + \mathbf{D}^T \mathbf{L}^T \mathbf{H}^T \mathbf{R}^{-1} (\mathbf{H}\mathbf{x}' - \mathbf{y}^{0'}) \tag{6}$$

L is interpolation from low to high resolution.

The gradients of the cost function (2) with respect to the new control variables

$$\nabla_{\mathbf{x}} J = \begin{pmatrix} \nabla_{\mathbf{x}_1'} J \\ \nabla_a J \end{pmatrix} = \mathbf{B}^{-1} \mathbf{x} + \mathbf{C}^T \mathbf{H}^T \mathbf{R}^{-1} (\mathbf{H}\mathbf{C}\mathbf{x} - \mathbf{y}^{0'}) = \mathbf{z} + \mathbf{C}^T \mathbf{H}^T \mathbf{R}^{-1} (\mathbf{H}\mathbf{C}\mathbf{x} - \mathbf{y}^{0'}) \tag{7}$$

Divide (5) and (6) by $\beta_1 \mathbf{B}_1{}^{-1}$ and $\beta_2 \mathbf{A}^{-1}$ respectively, the gradients of the new cost function with respect to $\beta_1 \mathbf{B}_1{}^{-1} \mathbf{x}'_1$ and $\beta_2 \mathbf{A}^{-1} \mathbf{a}$ are given by

$$\nabla_{\beta_2 \mathbf{B}_1^{-1} \mathbf{x}_1'} J = \mathbf{x}_1' + \frac{1}{\beta_1} \mathbf{B}_1 \mathbf{H}^T \mathbf{R}^{-1} (\mathbf{H}\mathbf{x}' - \mathbf{y}^{0'}) \tag{8}$$

$$\nabla_{\beta_2 \mathbf{A}^{-1} \mathbf{a}} J = \mathbf{a} + \frac{1}{\beta_2} \mathbf{A}\mathbf{D}^T \mathbf{L}^T \mathbf{H}^T \mathbf{R}^{-1} (\mathbf{H}\mathbf{x}' - \mathbf{y}^{0'}) \tag{9}$$

The gradient of cost function with respect to **z** is

$$\nabla_{\mathbf{z}} J = \begin{pmatrix} \nabla_{\beta_2 \mathbf{B}_1^{-1} \mathbf{x}_1'} J \\ \nabla_{\beta_2 \mathbf{A}^{-1} \mathbf{a}} J \end{pmatrix} = \mathbf{x} + \mathbf{B}\mathbf{C}^T \mathbf{H}^T \mathbf{R}^{-1} (\mathbf{H}\mathbf{C}\mathbf{x}' - \mathbf{y}^{0'}) \tag{10}$$

Compare (4), (7), (10) , we obtain

$$\nabla_{\mathbf{z}} J = \mathbf{B} \nabla_x J \tag{11}$$

Therefore, cost function (2) is minimized by iteration of (7) and (11). Note that **B** and **x** in (7) and (11) include extended background covariance and extended control variable.

The GSI hybrid dual resolution DA is realized by three steps: 1) Ensemble forecast perturbations $\mathbf{x}_k^e$ used for flow dependent covariance together with extended control variables $\mathbf{a}_k$ are calculated at 9-km grid. 2) The background fields and analysis increment $\mathbf{x}'$ are calculated at 3-km grid. 3) A linear interpolation is performed between 1) and 2) during DA minimization.

The ensemble for the hybrid ensemble-3DVAR system is updated by using an EnKF that is implemented as square root filter algorithm (EnSRF) (Whitaker and Hamill 2002) in this study. This EnKF code has been efficiently parallelized following Anderson and Collins (2007). In this algorithm, both the model state variables and the observation priors (the predicted observation variable ensemble members) are updated so as to avoid re-computing the forward operator after each observation is assimilated. The EnKF is interfaced with HWRF model by reading HWRF forecast data and outputting HWRF initial condition data. Meanwhile, the EnKF is interfaced with GSI 3DVAR system by using GSI's observation operators, pre-processing and quality control of assimilated data. In EnKF, sample covariance can be spurious due to sampling error related to limited ensemble size, model error, and other factors. To reduce spurious covariance, localization is used in the state update to limit the impact of observations to a specified distance (length scale) from the observation. The localization is realized through polynomial function (Gaspari and Cohn 1999) equivalent to $e^{-r/c}$ where r is distance normalized by the length scale and c is a constant (0.388). In this study, the cut-off localization length scale is 450 km in the horizontal direction, 1.0 scale height (neutral log of pressure) in the vertical direction,. In GSI hybrid system, the

ensemble covariance localization is realized by a recursive filter (Hayden and Purser 1995). The corresponding covariance localization length scale can be calculated through (Gaspari and Cohn 1999) function $L_h = \frac{\sqrt{0.15}}{\sqrt{2}} L_e$. L_e (450 km) and L_h (123 km) are EnKF and GSI hybrid localization length scales respectively. Note that the horizontal correlation length scale of GSI static covariance is reduced by a factor of 0.2, 0.4, and 0.8.

Usually, the ensemble based data assimilation algorithm will quickly reduce ensemble spread (standard deviation) after assimilating observations. To mitigate quick reduction of the spread, the multiplicative inflation method (Whitaker and Hamill 2012) is applied in the EnKF. We define "prior (forecast/background)" and "posterior (analysis)" for the state variables before and after data assimilation respectively. The posterior ensemble perturbations are inflated by a factor proportional to the amount of the reduction of the ensemble covariance due to the assimilation of observations. (Whitaker and Hamill 2012)

$$\mathrm{x}'_{\mathrm{new}} = \mathrm{x}'_a \left(b \frac{\delta_f - \delta_a}{\delta_a} + 1 \right) \tag{12}$$

In Eq. (3), $\mathrm{x}'_{\mathrm{new}}$ is inflated posterior perturbation, x'_a is posterior perturbation, b is inflation factor set to 0.99 in this study, and δ_f and δ_a are prior and posterior standard deviations at each model grid, respectively.4.3 Experimental design

a. The HWRF model configuration

The Hurricane Weather Research and Forecasting system (HWRF) model is used in this study. The model is a non-hydrostatic primitive equation model using rotated-E grid dynamic core. In this study the HWRF ensemble is configured at single grid while HWRF control run is at either single or nested grid. The horizontal spacing is 9 km (224x448 grid points) for single grid and 9 km (224x448 grid points) and 3 km (157x322 grid points) for nested grids (Fig.4.3). All grids have 61 vertical levels with The model top at 2 hPa. The time step is 15/5 s for 9/3 km grids respectively. These configuration parameters are also used by Environmental Modeling Center (EMC) operational runs. The microphysics scheme is based on the Eta Grid-scale Cloud and Precipitation scheme (Ferrier 2005). Since the grid resolution may not fully resolve the hurricane convective features, the Simplified Arakawa-Schubert scheme (SASS) cumulus parameterization (Han and Pan 2011) is included. Other physics parameterizations schemes include non-local planetary boundary layer parameterization

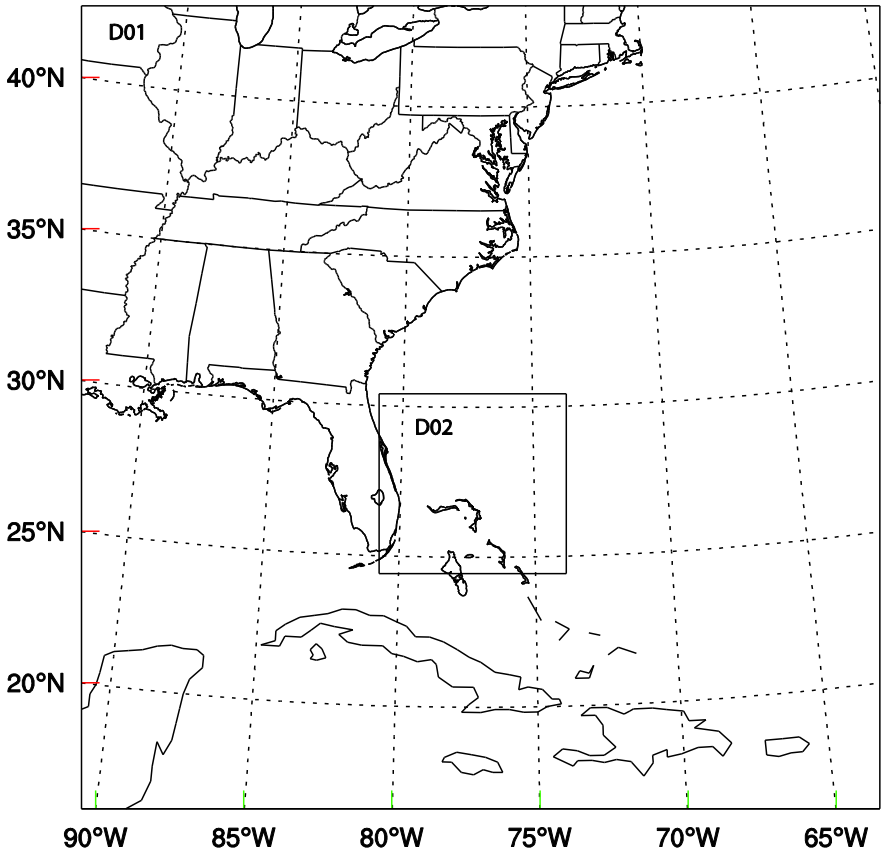

Fig. 4.3 An example of the HWRF model domain. D01 and D02 denote 9 and 3 km grids respectively.

(Troen and Mahrt 1986), surface layer parameterization (Sirutis and Miyakoda 1990) and Land/water surface parameterization scheme (Tuleya 1994), HWRF short wave (Lacis and Hanson 1974) and long wave (Fels and Schwarzkopf 1975; Schwartzkopf and Fels 1991) radiation parameterization schemes.

b. The airborne radar data processing

The radial velocity data retrieved from the tail Doppler radar aboard NOAA P-3 aircraft are assimilated in this study. The airborne radar observations are collected and processed for data quality control during flight missions. The data quality control includes several passes such as removing the observations that represent a reflection off sea surface, subtracting the projection of aircraft motion on the radials, and radar Nyquist velocity de-aliasing by the Hurricane Research Division (HRD; Gamache 2005). Then the data, encoded in Binary Universal Form for the Representation (BUFR) format, are sent off the aircraft for operational use.

c. The data assimilation setup

The data assimilation cycling and subsequent free forecast experiments were conducted for hurricane Irene (2011) for four NOAA aircraft missions. The TDR data were assimilated with the analysis time (also short forecast valid time) at the center of each flight leg. In other words, the TDR data were assimilated flight leg by flight leg. Other available observations such as SFMR, flight level onboard wind observations, and National Hurricane Center (NHC) best track, are used for verification. Various experiments are summarized in Table 4.1. Experiments differ based on what, if any, DA system is used for assimilating TDR data. Specifically, the experiments are designed to examine the influence of model resolution on the hurricane intensity and track forecast. The key technique is the dual resolution hybrid where ensemble covariance and extended control variable are calculated at 9 km grid and analysis (increment) is calculated at 3 km grid.

All DA experiments consist of three stages. 1) Spinup forecast to produce background fields and flow-dependent covariance at the beginning of DA cycles (the center of first flight leg). EnKF ensemble initial and lateral boundary conditions (BCs) are interpolated from the experimental Global Forecast System (GFS)/EnKF ensemble (Hamill et al. 2011), a high-resolution version (T382L64) of the NCEP GFS. HWRF control runs (NoDA, GSI, and hybrid) use the average of initial and boundary conditions of EnKF ensemble members. GFS/EnKF ensemble forecast are initialized every 6 hour. TDR data are usually available around 00 UTC and 12 UTC with a time window of about 6 hours. Therefore the spinup forecast time can be 3-9 hours. 2) DA cycles for assimilation of TDR data leg by leg. The length of the analysis cycle, determined by flight time between the centers of two legs, is usually 1-1.5 hours. The DA time window varies 2-5 hours for 2-5 cycles. 3) An about 48-h deterministic forecast initialized by the analysis at the end of the assimilation cycles in stage 2. Table 1 shows all experiments and their purpose performed in this study

Table 4.1 List of experiments

Experiments	Description	Purpose
dualHYB1way93	Hybrid analysis and free forecast are at 9 and 3 km grids. The 9 km and 3 km Hybrid background covariances are estimated from ensemble forecast updated by EnKF at 9 km grid.	Test if dual resolution hybrid DA is better than single resolution hybrid DA
dualHYB2way93	The same as dualHYB1way93 except that EnKF analysis mean is replaced by 9 km hybrid analysis.	Test if the re-center method is better than others.
sinHYBe1w9	Hybrid analysis and free forecast is at 9 km single grid only. Hybrid background covariances are estimated from ensemble forecast in dualHYB1way93.	Test single resolution hybrid DA
sinHYBe1w93	The same as sinHYB1way9 except that 9 km and 3 km nested grids are used during free forecast.	compare single resolution hybrid DA with dualHYB1way93
sinHYBe2w93	The same as sinHYBe1w93 except Hybrid background covariances are estimated from ensemble forecast in dualHYBe2w93.	Compare single resolution hybrid DA with dualHYB2way93

sinHYBe1w9 is a hybrid DA experiment using flow dependent covariance estimated from EnKF in one-way coupling. Single 9 km grid is used by HWRF model forecast and GSI analysis during spinup, DA cycling, and free forecast. Results from sinHYBe1w9 show how flow dependent covariance works. This experiment is a control run to be compared with all others.

sinHYBe1w93 is similar to sinHYBe1w9 with exception that 9/3 km nested grids are used for free forecast.

dualHYBe2w93 is a hybrid DA experiment using flow dependent covariance estimated from EnKF in two-way coupling. Nested 9/3 km grids are used by HWRF model forecast and GSI analysis during spinup, DA cycling, and free forecast. The EnKF ensemble perturbations and extended control variables remain at 9 km grid for 3 km analysis.

dualHYBe1w93 is similar to dualHYBe2w93 with exception that one-way coupling used between EnKF and hybrid.

Compared with early studies where same domain coverage is used by high (control run) and low (ensemble members) resolutions, using nested grids should be a cheaper method. Results from dualHYBe2w93 show how a combination of dual resolution, nest grids and two-way coupling works best. Additional experiments are performed to evaluate various configurations of forecast and analysis.

4.4 Results and discussion

a. Single observation test for equivalence between EnKF and Hybrid

As discussed in Section 2, a recursive filter is used by the hybrid 3DVAR while the Gaspari and Cohn (1999) fifth-order correlation function is used by EnKF for covariance localization. We configure and tune correlation length scales in hybrid 3DVAR and EnKF based on Gaspari and Cohn (1999) function so that the hybrid

3DVAR and EnKF may use equivalent localization.

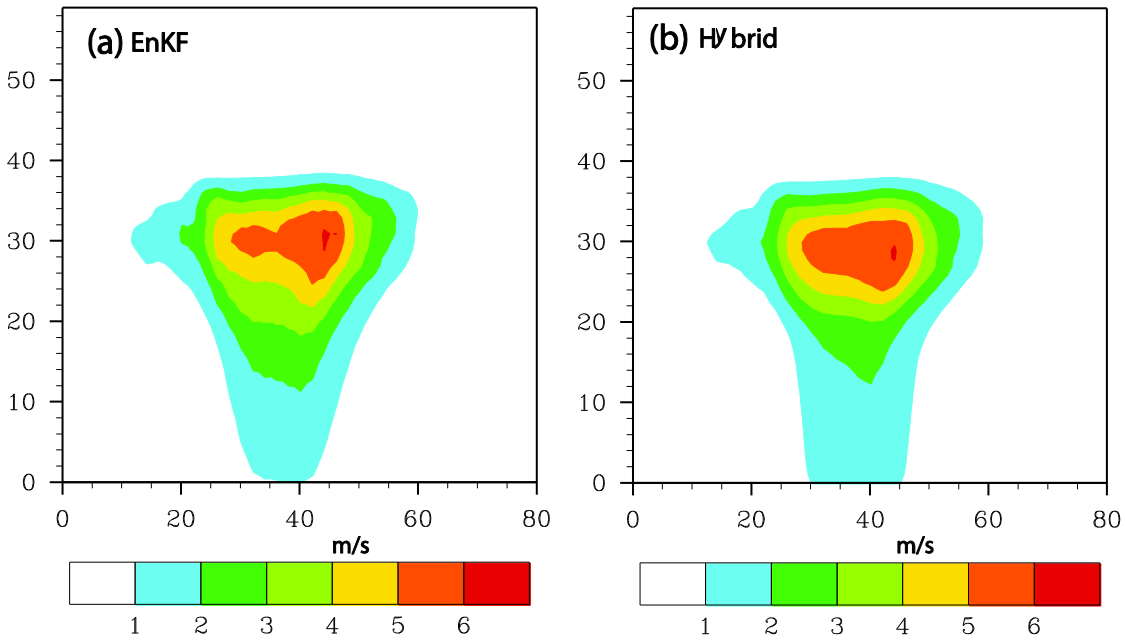

Fig. 4.4 Vertical cross sections of the wind speed increment (interval of 1 m s^{-1}) using a single radial velocity with an innovation of 8 m s^{-1} located at (34.78°N, 76.78°W; 535 hPa) for 2130 UTC 25 August 2011. Axis are marked by vertical levels and horizontal grid points.

Figure 4.4 shows the cross section of wind speed analysis increment from EnKF (Fig. 4.4a) and hybrid 3DVAR (Fig. 4.4b) using a single radial velocity with an innovation of 8 m s^{-1}. The overall increment patterns of EnKF and hybrid are very similar. Specifically, in both EnKF and hybrid 3DVAR, a maximum increment of about 6 m s^{-1} is found at level 30 and grid 44. The 1 m s^{-1} increment touches surface (level 0) and reaches level 38. At about level 30, the 1 m s^{-1} increment is found horizontally from grid 12 to grid 57. We also can see other increment contour lines such as 2, 3, 4, 5 m s^{-1} show very similar for location and shape. The similarity here is consistent with

that between EnKF and hybrid 3DVAR in Zhang et. al (2013), where a 1-K innovation is used.

b. Wind and temperature analysis increments

To evaluate the impact of dual resolution interpolation from 9 km grid to 3 km grid, we first look at the structure and magnitude of wind analysis increments. Fig.4.5 shows the 700 hPa wind increments with background from nested 9 km (Fig. 4.5a) and 3 km (Fig. 4.5b) grids for first DA cycle that assimilates radial velocity from first flight leg. Both analyses use the same 9 km grid forecast ensemble perturbations for covariance estimation. Meanwhile the 9 and 3 km grid background may be generally similar as two-way nested method is applied. The main difference between 9 and 3 km analysis is caused by dual resolution interpolation L, innovation $y^{0'}$, and H(x). We can see both increments show similar cyclonic increment near observed hurricane center. The increment patterns over other places are also close to each other. But the increment magnitude of 3 km grid (Fig. 4.5b) is obviously larger than that of 9 km grid at east and west sides of eye walls as higher resolution can capture more detailed features such as peak values. Based on these similarity and difference, we can deduce the dual resolution algorithm is effectively working.

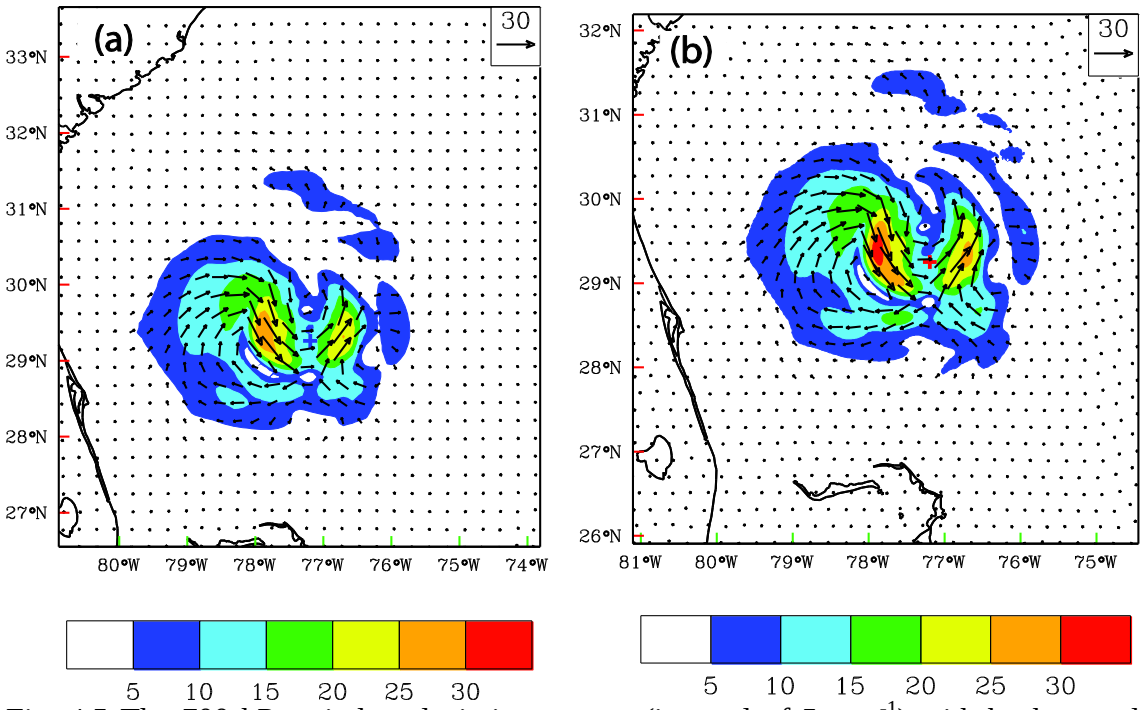

Fig. 4.5 The 700 hPa wind analysis increments (interval of 5 m s^{-1}) with background from nested grids at (a) 9 km, (b) 3 km at 0930 UTC 26 August 2011.

Because only radial velocity data is assimilated in this study, any increment in temperature is a result of balance relationship applied (if any) and/or due to cross covariance in the background error. Fig. 4.6 shows the 700-hPa temperature increments for dualHYBe2w93 (Fig. 4.6a) and sinHYBe1w9 (Fig. 4.6b) after assimilating radial velocity data for the first cycle. First of all, both dualHYBe2w93 and sinHYBe1w9 have warming core increment, with maximum ranging from 0.5^{o} to 1^{o}, near the observed hurricane center indicated by a cross sign. Based on the hydrostatic

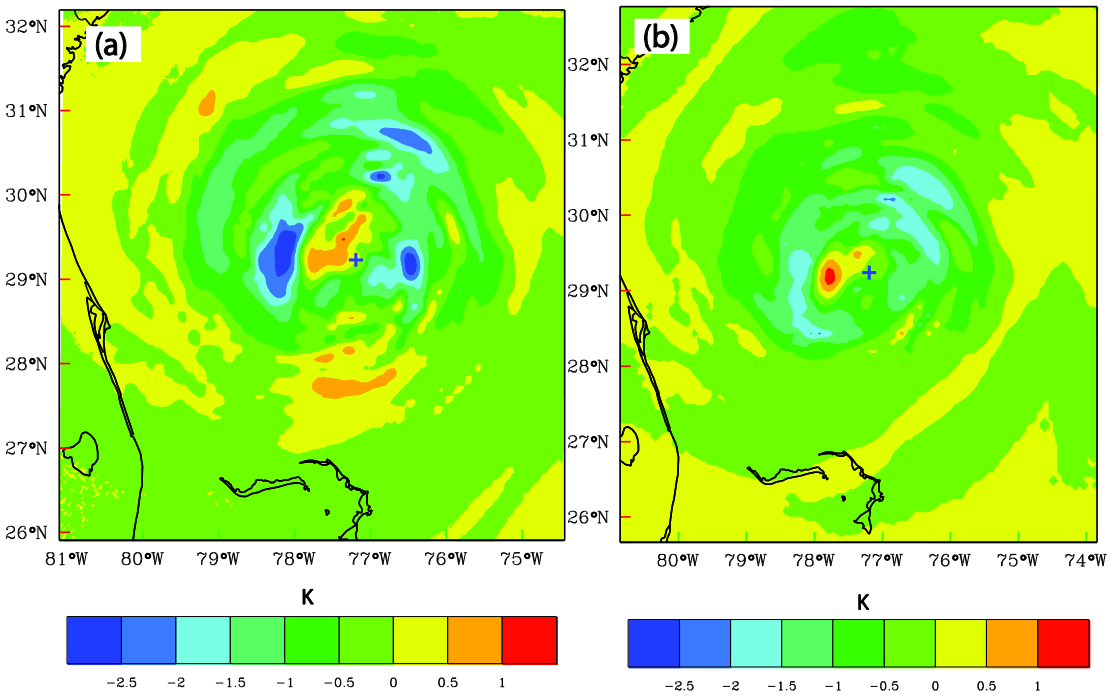

Fig. 4.6 The 700 hPa temperature analysis increments (at intervals of 0.5 K) for (a) dualHYBe2w93, (b) sinHYBe1w9 at 0930 UTC 25 August 2011.

relationship in core region the hurricane central pressure is negatively proportional to the temperature. In addition, gradient wind is the first order approximation. Therefore this warming core increment is consistent with cyclonic wind increment as both of them result in an enhancement of weaker background hurricane. Though we cannot make conclusion which experiment is better based on the temperature increment magnitude, the increment structures show that dualHYBe2w93 (Fig. 4.6a) contains more detailed hurricane like spiral bands than sinHYBe1w9 in the eye wall and outer area. We know small scale convections exist in hurricane circulation and are very important for hurricane sustaining. For this aspect, dualHYBe2w93 is superior to sinHYBe1w9. We

speculate such an advantage of dualHYBe2w93 comes from higher resolution background and corresponding innovation as covariance is of the same resolution for both experiments.

c. The hurricane structures

We now examine the structure of the hurricane at the end of the DA cycles at 1

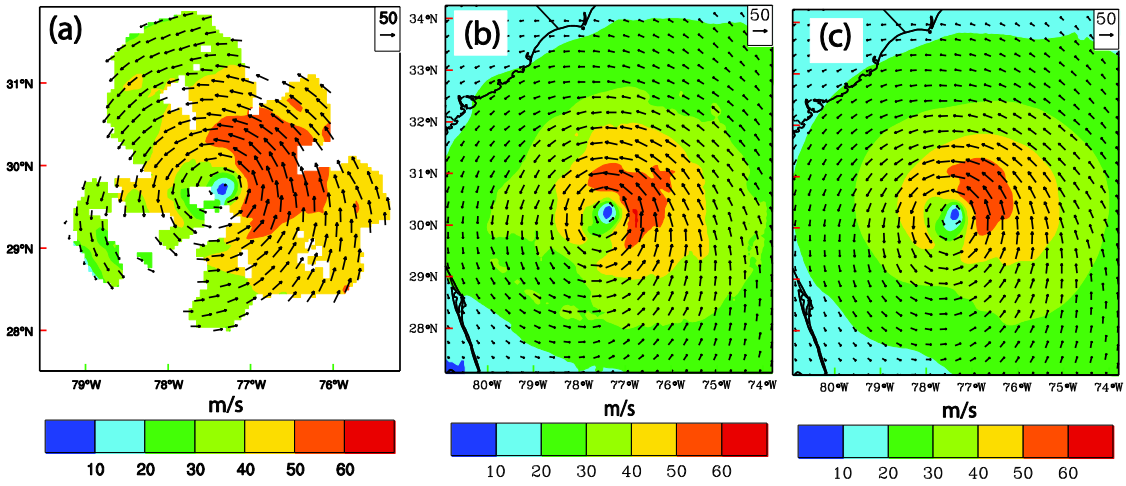

Fig. 4.7 Wind vector and speed (shaded, interval of 10 m s^{-1}) at 1-km height. (a) HRD TDR Vr analysis. The final analyzed wind for (b) dualHYBe2w93, and (c) sinHYBe1w93 at 1300 UTC 26 September 2011.

km height and at vertical cross section through the analyzed hurricane center at 13 UTC 26 Aug. 2011. The model winds from dualHYBe2w93 and sinHYBe1w93 (sinHYBe1w9 using the same analysis as sinHYBe1w93) are compared with the three dimensional hurricane-relative wind analysis derived by HRD based on the quality-controlled TDR radial velocity. Fig. 4.7 shows the model wind and TDR Vr wind

analysis at 1 km height. The Vr wind analysis covers most area of the hurricane inner core with maximum wind speed at northeast quadrant to the hurricane center. Similar to Vr wind analysis, maximum wind speed in dualHYBe2w93 and sinHYBe1w93 was also located northeast quadrant to the hurricane center. The maximum wind speed (50 - 60 m s^{-1}) in dualHYBe2w93 covers larger area and also closer to Vr wind analysis (50 – 60 m s^{-1}) than sinHYBe1w93. Therefore, dual resolution is superior to single low resolution for 1 km wind analysis.

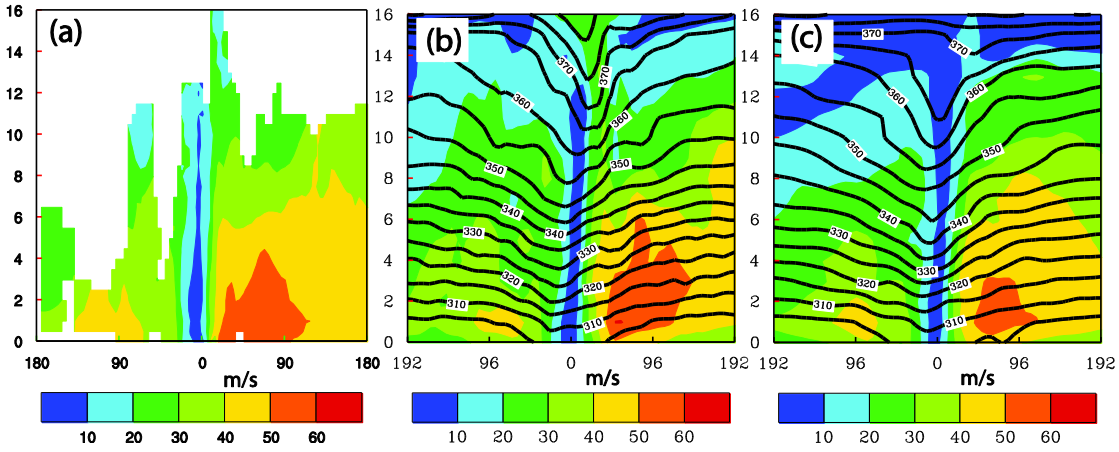

Fig. 4.8 Vertical cross section of wind speed (interval of 10 m s^{-1}, shaded). (a) HRD TDR Vr analysis. The final analysis wind for (b) dualHYBe2w93, and (c) sinHYBe1w93 at 1300 UTC 26 September 2011. Error! Reference source not found.

Figure 4.8 shows the vertical cross sections of horizontal wind speed and potential temperature for TDR Vr wind analysis, dualHYBe2w93 and sinHYBe1w93 final analysis at 13 UTC 26 Aug. 2011. The locations of cross sections are west-east through the analyzed hurricane center. First, the potential temperatures in eye region bend down for both dualHYBe2w93 and sinHYBe1w93 with an exception that sinHYBe1w93 has a little flat contour line above 14 km. This reflects the warm core with sinking motion

and therefore is consistent with existing theory. In Vr wind analysis, the hurricane eye is clearly shown with maximum wind speed on east eye wall where the large wind for 50 – 60 m s^{-1} is below 4 km height. Similar to Vr wind analysis, in dualHYBe2w93 and sinHYBe1w93, there is also large wind for 50 – 60 m s^{-1} on east eye wall below 4 km height. However, the area of 50-60 m s^{-1} wind in dualHYBe2w93 is larger and closer to Vr analysis than that in sinHYBe1w93. Based on both horizontal and vertical wind analysis, dualHYBe2w93 is better than sinHYBe1w93.

The experiments dualHYBe2w93, sinHYBe1w93, and sinHYBe1w9 are further evaluated by inter-comparison and comparison between model forecast winds and Vr analysis during forecast. Specifically, we compare 11 hour HWRF forecast winds with Vr analysis winds at 00 UTC 27 Aug. 2011. Fig. 4.9 shows the model wind and TDR Vr wind analysis at 1 km height. The Vr wind analysis roughly shows the hurricane inner core area with maximum wind speed at northeast quadrant (50-60 m s^{-1}). Similar to Vr wind analysis, maximum wind speed in dualHYBe2w93 was also

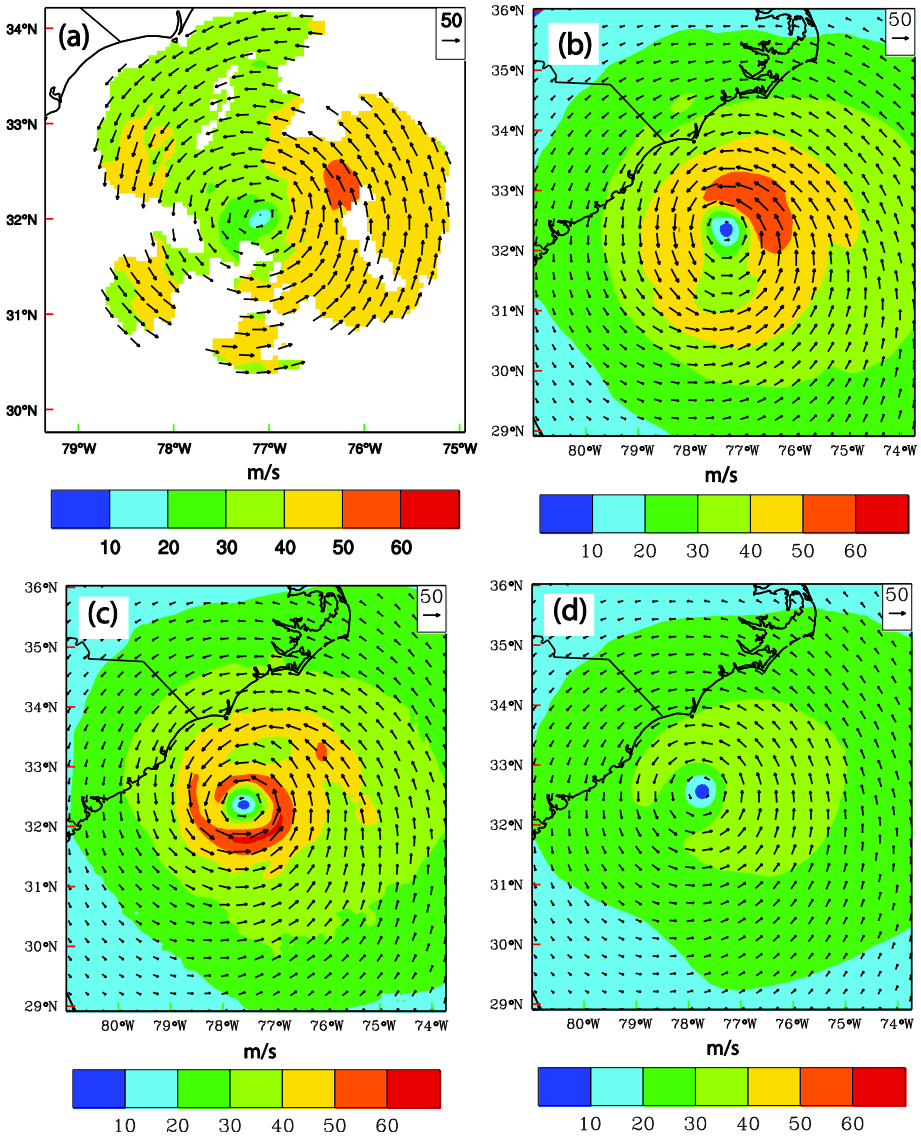

Fig. 4.9 Wind vector and speed (interval of 10 m s^{-1}, shaded) at 1-km height. (a) HRD TDR Vr analysis. The HWRF forecast wind for (b) dualHYBe2w93, (c) sinHYBe1w93, and (d) sinHYBe1w9 at 0000 UTC 27 September 2011.

located northeast quadrant (50-60 m s^{-1}). On contrary, the large wind speed (50 - 60 m s^{-1}) in sinHYBe1w93 almost forms a circular around hurricane center, significantly different from Vr analysis. Moreover, the maximum wind (>60 m s^{-1}) is found at south of the center rather than northeast. The sinHYBe1w9 shows too weak wind speed (< 40

m s^{-1}) that is consistent with its higher CSLP. Based on these comparisons dualHYBe2w93 forecast wind is better than both sinHYBe1w93 and sinHYBe1w9.

Figure 4.10 shows the vertical cross sections of forecast horizontal wind speed and

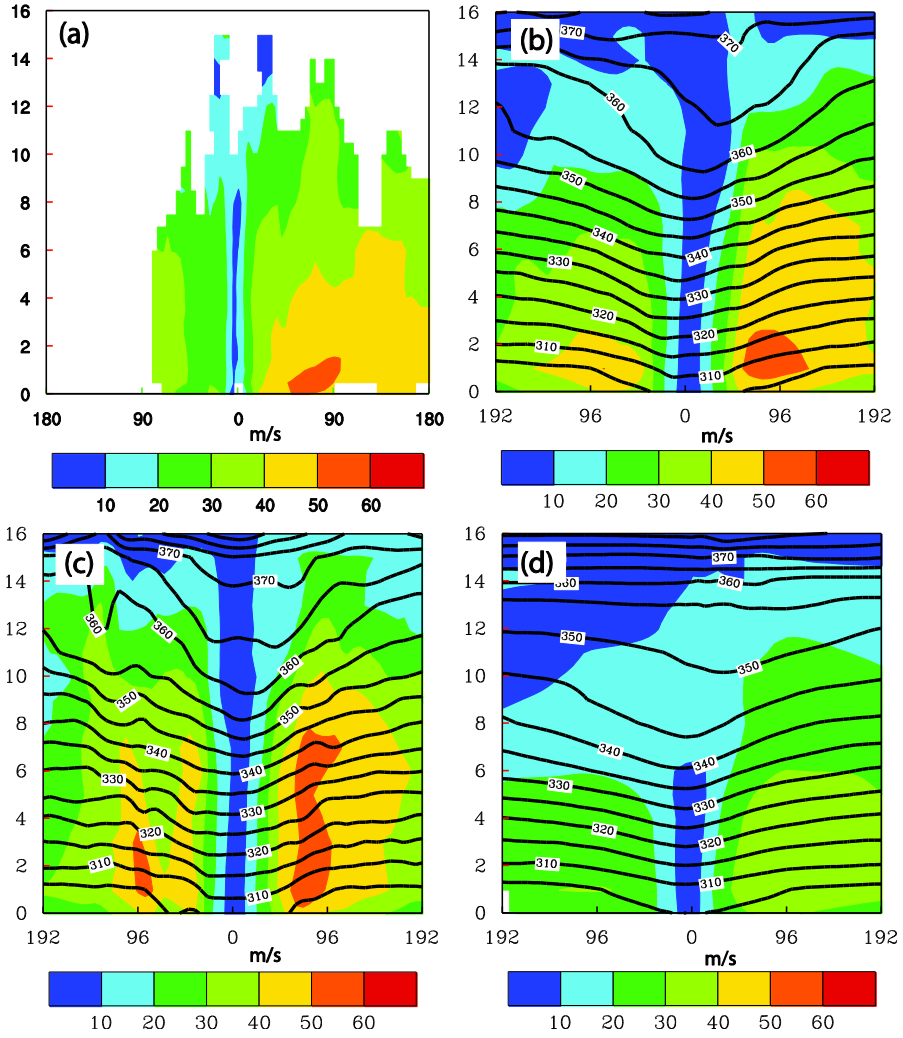

Fig. 4.10 Vertical cross section of wind speed (interval of 10 m s-1, shaded). (a) HRD TDR Vr analysis. The HWRF forecast wind for (b) dualHYBe2w93, (c) sinHYBe1w93, and (d) sinHYBe1w9 at 0000 UTC 27 September 2011.

potential temperature for dualHYBe2w93, sinHYBe1w93, and sinHYBe1w9, as well as TDR Vr wind analysis at 00 UTC 27 Aug. 2011. The locations of cross sections are

west-east through the analyzed hurricane center. In Vr wind analysis, the hurricane eye is clearly shown with low wind speed less than 10 m s^{-1} at the center and maximum wind speed (50 – 60 m s^{-1}) on east eye wall. Similar to Vr wind analysis, in dualHYBe2w93, there is also large wind for 50 – 60 m s^{-1} on east eye wall. On the contrary, sinHYBe1w9 shows too small wind speed with maximum wind less than 40 m s^{-1}. Meanwhile, the eye defined by wind speed less than 10 m s^{-1} is only found below 6 km. And the potential temperature contour lines above 10 km is much flattened compared with that in dulHYBe2w93. Both temperature and wind in sinHYBe1w9 show a weaker hurricane than Vr analysis. While sinHYBe1w93 shows similar magnitude of maximum wind (50-60 m s^{-1}) on east eye wall the coverage of such maximum wind extends up to 8 km height that is higher than counterpart in Vr analysis and dualHYBe2w93. We can also conclude that dualHYBe2w93 is better than sinHYBe1w93 and sinHYBe1w9 based on comparison among forecast wind and Vr analysis.

Base on CSLP and maximum wind forecast we can see sinHYBe1w9 produces weakest hurricane (weaker than best track) and intensities from dualHYBe2w93 and sinHYBe1w93 are mixing. Moreover the trend of forecast intensities from dualHYBe2w93 and sinHYBe1w93 generally follow the best track which is consistent with above hurricane structure comparison.

d. The precipitable water

In the previous sections, we see that the forecast winds in the sinHYBe1w9 are

weaker than that in dualHYBe2w93 and sinHYBe1w93. We speculate that simulated hurricanes in all these three experiments share the same environment such as large scale air flow and sea surface conditions. It is recognized that the same sea surface condition (e.g., sea water temperature) may affect hurricane differently due to various factors (e.g., surface wind). Nevertheless we examine other model fields such as precipitable water that may explain wind difference. We assume high precipitable water is related to large latent heating and then enhances hurricane intensity such as maximum winds. Fig. 4.11 shows precipitable water for dualHYBe2w93, sinHYBe1w93, and sinHYBe1w9. For precipitable water at final analysis at 1300 UTC 26 Aug. 2011, all dualHYBe2w93 (Fig. 4.11a), sinHYBe1w93 (Fig. 4.11b), and sinHYBe1w9 (Fig.4.11c) show hurricane like spiral bands. Generally speaking, the magnitude of precipitable water in dualHYBe2w93, sinHYBe1w93, and sinHYBe1w9 are similar where the maximum precipitable water in dualHYBe2w93 and sinHYBe1w93 (the same as sinHYBe1w9) is a little larger than 90 mm. The dualHYBe2w93 with dual resolution analysis shows more detailed small scale convective features than sinHYBe1w93 with low resolution

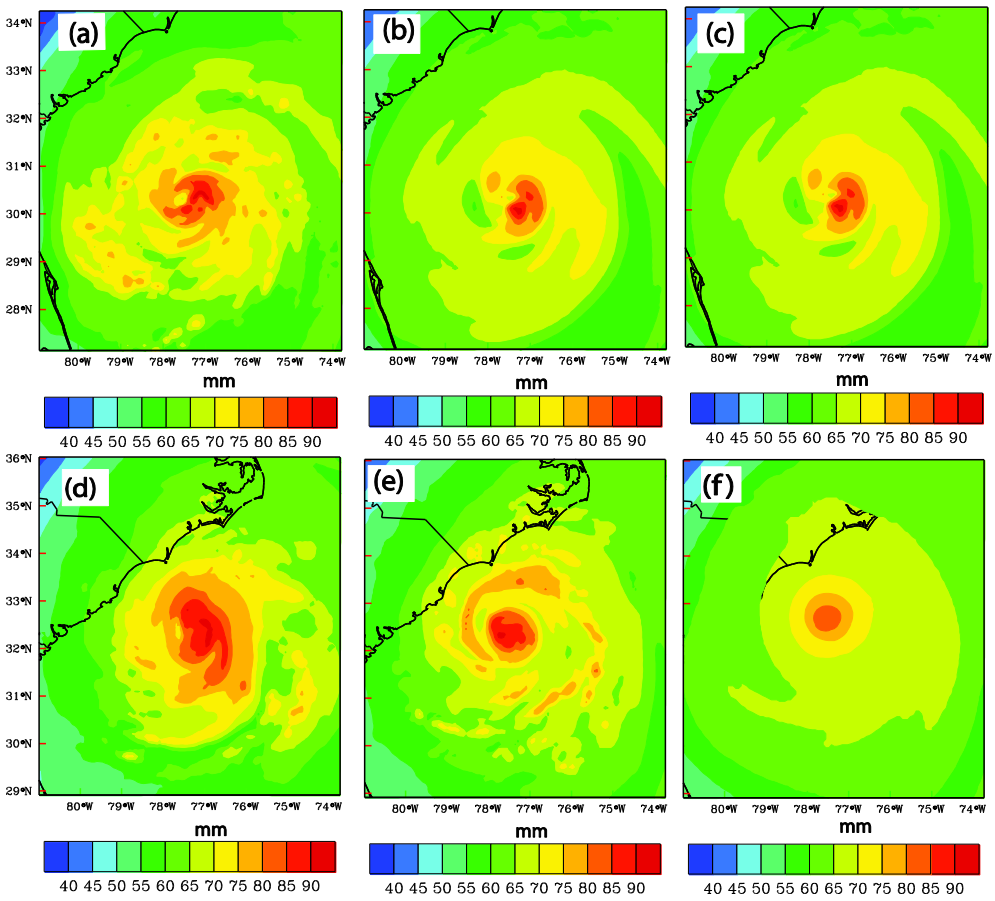

Fig. 4.11 Precipitable water (interval of 5 mm) for final analysis by (a) dualHYBe2w93, (b) sinHYBe1w93, and (c) sinHYBe1w9 at 1300 UTC 26 September 2011 and forecast by (a) dualHYBe2w93, (b) sinHYBe1w93, and (c) sinHYBe1w9 at 0000 UTC 27 September 2011.

analysis. For the 12-h forecast at 00 UTC 27 Aug. 2011, sinHYBe1w9 (Fig. 4.14f) shows much smoother and smaller precipitable water than dualHYBe2w93 (Fig. 4.11d) and sinHYBe1w93 (Fig. 4.11e). Specifically, the hurricane like spiral bands are found only in dualHYBe2w93 and sinHYBe1w93. The maximum precipitable water in dualHYBe2w93 and sinHYBe1w93 is about 90 mm while that in sinHYBe1w9 is about 80 mm. Recall that the 12-h wind forecast in sinHYBe1w9 (Fig. 4.10) is also obviously

smaller and smoother than dualHYBe2w93 and sinHYBe1w93. Thus the wind and precipitable water forecast are consistent with each other. We deduce latent heating that is positively proportional to precipitable water may play important role for hurricane intensity.

Having much difference of precipitable water, sinHYBe1w9 and sinHYBe1w93 share all settings except dual and single resolutions as well as cumulus parameterization turned on for sinHYBe1w9 and off for 3 km grid of sinHYBe1w93. To evaluate the cumulus parameterization contributing to precipitable water, a modified sinHYBe1w9 experiment with cumulus parameterization turned off was carried out and shows only small change of precipitable water compared with original sinHYBe1w9. Thus we speculate dual resolution may be major factor causing different precipitable water between sinHYBe1w9 and sinHYBe1w93.

e. The track and intensity forecast RMSEs

To further evaluate the quality of analyses produced by different DA methods including dualHYBe2w93, dualHYBe1w93, sinHYBe1w93, and sinHYBe1w9, deterministic forecasts initialized from the final analyses at 12 UTC 24, 12 UTC 25, 00 UTC 26, and 12 UTC 26 are launched. The 48 hours track forecasts based on the at 6-h interval output of four cases are verified by calculating RMSE against NHC best track in Fig. 4.12a. The position of the forecast hurricane of our experiments is defined by HWRF utility “GFDL Vortex Tracker”. The initial track errors are about 20-30 km for all four experiments. With some oscillation, the track errors increase with forecast lead

time. No matter what level of the errors among four experiments is, it is clearly seen that the forecast track errors increase in order of dualHYBe2w93, dualHYBe1w93, sinHYBe1w93, and sinHYBe1w9. By the end of the 48 hours forecast, the track errors are 80, 95, 110, and 135 km for dualHYBe2w93, dualHYBe1w93, sinHYBe1w93, and

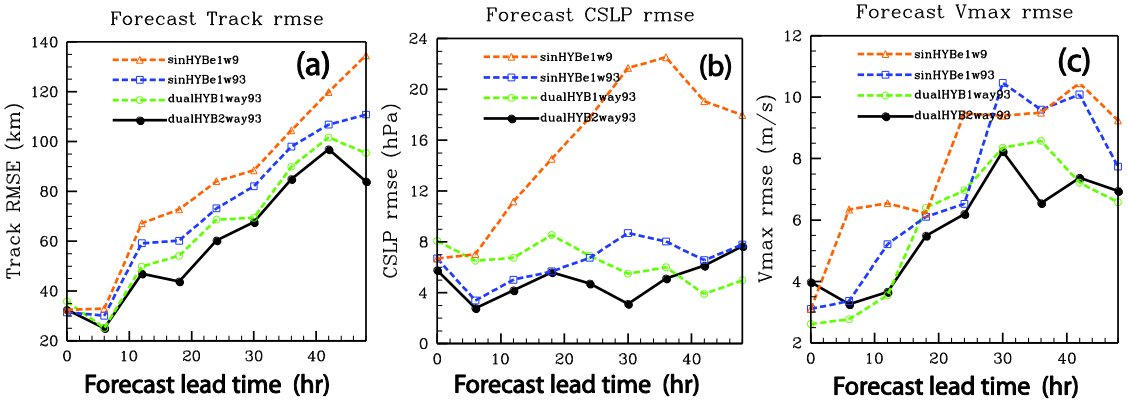

Fig. 4.12 Deterministic forecast RMSEs for (a) tracks and (b) central sea level pressure (hPa), (c) maximum wind by dualHYBe2w93, dualHYBe1w93, sinHYBe1w93, and sinHYBe1w9 as compared to NHC best track estimates from 1300 UTC 26 through 1200 UTC 28 August 2011.

sinHYBe1w9 respectively. Given that our DA experiments do not include environmental observations, the main effect on the track should come from the changes to the inner core structure of the analyzed hurricane that is related to different analysis methods. We may deduce that, in terms of track forecast, dual resolution is better than single coarse resolution for either DA step or free forecast. And two-way coupling is better than one-way coupling. Using the same numerical model and observations

assimilated, better DA method results in better analysis and further produces smaller track forecast errors.

The forecast CSLP RMSEs are shown in Fig. 4.12b. It is seen that CSLP RMSEs ranges from 6-8 hPa for all experiments of dualHYBe2w93, dualHYBe1w93, sinHYBe1w93, and sinHYBe1w9. As forecast lead time increases, the RMSEs depart for experiments that CSLP RMSE for sinHYBe1w9 grows up to 18 hPa while the RMSEs for the other three experiments still range from 4-8 hPa at 48 hour forecast lead time. For most forecast valid time dualHYBe2w93 produces smallest CSLP RMSEs while sinHYBe1w9 has largest RMSEs. It is noted that comparison between dualHYBe1w93 and sinHYBe1w93 is mixing. We further examine maximum wind RMSEs (Fig. 4.12c). It is found that the error levels increase in the order of dualHYBe2w93, dualHYBe1w93, sinHYBe1w93, and sinHYBe1w9 for most forecast lead times. We notice maximum wind RMSE for sinHYBe1w9 is largest though it does not depart from others too much as in CSLP RMSEs. Based on both CSLP and maximum wind RMSEs, dualHYBe2w93 performs best and sinHYBe1w9 is worst.

4.5 Summary and conclusions

In this study, the GSI 3DVar-based hybrid EnKF-Var data assimilation system including both the Var and EnKF components were expanded to HWRF for the prediction of hurricanes Irene (2011). In the hybrid DA system, the flow-dependent ensemble covariances were estimated from an EnKF-generated ensemble and incorporated into the variational minimization by using the extended control variable

method. Forecasts of a 40 member ensemble and control runs are performed. The analysis ensemble is generated by updating each forecast ensemble member with EnKF in a manner of a serial implementation of the square root ensemble Kalman filter (EnSRKF) system. The NOAA P-3 air borne Doppler radar radial velocity is for first time assimilated by this EnKF system, which is interfaced with GSI by using the same data quality control and observation operator. In GSI system, the radar data thinning method is further enhanced (e.g., fore and aft sweeps are separated when thinning). Thus in a three dimensional box two radial velocities are selected from two different directions (e.g., 50^o from each other). Such an enhanced part of the thinning method is implemented into EMC operational data assimilation system.

The tail Doppler radar radial velocity is assimilated leg by leg of an NOAA P-3 flight missions around 12 UTC 24, 12 UTC 25, 00 UTC 26, 12 UTC 26 Aug. 2011. We examine the difference of using dual resolution and single resolution methods when assimilating airborne radar observations by comparing both analysis and forecast with various kinds of observations. The examinations are based on four experiments in this study. A DA experiment sinHYBe1w9 is a hybrid DA experiment using flow dependent covariance estimated from EnKF in one-way coupling between EnKF and hybrid. Single 9 km grid is used by HWRF model forecast and GSI analysis during spinup, DA cycling, and free forecast. Results from sinHYBe1w9 show how flow dependent covariance works. This experiment is a control run to be compared with all others. sinHYBe1w93 is similar to sinHYBe1w9 with exception that 9/3 km nested grids are used for free forecast.

dualHYBe2w93 is a hybrid DA experiment using flow dependent covariance

estimated from EnKF in two-way coupling. Nested 9/3 km grids are used by HWRF model forecast and GSI analysis during spinup, DA cycling, and free forecast. The EnKF ensemble perturbations and extended control variables remain at 9 km grid and all other steps are performed at 3 km grid during DA minimization so that computation is reduced. dualHYBe1w93 is similar to dualHYBe2w93 with exception that one-way coupling used between EnKF and hybrid.

The results of analyses and forecasts from the four experiments are verified against best-track data, radar wind measurements. The main conclusions are summarized in the following.

Comparison between dual resolution and single resolution increments shows that dual resolution produces more detailed TC-like spiral bands structures than single low resolution, while the overall patterns of increment are alike between them (e.g., both has warm core increment). Case study shows dual resolution forecast wind is closer to radar composite wind than single resolution forecast wind though dual and single resolutions produce similar analysis wind. These demonstrate dual resolution method works well and is superior to single resolution.

The track forecast root mean square errors (RMSE) based on 4 cases and NHC best track are compared among four experiments. The error level at all forecast leading times increases with experiments of dualHYBe2w93, dualHYBe1w93, sinHYBe1w93, sinHYBe1w9. It means, for track forecast, two-way coupling is better than one-way coupling. Dual resolution analysis is better than single resolution analysis. Nested grids are better than single low resolution for free forecast.

We use central sea level pressure (CSLP) and maximum wind to evaluate the

hurricane intensity forecast. For central sea level pressure RMSE, dualHYBe2w93 performs best with least RMSE at most forecast lead times. Meanwhile, sinHYBe1w9 produces largest RMSE for almost all forecast lead time. The comparison between dualHYBe1w93 and sinHYBe1w93 is mixing. Yet dualHYBe1w93 and sinHYBe1w93 are much closer to dualHYBe2w93 than to sinHYBe1w9 in terms of CSLP RMSE. We may draw that dual resolution analysis and forecast is superior to single resolution as the former can process more detailed feature than the latter.

Maximum wind RMSEs among four experiments do not show as much difference as CSLP RMSEs. Even so, we still can see dualHYBe2w93 and dualHYBe1w93 perform better than sinHYBe1w9. The performance of sinHYBe1w93 is between them. The dual resolution again is better than single resolution for maximum wind forecast.

Through one Vr observation test, we see that the analysis increment sinHYBe1w9 and EnKF are very similar to each other. There are a little more difference between sinHYBe1w9 and EnKF when many observations are used. This may be caused by the complex interactions among data and DA methods. We need to do further investigation on the compatibility between sinHYBe1w9 and EnKF.

We note that this study represents the first attempt of applying the GSI 3DVar-based dual resolution hybrid EnKF-Var data assimilation method interfaced with HWRF model to hurricane and radar data assimilation. We also note that the above conclusions and findings are based on only 4 flight mission of a hurricane reconnaissance. This paper may be considered as a pioneer of afterwards research for many hurricane cases and operational runs with the same procedures presented here.

Chapter 5

Summary and Future Plan

5.1 General Summary

Atmospheric data assimilation that combines observation and forecast model state can provide initial condition for weather forecast numerical models. The quality of the initial conditions relies on greatly the data assimilation algorithms. Traditional 3DVAR used static background error covariance that usually is a statistics of history atmosphere state. Therefore such a covariance does not reflect current atmosphere flow and is not suitable for weather systems such as hurricane. Recently Ensemble Kalman filter (EnKF) is applied for atmosphere data assimilation, where ensemble forecasts are used to estimate and evolve flow-dependent error covariance statistics. While EnKF using flow-dependent covariance is superior over traditional 3DVAR using static covariance, it is not easy to incorporate constraints into EnKF. Now the ensemble variational (EnsVar) method is developed and applied for atmosphere data assimilation. In ensemble variational method static covariance is replaced (or partly) by flow dependent covariance calculated from ensemble forecasts. Therefore ensemble variational method takes advantages from both EnKF and variational method. In this research we refer ensemble variational method also as hybrid. Today ensemble variational method has several combinations. For example, both ensemble and variational methods are three dimensional. Second, ensemble is four dimensional but variational method is three dimensional. Also ensemble is three dimensional and varitional is four dimensional. For terminologies and differences among these combinations, please see Wang and Lei 2014. In this research we mainly use three

dimensional ensemble and variational method, which is very easily modified to include four dimensional ensemble. Ensemble variational method is one of the most popular data assimilation methods among the research community today.

One of the important applications of hybrid method is numerical analysis and prediction of hurricanes. Study of hurricane has not only practical but also theoretical significances. Hurricane could make tremendous damage of property and life. Meanwhile further investigation for hurricane formation, development, structure, and movement is still needed.

Radar is one of the most important observations for hurricane as there is little or none of other observations oversea. While radar could provide spatially and temporarily dense data, it is still a challenge to assimilate it. Both radar radial velocity and reflectivity are not model state quantity. Proper assimilation method is naturally required.

This research consists of advanced data assimilation methods such as EnKF and ensemble-variational algorithms. The first part is for ground based radar WSR 88D data assimilation and the second and third parts are for airborne tail Doppler radar data assimilation. WSR 88D radar radial velocity data is assimilated by the WRF ensemble-3DVar hybrid system for the prediction of Hurricane Ike (2008). The airborne tail Doppler radar radial velocity data is assimilated by GSI-based hybrid EnKF 3DVar system for the prediction of Hurricane Irene (2011).

In Chapter 2 of this research, the WRF hybrid ensemble-3DVAR data assimilation (DA) system is applied for the first time to the assimilation of radial velocity data for a landfalling hurricane. Basically, radial velocity data from two land

base WSR-88D radars along the Gulf of Mexico coast are assimilated after Hurricane Ike (2008) moved into the coverage of the two radars.

We conducted five experiments including a forecast experiment without assimilating any radar data or other observation is initialized directly from the operational GFS analysis; 3DVAR methods that use the static covariance; the hybrid DA system using purely flow-dependent background covariance or using half static and half flow-dependent covariance, respectively. The main conclusions are summarized in the following.

For temperature analysis, hybrid method produces hurricane warm core structure with positive temperature increment at the center. On the contrary, 3DVAR method produces negative temperature anomalies at lower levels in the eye region with much weaker and smoother temperature increments that are negative at the center of hurricane. All three radar DA experiments created analyses that fit the Vr data well. Most of the minimum sea level pressure reduction is achieved through WRF model adjustment during the short forecast step of the assimilation cycles

Compared with experiments without radar DA, the hybrid experiments improve the Ike track forecast slightly. All radar DA experiments produce intensity forecasts closer to the NHC best track observation.

Compared with 3DVAR method, hybrid produces much better fit of forecast radial velocity to radar observations. This means hybrid analysis is of overall better quality than 3DVAR, producing more dynamically consistent state estimations that lead to later slower error growth during forecast. The equitable threat scores (ETSs) for 3-hour accumulated precipitation forecasts in the hybrid experiments are higher than those of

3DVAR for the thresholds and lead times considered indicating again the superior quality of the hybrid DA method. We also notice that combination of half static and half ensemble background covariance did not improve the results over pure flow-dependent covariance.

In Chapter 3 of this research, the GSI 3DVar-based hybrid EnKF-Var data assimilation system including both the Var and EnKF components were expanded to HWRF for the prediction of hurricane Irene (2011). We couple EnKF and GSI 3DVar to provide the flow-dependent ensemble covariances into the variational minimization by using the extended control variable method. A serial implementation of the square root ensemble Kalman filter (EnSRF) system is used to update each forecast ensemble member. To the author's best knowledge, the air borne Doppler radar radial velocity is for first time assimilated by this hybrid system. In GSI system, the original radar data thinning method is further enhanced. Such an enhanced part of the thinning method is transferred and implemented into EMC operational data assimilation system.

The tail Doppler radar radial velocity is assimilated for an NOAA P-3 flight mission on 25 – 26 August 2011. We compared the results from hybrid method using flow-dependent with the results from 3DVAR using static background covariance. Four experiments are carried out in this study including a forecast experiment without assimilating any radar data initialized directly from the global GFS analysis; a GSI 3DVAR using the static covariance; the GSI hybrid DA system using purely flow-dependent background covariance; and EnKF. The results of analyses and forecasts from the four experiments are intercompared and compared with EMC operational

forecast, NHC best-track data, radar wind measurements, in situ data, and remote sensed observations. The main conclusions are summarized in the following.

Verified with observation, we found that the hybrid analyses using flow dependent covariance successfully capture the inner-core structure of the hurricane vortex. Compared with 3DVAR and EMC operational forecast, GSI hybrid and EnKF initialized by assimilating airborne radar observations improved the hurricane track and intensity forecasts.

In chapter 4 of this research, we investigated dual resolution method. A series of experiments were performed including hybrid DA experiment using flow dependent covariance estimated from EnKF in one-way or two way coupling manner; hybrid DA dual resolution experiment with ensemble covariance at 9 km grid and analysis at 3 km grid; experiment with DA cycling at 9 km grid and free forecast at 9/3 km nested grids.

Comparison between dual resolution and single resolution increments shows that dual resolution produces more detailed TC-like spiral bands structures than single low resolution. Compared with radar wind composite for a case study, dual resolution forecast wind is better than single resolution forecast wind. This demonstrates dual resolution method is superior to single resolution.

Based on the NHC best track and for model forecast track, two-way coupling is better than one-way coupling. Dual resolution analysis is better than single resolution analysis. Nested grids are better than single low resolution for free forecast.

Central sea level pressure and maximum wind RMSE is used to evaluate the hurricane intensity forecast. According to central sea level pressure RMSE, dual resolution method using 9/3 km grids at all performs best with least RMSE at most

forecast lead times. Meanwhile, single resolution method using 9 km grid at all produces largest RMSE for almost all forecast lead time. Maximum wind RMSEs also show the dual resolution again is better than single resolution for maximum wind forecast. Therefore we may draw that dual resolution analysis and forecast is superior to single resolution as the former can process more detailed feature than the latter.

5.2 Future plan

While many experiments had been carried out during last several years, some additional research is still needed. It is supposed that using flow dependent covariance should result in better analysis and subsequent forecast than using static covariance. We still need to do more diagnostic based on existing simulations. The dual resolution analysis for 3DEnsVar is an interesting topic. The advantage of dual resolution analysis is that ensemble members can be at coarse grid and variational analysis is performed at fine grid. The capability is already available in this data assimilation system. We just use the same data and procedure to compare the results from single resolution and dual resolution analysis. Furthermore, we will assimilate satellite data such as radiance and wind, drop sounding data, and so on with this method.

References

Aksoy, A., S. Lorsolo, T. Vukicevic, K. J. Sellwood, S. D. Aberson and F. Zhang, 2012: The HWRF Hurricane Ensemble Data Assimilation System (HEDAS) for high-resolution data: The impact of airborne Doppler radar observations in an OSSE. *Mon. Wea. Rev.,* in press.

Barker, D. M., W. Huang, Y. R. Guo, A. J. Bourgeois, and Q. N. Xiao, 2004: A Three-Dimensional Variational Data Assimilation System for MM5: Implementation and Initial Results. *Mon. Wea. Rev.* , 132, 897-914.

Buehner, M., 2005: Ensemble-derived stationary and flow-dependent background-error covariances: Evaluation in a quasi-operational NWP setting. *Quart. J. Roy. Meteor. Soc.*, 131, 1013-1043.

---, P. L. Houtekamer, C. Charette, H. L. Mitchell, and B. He, 2010a: Intercomparison of variational data assimilation and the ensemble Kalman filter for global deterministic NWP. Part I: Description and single-observation experiments. *Mon. Wea. Rev.*, 138, 1550-1566.

---,--,--,--, and --, 2010b: Intercomparison of variational data assimilation and the ensemble Kalman filter for global deterministic NWP. Part II: One-month experiments with real observations. *Mon. Wea. Rev.*, 138, 1567-1586.

Burgers, G., P. J. van Leeuwen, and G. Evensen, 1998: Analysis scheme in the ensemble Kalman filter, *Mon. Wea. Rev*., 126, 1719--1724.

Cavallo, S. M., R. D. Torn, C. Snyder, C. Davis, W. Wang, and J. Done, 2013: Evaluation of the Advanced Hurricane WRF Data Assimilation System for the 2009 Atlantic Hurricane Season. Mon Weather Rev, 141, 523-541.

Courtier, P., Thépaut, J.-N. and Hollingsworth, A., 1994: A strategy for operational implementation of 4D-Var, using an incremental approach. Q. J. R. Meteorol. Soc., 120, 1367-1388

Dong, J., and M. Xue, 2013: Coastal WSR-88D Radar Data Assimilation with Ensemble Kalman Filter for Analysis and Forecast of Hurricane Ike (2008). *Quart. J. Roy. Meteor. Soc.*, 139, 467-487.

Dowell, D. C. and L. J. Wicker, 2009: Additive Noise for Storm-Scale Ensemble Data Assimilation. *J. Atmos Ocean Tech*, 26, 911-927.

Du, J., 2004: Hybrid ensemble prediction system: A new ensembling approach. Preprints, *Symp. 50th Anniversary of Operational Numerical Weather Prediction,* College Park, MD, NCEP, 4.2. [Available online at

http://www.emc.ncep.noaa.gov/mmb/SREF/hybrid_50thNWP.pdf.]

Du, N. Z., M. Xue, K. Zhao, and J. Z. Min, 2012: Impact of assimilating airborne Doppler radar velocity data using the ARPS 3DVAR on the analysis and prediction of Hurricane Ike (2008). *J Geophys Res-Atmos*, 117.

Dudhia, J., 1989: Numerical study of convection observed during the Winter Monsoon Experiment using a mesoscale two-dimensional model. J. Atmos. Sci., 46, 3077-3107.

Etherton, B. J., and C. H. Bishop, 2004: The resilience of hybrid ensemble/3D-Var analysis schemes to model error and ensemble covariance error. *Mon. Wea. Rev.*,132, 1065-1080.

Evensen G., 1994: Sequential data assimilation with a nonlinear quasi-geotropic model using Montre Carlo methods to forecast error statics [J] . J Geophys Res, 99(C5): 10143-10162.

Evensen, G., 2003: The ensemble Kalman filter: Theoretical formulation and practical implementation. *Ocean Dynamics*, 53, 343-367.

Fels, S. B. and M. D. Schwarzkopf, 1975: The simplified exchange approximation: A new method for radiative transfer calculations. *J. Atmos. Sci.*, 32, 1476-1488.

Gao, J. and M. Xue, 2008a: An efficient dual-resolution approach for ensemble data assimilation and tests with assimilated Doppler radar data. *Mon. Wea. Rev.*, 136, 945-963.

Gao, J. and M. Xue, 2008b: An Efficient Dual-Resolution Approach for Ensemble Data Assimilation and Tests with Simulated Doppler Radar Data. *Mon Weather Rev*, 136, 945-963.

Gao, J. and D. J. Stensrud, 2014: Some Observing System Simulation Experiments with a Hybrid 3DEnVAR System for Stormscale Radar Data Assimilation. *Mon Weather Rev*.

Gaspari, G. and S. E. Cohn, 1999: Construction of correlation functions in two and three dimensions. *Quart. J. Roy. Meteor. Soc.*, 125, 723-757.

Grell, G. A. and D. Devenyi, 2002: A generalized approach to parameterizing convection combining ensemble and data assimilation techniques. *Geophys Res Lett*, 29(14), Article 1693.

Halverson, J. B., J. Simpson, G. Heymsfield, H. Pierce, T. Hock, and L. Ritchie, 2006: Warm core structure of Hurricane Erin diagnosed from high altitude dropsondes

during CAMEX-4. *J Atmos Sci*, 63, 309-324.

Hamill, T. M. and C. Snyder, 2000: A hybrid ensemble Kalman filter-3D variational analysis scheme. *Mon. Wea. Rev.*, 128, 2905-2919.

Hamill, T. M., J. S. Whitaker, M. Fiorino, and S. G. Benjamin, 2011: Global ensemble predictions of 2009's tropical cyclones initialized with an ensemble Kalman filter. Mon. Wea. Rev., 139, 668-688.

Han, J. and H. L. Pan, 2011: Revision of Convection and Vertical Diffusion Schemes in the NCEP Global Forecast System. *Weather Forecast*, 26, 520-533.

Hayden, C. M. and J. Purser, 1995: Recursive filter objective analysis of meteorological fields: Applications to NESDIS operational processing. *J. Appl. Meteor.*, 34, 3-15.

Haurwitz, B., 1935: The height of tropical cyclones and the eye of the storm. *Mon. Wea. Rev.*, 63, 45-49.

Hawkins, H. F. and S. M. Imbembo, 1976: The structure of a small, intense hurricane-Inez 1966. *Mon. Wea. Rev.*, 104, 418-442.

Holland, G. J., 1997: The maximum potential intensity of tropical cyclones. *J. Atmos. Sci.*, 54, 2519-2541.

Hong, S.-Y., J. Dudhia, and S.-H. Chen, 2004: A revised approach to ice microphysical processes for the bulk parameterization of clouds and precipitation. *Monthly Weather Review*, 132, 103-120.

Houtekamer, P. L., and H. L. Mitchell, 1998: Data Assimilation Using an Ensemble Kalman Filter Technique. *Mon. Wea. Rev.*, 126, 796–811.

Hu, M., M. Xue, J. Gao, and K. Brewster, 2006: 3DVAR and cloud analysis with WSR-88D level-II data for the prediction of Fort Worth tornadic thunderstorms. Part II: Impact of radial velocity analysis via 3DVAR. *Mon. Wea. Rev.*, 134, 699-721.

James, C. N. and R. A. Houze, 2001: A real-time four-dimensional Doppler dealiasing scheme. *J Atmos Ocean Tech*, 18, 1674-1683.

Kleist, D., K. Ide, J. Whitaker, J. C. Derber, D. Parrish and X. Wang, 2011: Expanding the GSI based hybrid ensemble-variational system to include more flexible parameter settings. Paper J16.4. AMS Annual meeting, Seattle, WA. Jan. 23-27, 2011.

Kurihara, Y., M. A. Bender, R. E. Tuleya, and R. Ross, 1995: Improvements in the GFDL hurricane prediction system. *Mon. Wea. Rev.,* 123, 2791-2801.

Lacis, A. A. and J. E. Hanson, 1974: A parameterization for the absorption of solar radiation-in the earth's atmosphere. *J. Atmos. Sci.*, 31, 118-133.

La Seur, N. E., and H. F. Hawkins, 1963: An analysis of Hurricane Cleo (1958) based on data from research reconnaissance aircraft. *Mon. Wea. Rev.*, 91, 694-709.

Liu, C., Q. Xiao, and B. Wang, 2008: An ensemble-based four-dimensional variational data assimilation scheme. Part I: Technical formulation and preliminary test. Mon. Wea. Rev., 136, 3363–3373.

——, ——, and ——, 2009: An ensemble-based four-dimensional variational data assimilation scheme. Part II: Observing System Simulation Experiments with Advanced Research WRF (ARW). Mon. Wea. Rev., 137, 1687–1704.

Li, J., and H. Liu, 2009: Improved hurricane track and intensity forecast using singlefield-of-view advanced IR sounding measurements. *Geophy. Res. Lett.*, 36, L11813.

Li, Y., X. Wang, and M. Xue, 2012: Assimilation of radar radial velocity data with the WRF ensemble-3DVAR hybrid system for the prediction of hurricane Ike (2008). *Mon. Wea. Rev.*, 140,3507-3524.

Liu, C. S., Q. N. Xiao, and B. Wang, 2008: An ensemble-based four-dimensional variational data assimilation scheme. Part I: Technical formulation and preliminary test. *Mon Weather Rev*, 136, 3363-3373.

Liu, C. S., Q. N. Xiao, and B. Wang, 2009: An Ensemble-Based Four-Dimensional Variational Data Assimilation Scheme. Part II: Observing System Simulation Experiments with Advanced Research WRF (ARW). *Mon Weather Rev*, 137, 1687-1704.

Liu, Q., T. Marchok, H.-L. Pan, M. Bender, and S. J. Lord, 2000: Improvements in hurricane 2 initialization and forecasting at NCEP with global and regional (GFDL) models. Tech. rep., 3 NOAA Tech. Procedures Bull. 472, 7 pp., Camp Springs, MD.

Liu, S., M. Xue, J. Gao, and D. Parrish, 2005: Analysis and impact of super-obbed Doppler radial velocity in the NCEP grid-point statistical interpolation (GSI) analysis system. *Extended abstract, 17th Conf. Num. Wea. Pred.*, Washington DC, Amer. Meteor. Soc., 13A.4.

Lorenc, A., 2003: The potential of the ensemble Kalman filter for NWP - a comparison

with 4D-Var. *Quart. J. Roy. Meteor. Soc.*, 129, 3183-3204.

Marks, F. D. and R. A. Houze, 1984: Airborne Doppler radar observations in Hurricane Debby. *Bull. Amer. Meteor. Soc.*, 65, 569-582.

Marks, F. D., R. A. Houze, and J. F. Gamache, 1992: Dual-aircraft investigation of the inner core of Hurricane Norbert. Part I: Kinematic structure. *J. Atmos. Sci.*, 49, 919-942.

Marks, F. D., Jr. and R. A. Houze, 1987: Inner-core structure of Hurricane Alicia from airborne Doppler-radar observations. *J. Atmos. Sci.*, 44, 1296-1317.

Mlawer, E. J., S. J. Taubman, P. D. Brown, M. J. Iacono, and S. A. Clough, 1997: Radiative transfer for inhomogeneous atmospheres: RRTM, a validated correlated-k model for the longwave. *J. Geophys. Res.*, 102, 16663-16682.

Noh, Y., W. G. Cheon, S. Y. Hong, and S. Raasch, 2003: Improvement of the K-profile model for the planetary boundary layer based on large eddy simulation data. *Bound-Lay Meteorol*, 107, 401-427.

Parrish, D. F. and J. C. Derber, 1992: The National Meteorological Center's spectral statistical-interpolation analysis system. *Mon. Wea. Rev.*, 120, 1747-1763.

Pielke, R. A., J. Gratz, C. W. Landsea, D. Collins, M. A. Saunders, and R. Musulin, 2008: Normalized hurricane damage in the United States: 1900-2005. *Natural hazards Review*, 29-42.

Rainwater, S. and B. Hunt, 2013: Mixed-Resolution Ensemble Data Assimilation. *Mon Weather Rev*, 141, 3007-3021.

Schwartz, C. S. and Z. Liu, 2014: Convection-Permitting Forecasts Initialized with Continuously Cycling Limited-Area 3DVAR, Ensemble Kalman Filter, and "Hybrid" Variational–Ensemble Data Assimilation Systems. *Mon Weather Rev*, 142, 716-738.

Schwartz, C. S., Z. Liu, X.-Y. Huang, Y.-H. Kuo, and C.-T. Fong, 2013: Comparing Limited-Area 3DVAR and Hybrid Variational-Ensemble Data Assimilation Methods for Typhoon Track Forecasts: Sensitivity to Outer Loops and Vortex Relocation. *Mon Weather Rev*, 141, 4350-4372.

Schwartzkopf, M. D. and S. B. Fels, 1991: The simplified exchange method revisited: An accurate, rapid method for computation of infrared cooling rates and fluxes. *J. Geophys. Res.*, 96, 9075-9096.

Schenkman, A., M. Xue, A. Shapiro, K. Brewster, and J. Gao, 2011: The analysis and

prediction of the 8-9 May 2007 Oklahoma tornadic mesoscale convective system by assimilating WSR-88D and CASA radar data using 3DVAR. *Mon. Wea. Rev.*, 139, 224-246.

Schwartzkopf, M. D. and S. B. Fels, 1991: The simplified exchange method revisited: An accurate, rapid method for computation of infrared cooling rates and fluxes. *J. Geophys. Res.*, 96, 9075-9096.

Sirutis, J. and K. Miyakoda, 1990: Subgrid scale physics in 1-month forecasts. Part I: Experiment with four parameterization packages. *Mon. Wea. Rev.*, 118, 1043-1064.

Skamarock, W. C., J. B. Klemp, J. Dudhia, D. O. Gill, D. M. Barker, M. Duda, X.-Y. Huang, W. Wang and J. G. Powers, 2008: A Description of the Advanced Research WRF Version 3. NCAR Technical Note TN-475+STR, 113 pp .

Sugimoto, S., N. A. Crook, J. Sun, Q. Xiao, and D. Barker, 2009: Assimilation of Doppler Radar Data with WRF 3DVAR: Evaluation of its Potential Benefits to Quantitative Precipitation Forecasting through Observing System Simulation Experiments. Mon. Wea. Rev., 137, 4011-4029.

Tallapragada, V., C. Kieu, Y. Kwon, S. Trahan, Q. Liu, Z. Zhang, and I.-H. Kwon, 2014: Evaluation of Storm Structure from the Operational HWRF Model during 2012 Implementation. *Mon Weather Rev.*

Torn, R. D., and G. J. Hakim, 2009: Initial condition sensitivity of western-Pacific extratropical transitions determined using ensemble-based sensitivity analysis. *Mon. Wea. Rev.* 137, 3388-3406.

−, −, and C. Snyder, 2006: Boundary conditions for limited-area ensemble Kalman filters. Mon. Wea. Rev., 134, 2490–2502.

Troen, I. and L. Mahrt, 1986: A simple model of the atmospheric boundary layer; sensitivity to surface evaporation. *Bound.-Layer Meteor.*, 37, 129-148.

Tuleya, R. E., 1994: Tropical storm development and decay: Sensitivity to surface boundary conditions. *Mon. Wea. Rev.*, 122, 291-304.

Wang, X., T. M. Hamill, J. S. Whitaker and C. H. Bishop, 2007a: A comparison of hybrid ensemble transform Kalman filter-OI and ensemble square-root filter analysis schemes. *Mon. Wea. Rev.*, 135, 1055-1076.

---, C. Snyder, and T. M. Hamill, 2007b: On the theoretical equivalence of differently proposed ensemble/3D-Var hybrid analysis schemes. *Mon. Wea. Rev.*, 135, 222-227.

---, D. M. Barker, C. Snyder, and T. M. Hamill, 2008a: A Hybrid ETKF-3DVAR Data Assimilation Scheme for the WRF Model. Part I: Observing system simulation experiment. *Mon. Wea. Rev.*, 136, 5116-5131.

---,--,--,and --, 2008b: A hybrid ETKF-3DVAR data assimilation scheme for the WRF model. Part II: Real observation experiment. *Mon. Wea. Rev.*, 136, 5132-5147.

---, T. M. Hamill, J. S. Whitaker, C. H. Bishop, 2009: A comparison of the hybrid and EnSRF analysis schemes in the presence of model error due to unresolved scales. *Mon. Wea. Rev.*, 137,3219-3232.

---, 2010: Incorporating ensemble covariance in the Gridpoint Statistical Interpolation (GSI) variational minimization: a mathematical framework. *Mon. Wea. Rev.*, 138,2990-2995.

---, 2011: Application of the WRF hybrid ETKF-3DVAR data assimilation system for hurricane track forecasts. *Wea. Forecasting*, 26, 868-884.

----, T. Lei, J. Whitaker, D. Parrish, and D. Kleist, 2011: GSI-based hybrid ensemble-variational data assimilation system for the Global Forecast system model: 3DVAR-based hybrid and ensemble 4DVAR. Paper J16.5. AMS Annual meeting, Seattle, WA. Jan. 23-27, 2011.

----, D. Parrish, D. Kleist, and J. Whitaker, 2013: GSI 3DVar-based Ensemble-Variational Hybrid Dara Assimilation for NCEP Global Forecast System: Single Resolution Experiments [J]. Mon. Wea. Rev., 141, 4098-4117.

----, and T. Lei, 2014: GSI-based four dimensional ensemble-variational (4DEnsVar) data assimilation: formulation and single resolution experiments with real data for NCEP Global Forecast System . *Mon. Wea. Rev.*, **142**,3303-3325.

Wang, X., J. Whitaker, D. T. Kleist, D. F. Parrish, and B. W. Holland, 2011: A GSI-based hybrid ensemble-variational data assimilation system and its comparison with GSI and ensemble Kalman filter *24th Conf. Wea. Forecasting/20th Conf. Num. Wea. Pred.*, Amer. Meteor. Soc., Paper J16.5.

Weng, Y., M. Zhang, and F. Zhang, 2011: Advanced data assimilation for cloud-resolving hurricane initialization and prediction. Comput. Sci. Eng., 13, 40-49.

Weng, Y. and F. Zhang, 2012: Assimilating Airborne Doppler Radar Observations with an Ensemble Kalman Filter for Convection-Permitting Hurricane Initialization and Prediction: Katrina (2005). Mon. Wea. Rev., 140, 841-859.

Whitaker, J. S. and T. M. Hamill, 2002: Ensemble data assimilation without perturbed observations. *Mon Weather Rev*, 130, 1913-1924.

Whitaker, J., D. Kleist, X. Wang and T. Hamill, 2011: Tests of a hybrid variational-ensemble global assimilation system for hurricane prediction. Paper J16.2. AMS annual meeting, 2011, Seattle, WA.

Whitaker, J. S. and T. M. Hamill, 2012: Evaluating Methods to Account for System Errors in Ensemble Data Assimilation. *Mon Weather Rev*, 140, 3078-3089.

Willoughby, H. E., 1990: Temporal changes in the primary circulationin tropical cyclones. *J. Atmos. Sci.*, 47, 242–264.

Wu, W.-S., R. J. Purser, and D. F. Parrish, 2002: Three-dimensional variational analysis with spatially inhomogeneous covariances. *Mon Weather Rev*, 130, 2905-2916.

Xiao, Q. N., and J. Sun, 2007: Multiple radar data assimilation and short-range quantitative precipitation forecasting of a squall line observed during IHOP_2002. *Mon.Wea.Rev.*, 135, 3381-3404.

---, X. Y. Zhang, C. Davis, J. Tuttle, G. Holland, and P. J. Fitzpatrick, 2009: Experiments of Hurricane Initialization with Airborne Doppler Radar Data for the Advanced Research Hurricane WRF (AHW) Model. *Mon Weather Rev*, 137, 2758-2777.

Xu, Q. and J. D. Gong, 2003: Background error covariance functions for Doppler radial-wind analysis. *Q J Roy Meteor Soc*, 129, 1703-1720.

Zhang, F., C. Snyder, and J. Sun, 2004: Impacts of initial estimate and observations on the convective-scale data assimilation with an ensemble Kalman filter. *Mon. Wea. Rev.*, 132, 1238-1253.

Zhang, F., Y. Weng, J. A. Sippel, Z. Meng, and C. H. Bishop, 2009: Cloud-resolving hurricane initialization and prediction through assimilation of Doppler radar observations with an ensemble Kalman filter. *Mon. Wea. Rev.*, 137, 2105-2125.

Zhang, F., M. Zhang and J. A. Hansen, 2009: Coupling ensemble Kalman filter with four-dimensional variational data assimilation. *Advances in Atmospheric Sciences* , 26, 1-8.

Zhang, F., Y. Weng, J. F. Gamache, and F. D. Marks, 2011: Performance of convection-permitting hurricane initialization and prediction during 2008-2010 with ensemble data assimilation of inner-core airborne Doppler radar observations. Geophys. Res. Lett., 38, L15810, doi:10.1029/2011GL048469.

Zhang, F., M. Zhang, and J. Poterjoy, 2013a: E3DVar: Coupling an Ensemble Kalman Filter with Three-Dimensional Variational Data Assimilation in a Limited-Area Weather Prediction Model and Comparison to E4DVar. *Mon Weather Rev*, 141, 900-917.

Zhang, M. and F. Zhang, 2012: E4DVar: Coupling an Ensemble Kalman Filter with Four-Dimensional Variational Data Assimilation in a Limited-Area Weather Prediction Model. *Mon Weather Rev,* 140, 587-600.

Zhang, M., M. Zupanski, M.-J. Kim, and J. A. Knaff, 2013b: Assimilating AMSU-A Radiances in the TC Core Area with NOAA Operational HWRF (2011) and a Hybrid Data Assimilation System: Danielle (2010). *Mon Weather Rev*, 141, 3889-3907.

Zhao, K. and M. Xue, 2009: Assimilation of coastal Doppler radar data with the ARPS 3DVAR and cloud analysis for the prediction of Hurricane Ike (2008). *Geophy. Res. Lett.*, 36, L12803.

Zou, X. L. and Q. N. Xiao, 2000: Studies on the initialization and simulation of a mature hurricane using a variational bogus data assimilation scheme. *J. Atmos. Sci.*, 57, 836-860.

Zupanski, M., 2005: Maximum Likelihood Ensemble Filter: Theoretical Aspects. *Mon. Wea. Rev.*, 133, 1710-1726.